HSE
Health & Safety Executive

A REVIEW OF RESIDUAL STRESS DISTRIBUTIONS IN WELDED JOINTS FOR THE DEFECT ASSESSMENT OF OFFSHORE STRUCTURES

Prepared by AEA Technology plc
for the Health and Safety Executive

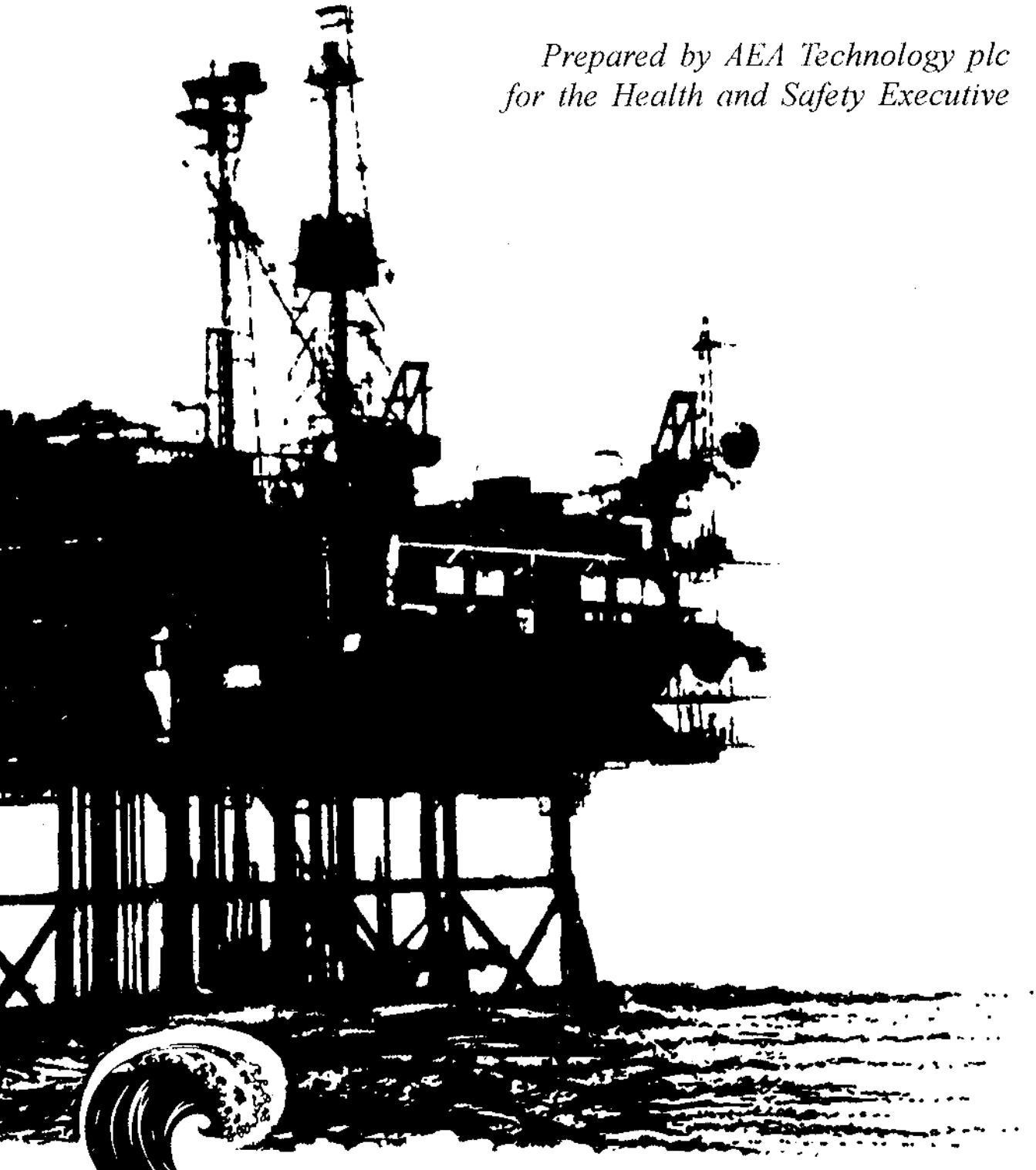

Offshore Technology Report

Health and Safety Executive

A REVIEW OF RESIDUAL STRESS DISTRIBUTIONS IN WELDED JOINTS FOR THE DEFECT ASSESSMENT OF OFFSHORE STRUCTURES

Authors

S K Bate, D Green

AEA Technology plc
Risley, Warrington
Cheshire
WA3 6AT

D Buttle

AEA Technology plc
Culham, Abingdon
Oxfordshire
OX14 3DB

HSE BOOKS

Health and Safety Executive - Offshore Technology Report

First published 1997

ISBN 0-7176-2411-0

This report is published by the Health and Safety Executive as part of a series of reports of work which has been supported by funds provided by the Executive. Neither the Executive, or the contractors concerned assume any liability for the report nor do they necessarily reflect the views or policy of the Executive.

Results, including detailed evaluation and, where relevant, recommendations stemming from their research projects are published in the OTH/OTI series of reports.

SUMMARY

A review of residual stress distributions in welded joints and the treatment of residual stresses in defect assessment procedures is presented. A review of the literature has been carried out on residual stress distributions in welded joints, with particular emphasis on offshore structures, in order to identify representative distributions. Consideration has also been given to the current methods for the treatment of residual stress in defect assessment procedures, such as British Standard PD 6493:1991 and the Nuclear Electric R6 procedure, and the methods for measuring residual stresses. Areas of further work have been identified for establishing a comprehensive catalogue of stress distributions.

TABLE OF CONTENTS

1. INTRODUCTION

Residual stresses can have a detrimental effect on structural integrity and are an important consideration in failure assessment of structures. The stresses are introduced inherently, to varying degrees, by a number of manufacturing processes although their adverse effects are particularly apparent in welded joints. The superposition of high tensile residual stresses with the high operating stresses to which offshore structures are subjected can promote failure by fracture.

Residual stresses in as-welded structures may be up to yield magnitude in tension; with post-weld heat treatment (PWHT), however, they are generally relaxed to about 10-25% of this value. The magnitude and distribution of residual stresses introduced by welding operations are strongly influenced by the geometry of the structure. Understanding the influence of residual stresses is of fundamental importance in analysing the integrity of welded structures, especially heavy section structures such as those used offshore.

In combination with stresses due to service loads, residual stresses may change the susceptibility to failure modes such as corrosion fatigue, stress corrosion cracking and fracture. These residual stresses can influence the fatigue life such that when the residual stresses are tensile, the mean stress is increased and this can adversely influence the initiation of fatigue crack growth and fracture. Conversely, when the residual stresses are compressive the interaction with the applied stresses can result in an overall reduction in the effective stress level, thus enhancing the fatigue life and the resistance to fracture.

The purpose of the current work is to review residual stress distributions typical of those due to welding in offshore structures and to identify representative distributions and their classifications. An overview is given of methods currently recommended for the treatment of residual stress in the BS PD 6493 1991 procedure [1] and in the Nuclear Electric R6 procedure [2]. Recent investigations which comment on the suitability of these procedures are also reviewed. Residual stress profiles have been collated from world-wide literature available in the public domain. Steels studied include structural steels utilised by the offshore industry (BS7191 1989 [3] and BS4360 1990 [4]) as well as those used primarily in the nuclear industry.

The data obtained have been classified by the welded joint type. For each joint classification, the surface and through-thickness residual stress profiles have been obtained where possible. Stress profiles are provided for both longitudinal (parallel to the weld) and transverse (normal to the line of the weld) directions. Figure 1 shows the stress directions identified for each of the joint types. To enable comparison between joint types, the stress profiles have been normalised to the 0.2% proof strength or yield stress of the weld or parent material (if material data are available), as appropriate. The through-thickness profiles have also been normalised with respect to the wall thickness.

Factors affecting the residual stress distributions in the welded joints are also studied. These include the thickness of the parent plate/chord, the boundary restraint applied during the welding process, the heat input supplied by welding (presented as energy per unit length, kJ/mm), and the effect of post-weld heat treatment (PWHT). The general principles of stress redistribution are discussed, along with fatigue crack growth and plasticity.

Conclusions and areas of further work for establishing a comprehensive catalogue of residual stress distributions are presented in Chapter 7. Consideration of the methods for evaluating residual stresses and their distribution using destructive, semi-destructive, non-destructive and numerical techniques is presented in Appendix 1. The methods are assessed with reference to their potential for offshore use.

2. DEFECT ASSESSMENT PROCEDURES

2.1 OVERVIEW OF UK PROCEDURES

The importance of residual stress on structural integrity behaviour is reflected in defect assessment procedures and in the current recommendations of the Health and Safety Executive (HSE) Guidance Notes [5] which recommend when post-weld heat treatment (PWHT) should be used to alleviate residual stress. PWHT is recommended in plated and tubular nodal joints for which the hot-spot stress, calculated for the maximum design load, exceeds 0.8 of the specified minimum yield strength of the parent plate material and when the plate thickness being joined exceeds 40 mm. For other regions, PWHT is recommend when the plate thickness being joined exceeds 50 mm.

The Guidance Notes recommend that paragraphs 4.4.3-5 of BS5500 be used as the basis for PWHT procedures. BS5500 specifies the PWHT temperature and time at temperature for a range of ferritic steels (BS5500 1994 Table 4.4.3.1) and a rate for heating and cooling.

The significance of residual stress is also very apparent on implementation of HSE Guidance Notes with respect to fitness for purpose assessment in the presence of defects. The Guidance Notes allow the use of assessment procedures which can be used to assess fabrication defects or defects which develop in service.

The defect assessment procedures commonly used in UK industry, BS PD6493:1991 [1] and R6/Rev3 [2], are based on the concept of the Failure Assessment Diagram (FAD) which combines considerations of failure by plastic collapse and fracture. This requires the evaluation of two parameters designated S_r (or L_r) and K_r. S_r is defined as the ratio of the applied load to the collapse load based on flow stress, i.e. the mean value of the yield stress and ultimate tensile stress, whereas L_r is the ratio of the applied load to the plastic limit load based on yield stress. K_r is defined as the ratio of the stress intensity factor to the fracture toughness. A failure assessment curve is obtained by plotting values of S_r (or L_r) and K_r that cause limiting conditions. To achieve the critical crack size for a given load, crack dimensions can be adjusted until the (S_r,K_r) (or L_r,K_r) co-ordinates fall on the assessment curve. Alternatively, to calculate the critical load for a given crack size, the applied load can be adjusted until the (S_r,K_r) (or L_r,K_r) co-ordinates fall on the assessment curve. Typical FADs are presented in [1] and [2].

In BS PD6493:1991, three levels of assessment are provided, the degree of complexity increasing with each level in order to obtain greater accuracy in the assessment. The level 1 method is used as a conservative preliminary assessment. Level 2 is the most commonly used method and provides realistic predictions of fracture. Level 3 is the most accurate method but requires very detailed analysis.

R6/Rev3 has three options of failure assessment curve, the degree of complexity increasing with each option. Option 1 is a general curve, Option 2 is a material specific curve obtained by detailed knowledge of material stress-strain behaviour, and Option 3 is a material and geometry specific curve usually obtained from the results of elastic-plastic finite element calculations. In addition, there is a further failure assessment curve given in Appendix 8 of R6/Rev3 which is specifically applicable to structures made of carbon manganese (mild) steels.

2.2 TREATMENT OF RESIDUAL STRESSES IN FRACTURE ASSESSMENTS

The effects of residual stresses are determined by dividing them into two categories. Long range residual stresses produce primary stresses (σ^P) which contribute to plastic collapse. Short range residual stresses produce secondary stresses (σ^S) which do not contribute to plastic collapse and hence are not included in the S_r (or L_r) parameter. The σ^P and σ^S components caused by residual stresses are added to the other primary and secondary stresses generated by the applied loading system.

When there is a combination of σ^P and σ^S stresses, plasticity effects occur which cannot be evaluated by a simple linear addition of the stresses resulting from the two independent stress systems. A term ρ is included in PD6493 and in R6/Rev3 to cover interactions between these two systems such that:

$$K_r = K_I / K_{mat} + \rho \qquad (3)$$

where K_{mat} is material fracture toughness, and

$$K_I = K_I^P + K_I^S \qquad (4)$$

where K_I^P and K_I^S is the stress intensity factor resulting from σ^P and σ^S respectively.

Values for ρ in both PD6493 and R6/Rev3 are given as a function of $K_I^S L_r / K_I^P$.

It should be noted, though, that residual stresses which are self-equilibrating in the whole structure may not be self-equilibrating on the section containing the flaw. Such stresses are not necessarily classifiable as σ^S stresses and if in doubt the stress category σ^P should be assumed.

It is evident from the above that the effect of the residual stress distribution can be significant and needs to be given careful consideration in the application of defect assessment procedures.

2.3 MAGNITUDE OF RESIDUAL STRESSES

At Level 1 in PD6493, for structures in the as-welded condition, tensile residual stresses are conservatively assumed to be uniform and equal to the room temperature yield stress of the weld or parent metal depending in which the flow is located. For structures subjected to PWHT, the level of remaining residual stress may be estimated on the basis of stress relaxation tests. Where such data are unavailable, it may be assumed in carbon manganese and lower alloy steels that the stresses after heat treatment are 30% of the room temperature weld metal yield strength for stresses parallel to the weld, and 15% of the room temperature weld metal yield strength for stresses transverse to the weld. These assumptions are in accordance with BS5500.

Assessments at Levels 2 and 3 in PD6493 are based on the actual distribution of stresses in the vicinity of the flaw. When the distribution of residual stress in an as-welded structure is unknown, the residual stress component may be assumed to be uniform and equal to the appropriate material yield strength as for Level 1. The residual stress assumed in the analysis can be reduced to the lower of

$$\sigma_y \quad \text{or} \quad (1.4 - \sigma_n / \sigma_L)\,\sigma_y, \qquad (1)$$

where:

σ_n is the effective net section stress under the proof load conditions

σ_L is σ_f for Level 2 and $1.2\sigma_{y'}$ for Level 3

$\sigma_{y'}$ is the appropriate material yield strength at the proof test temperature

σ_f is the flow strength (assumed to be the average of the yield and tensile strengths) at the proof test temperature

Typical distributions of residual stress are provided in BS PD-6493 for the through-thickness base plate stress for fillet and butt welds. At the toe of a fillet or T-butt weld, the distribution of transverse residual stresses has been idealised and expressed as a function of the heat input and yield strength, i.e.

$$y = [(122 / \sigma_y) (q / v)]^{0.5} \qquad (2)$$

where:

y is the depth of the idealised residual stress field at the weld toe in a fillet or T-butt weld.

σ_y is the yield strength or 0.2% proof strength

q / v is the heat input of the weld run

The guidance given in BS PD 6493:1991 [1] for quantifying residual stress distributions is very limited and in many cases over-conservative. The recommendations on residual stresses are being revised in the forthcoming revision to BS PD6493:1991. Although no detailed guidance as such is currently given in R6/Rev3 on residual stress distributions, a new Appendix 12 on determination of residual stresses is due to be published.

3. RECENT DEVELOPMENTS IN THE TREATMENT OF RESIDUAL STRESS IN FRACTURE ASSESSMENT

3.1 STRESS CLASSIFICATION

The nature of residual stress is that it is self-balancing. It has been proposed [6, 7] that this balance can be achieved in three fundamental ways although some interaction between residual stress types and structure loading will also occur [8].

(i) Residual stress can be balanced globally throughout the structure so that some members experience membrane tension load and other members provide a balancing membrane compression load. An example is diagonal cross-bracing members between nodes.

(ii) Residual stress can be balanced in the plane of plate material. An example is at a girth weld between tubes where meridian and hoop stresses are in balance up to a characteristic distance away from the weld.

(iii) Residual stress can be balanced through the thickness of a plate. An example of this is a butt weld between plates where the plate surface near to the weld will experience tensile stress and the plate mid-thickness will experience a balancing compressive stress.

These three respectively residual stress types have been classified as long range, medium range and short range [6, 7]. The classification depends on the characteristic distance away from the weld at which the residual stress decays to zero. For example, the characteristic decay length for a girth weld between tubes, which would be classed as a medium range stress, is $2.5\sqrt{rt}$ where r is the tube radius and t is the wall thickness. The decay length for the through-thickness stress at a plate butt weld, which would be classed as a short range stress, is much smaller, being equal to the plate thickness.

In summary, residual stress can be partitioned into membrane, through-wall bending and through-wall self-balancing components which are characterised as long range, medium range or short range respectively. This characterisation depends on two factors which are first, whether the stress produces a progressively increasing stress intensity factor with increasing crack length and, secondly, whether the stress produces a change in ligament net stress with increasing crack length. Long range stresses result in an increase of both the stress intensity factor and ligament net stress with increasing crack length. Short range stress influences neither the stress intensity factor nor the ligament net stress as crack length increases. Medium range stress only influences the stress intensity factor as the crack length increases. Short range stresses have the least effect on fracture behaviour and long range stresses the most.

This classification of stress is also important with respect to the influence of heat treatment. Short range residual stress will be reduced by local heat treatment whereas it is well known that long range residual stress, acting as primary stress, does not readily reduce through local heat treatment.

The existing PD6493 and R6 procedures allow for the difference in behaviour between long-range and medium-range residual stress to be included where the stresses distributions are known but the considerable benefit to be gained by characterising residual stress as short-range where appropriate is not acknowledged.

3.2 FRACTURE OF THROUGH-THICKNESS CRACKS

In recognition of the over-conservative treatment of residual stress in fracture assessment, recent research work has been specifically aimed at identifying a realistic treatment for assessing the integrity of through-thickness cracks.

Considering the treatment of in-plane, self-balancing residual stress (medium range) in the presence of through-thickness defects, it was concluded from experimental work [8] that there is a large influence of residual stress on load carrying capacity for low Lr values where Lr is defined as the applied load divided by the plastic limit load accounting for the presence of the defect. Since Lr is determined using primary loads only, the residual stress is very important where primary loads are low. However, the influence of residual stress reduces to zero at Lr values greater than unity. This recognises that high primary loads can act to relieve residual stress through mechanical stress relief induced by plastic flow. The PD 6493 procedure predicts the effects of primary stresses satisfactorily provided that the magnitude and distribution of the residual stress are known. Otherwise, considerable conservatism may result.

Considering the treatment of through-thickness, self-balancing (i.e. short range) residual stress in the presence of through-thickness defects, it has been acknowledged [6, 7] that the stress intensity factor is primarily dependent on plate thickness rather than crack length. This means that the stress intensity factor is a constant which can be included in the fracture assessment as an effective reduction in fracture toughness. As reported in Section 2.3. the current PD 6493 procedure for including secondary stresses can be expressed in the form:

$$K_r = K_r^p + K_r^s + \rho \qquad (5)$$

where $K_r^p = K_I^p / K_{mat}$

and $K_r^s = K_I^s / K_{mat}$

K_{mat} is the fracture toughness

It has been proposed that a more realistic and less conservative treatment of residual stress is:

$$K_r = K_r^p + K_r^s(\text{long range}) + [K_r^s(\text{medium range}) + \rho] \pm \gamma(\text{short range}) \qquad (6)$$

where ρ is a correction factor accounting for the influence of plasticity on medium range residual stress, and is identical to the ρ factor currently incorporated into PD6493 (see Section 2.3).

$$\gamma = [C \sigma \sqrt{(\pi t)}] / K_{mat} \qquad (7)$$

which is positive at the plate surface and negative at the plate mid-thickness

σ is the surface value of the through-thickness, self-balancing residual stress

C is a constant

and t is the plate thickness.

In Eqn.(6) the long range, medium range and short range residual stress types are identified separately and their individual influences considered. The important point to note is that the stress intensity factor of a through-thickness crack with through-wall, self-balancing stress is dependent on plate thickness rather than crack length and achieves a maximum value when the crack length is approximately equal to the plate thickness.

For a through-thickness crack, the constant C in Eqn.(7) is 0.43 for the case of a through-wall, self-balancing stress in the form of a cosine wave. Triangular and square through-wall, self-balancing stress distributions have constants of 0.38 and 0.48 respectively [9].

3.3 FRACTURE OF EXTENDED SURFACE CRACKS

For extended surface cracks the same stress classification may be used. For short range, through-wall, self-balancing stress, the stress intensity factor for an extended surface crack achieves a maximum value at a crack depth approximately equal to the zero stress depth in the uncracked plate. For crack depths greater than this, the stress intensity factor reduces. Thus the treatment of short range stress through the γ (short range) factor is again applicable since the maximum achievable stress intensity factor depends on plate thickness. Coincidentally, the constant C in Eqn. (7) for the extended surface crack is also equal to 0.43 for a through-wall cosine stress distribution. For triangular and square through-wall, self-balancing stress distributions, the constants for the extended surface crack are 0.33 and 0.72 respectively [9].

3.4 FRACTURE OF SEMI-ELLIPTICAL SURFACE CRACKS

For semi-elliptical surface cracks, fracture may initiate from the maximum depth or from the surface breaking position. For long range and medium range stress types, stress intensity factor solutions are available in the literature. For the short range through-thickness, self-balancing stress, the stress intensity factor at the maximum depth position is conservatively given by the extended surface crack solution and for the surface breaking position by the through-thickness crack solution.

4. RESIDUAL STRESS DISTRIBUTIONS FOR AS-WELDED JOINTS

4.1 INTRODUCTION

Residual stress distributions within welded joints can be classified according to the geometry type, and hence the results presented in this section have been grouped into the following categories:

i) Plate butt welded joints
ii) T-butt welded joints
iii) Pipe butt welded joints
iv) Pipe seam welds
v) Repair welds
vi) Closure welds

For each of the above geometries, the following data were obtained (where available) in order to characterise the residual stress distributions:

a) reference
b) measurement method
c) plate thickness
d) boundary restraint
e) heat input
f) residual stress direction relative to the weld bead

The data taken from the literature for welded joints are summarised in Tables 1-5 according to each of the categories. The residual stress distributions that are presented are mainly based on measured experimental data from tests and as such they are subject to the accuracy of the methods of measurement (see Appendix).

4.2 PLATE BUTT WELDED JOINTS

Plate butt welds obtained in this study are shown in Table 1, the data which relates mostly to ferritic steels of the nuclear industry. Work by Leggatt [16, 17] and Porter Goff and Tsiagbe [20] relate to steel similar to BS 4360 grade 50E carbon manganese steel. Work by Zhou et al. [10] and Lidbury [21] studied residual stresses in heavy section weldments, while Ueda et al. [19] studied finite element analyses also on heavy section weldments. Transverse residual stress distributions, normalised against the yield stress and plate thickness are presented in Figure 2.

The longitudinal stresses measured by Leggatt [17] are shown in Figure 3. The work by Leggatt presented the residual stress distribution in butt welded plates of 25.4 mm thickness BS 4360 grade 50E carbon manganese steel. The welds used a double V preparation. The strains were measured using the neutron diffraction method, and then residual stresses deduced. The plates were held flat during the welding root runs (first two passes), but were then unrestrained for the remaining passes. The longitudinal residual stresses in the welds of the butt welded panels were in the range 320 to 576 MPa, compared to the mean weld metal yield strength of 517 MPa. The transverse stresses were in the range 21 to 144 MPa.

A review was carried out by Ruud and Dimascio [11] on the prediction of residual stresses in heavy plate butt welds. They referred to the residual stresses due to submerged arc welding in a 170 mm thick plate, measured by the X-ray double diffraction technique. The surface and mid-thickness stress distributions determined from the survey are shown in Figure 4. The tensile stresses are those obtained at the surfaces, whilst the compressive stresses are representative of stresses at the mid-thickness. The solid and dotted lines represent the transverse stresses and the stresses parallel to the weld centreline respectively on a traverse from the weld fusion line to a distance of about two plate thicknesses. The principal stresses were found to be perpendicular to, and parallel with, the weldment in the plane of the plate. It was noted that the stress perpendicular to the weld at the surface varied from close to the yield strength at the weld toe to near zero at a distance of one plate thickness from the weld toe. The stresses decreased in magnitude with depth into the plate, reaching the magnitude of the yield strength in compression in the centre of the plate.

Zhou et al. [10] studied residual stresses in welded heavy section plates of pressure vessel steels using the hole drilling method. The weldment was 595 mm long, 256 mm wide and 150 mm thick. The weld preparation was a single V and the heat input was 4 kJ/mm. After welding, the weldment was heat treated at 315°C for 6 hours and air-cooled to prevent cracking. Two other specimens of A737 grade B and A737 grade C were used to study the effect of post-weld heat treatment (PWHT) on residual stresses. The weld preparation was 'K' shaped and the heat input was 2.77 kJ/mm. They found that the residual stresses perpendicular and parallel to the weld were tensile at the surface, or near the surface, and compressive at the centre of the weldment thickness. The largest residual tensile stress was located in the longitudinal direction, parallel with the weld, at the centre of the weldment; whereas the largest compressive residual stress was in the transverse direction, perpendicular to the weld, at the centre of the weldment. Two different measuring techniques were used to quantify the residual stresses. The Battelle chip-removal technique was found to produce stress level measurements comparable in magnitude, but more consistent and less scattered than those from the hole drilling technique.

The surface stresses measured along the weld and transverse to the weld by Zhou et al. [10] are shown in Figure 5. It can be seen that stresses along the weld are tensile and are at a maximum in the centre of the plate. In the transverse direction, the distribution shows a similar trend, with the maximum stresses at the centre of the weld. Zhou et al. concluded that for heavy section welds, the tensile stresses are always substantially less than the yield strength of the steel in the high strength steel weldment.

Karthick and Radhakrishnan [12] developed a theoretical analysis of the residual stresses that was based upon the variation of thermal and mechanical properties of the material with temperature. The results were verified against experimental results carried out on low carbon steels which are presented in Table 1. Three welded plate specimens with a thickness of 12 mm were studied using the X-ray diffraction technique. They found that as the heat input increased, the extent of tensile residual stress that was adjacent to the weld line increased, but its magnitude decreased.

Sandstrom et al. [13] evaluated the residual stress distribution in heavy weldments of A533B steel. The plates had a thickness of 130 mm and the heat input was approximately 1.8 kJ/mm. The results were in good agreement with those on other weldments of similar geometry in heavy plates. In the weld metal the longitudinal stresses were essentially tensile with a minimum value around the centre of the plate. Transverse stresses were compressive in the

centre of the plate and tensile towards the plate surfaces. The stresses in the short transverse direction were smaller than those in the other two directions.

Ueda and Nakacho [14] studied the distribution of residual stresses in multi-pass weldments of 2¼Cr-1Mo A336 grade F22 steel. The submerged arc weld was prepared with a double U-groove (as used in cylinder-head joints) with plate thicknesses of 200 and 300 mm. No restraint was applied during the welding process. They also presented results from previous work which studied welded plates of thicknesses of 50 and 100 mm. The surface measurements by Ueda and Nakacho [14] for a 50 mm mild steel plate are shown at the top and bottom surfaces in Figures 6 and 7 respectively. The longitudinal stresses were at a maximum in the weld on the top surface. Transverse stresses were at a maximum in the weld on the bottom surface, and in the plate on the top surface. Ueda and Kim [24] reported the results of an investigation into calculating three-dimensional residual stress components, based upon the experimental results presented by Ueda and Nakacho [14].

Fidler [15] investigated surface residual stresses in 76 mm thick welded plate with three different types of welding - weave, stringer bead and horizontal/vertical welding. The conclusion was that the residual stresses in the weld metal of a plate welded with a weave weld were generally lower than those in a plate welded with a stringer weld. The results also showed that although the residual stresses measured in the weld metal of all three weld types were high, the standard stress relieving cycle of one hour per 25 mm thickness was sufficient to reduce the stresses to acceptable levels of less than 50 MPa for both weave and stringer and less than 103 MPa for the horizontal/vertical weld type.

Porter Goff and Tsiagbe [20] studied residual stresses in 12 mm welded grade 50D plate. Two different welding types were used - TIG (with a heat input of 2.9 kJ/mm) and MIG (with a heat input of 2.2 kJ/mm). Two different filler wires were used for the MIG specimens (BOC/LW1 and Linde 95). The plate was single pass welded to just fill a 60° V-groove that was 9 mm deep, machined on the longitudinal centre-line of each plate. The welded plates were subjected to PWHT, and then the surface residual stresses were measured using the hole drilling technique.

Lidbury [21] undertook a review of the significance of residual stresses in relation to the integrity of nuclear reactor pressure vessels. In this document, he presented results obtained from previous work by a number of different authors. Only three results were not previously published and these are included in Table 1. Two results were from investigations using A533 grade B class 1 steel plate with a plate thickness of 279 mm and 172 mm. The methods of measurement of the residual stresses used were hole drilling and x-ray diffraction respectively.

Through-thickness stress distributions presented by Stout [22] were obtained from a previous study on 24 mm thick plate welded by a multiple pass butt weld with no boundary restraints.

Ueda et al. [19] studied theories and procedures of the analysis of residual stresses using different finite element (FE) analysis techniques. The data included in Table 1 is for the FE results. The FE was performed on welded plates with thicknesses of 200 and 300 mm. Results were presented for the though-thickness transverse residual stresses, as shown in Figure 2.

Work undertaken by Wu and Carlsson [23] presented parametric equations that could be used to describe residual stress fields, with diagrams showing the typical distribution of residual stresses in plates joined by butt welds.

The effects of PWHT on residual stresses in submerged-arc welded 50 mm thick C-Mn-Nb-Al parent steel were studied by Leggatt [16], using a hole drilling measuring technique to determine the surface stresses, and a block removal technique to quantify the through-thickness stress distribution. It was noted that the maximum residual stresses in the welds lay in the longitudinal direction parallel to the weld length, while the transverse stresses were found to be much lower. The differences were attributed to the different restraint conditions as strong backs had been used.

A summary of investigations into residual stresses as a consequence of different welding passes was reported by Wohlfahrt [18], who included data previously derived for multi-pass welded sheet of high strength structural steel StE 690. It was noted that the transverse residual stress distribution followed a typical "W" shape at both the bottom and top surfaces, with the maximum being at the weld centre-line, as shown in Figure 8.

Overall, the transverse through-thickness stress distributions were found to have greater variation than the longitudinal though thickness stress distribution. This may be due to the greater variation of constraint in the transverse direction than in the longitudinal direction, during welding. Constraint was not quantified in any of the references and as a result this effect cannot be confirmed. The restraint may also cause similar variations between the transverse and the longitudinal through-thickness distributions, but there is insufficient data to confirm this.

4.3 T-BUTT WELDED JOINTS

Table 2 summarises the information that has been collated on T-butt welded joints [23-30]. The results have been discussed according to the following categories:

- T-Plate joints
- Pipe-on-plate joints
- Tubular joints

4.3.1 T-Plate Welded Joints

A total of six experimental residual stress results were obtained for T-plate welded joints, with one result relating to a finite element analysis.

Allen et al. [38] made measurements on model T-butt plate weldments to determine the ability of the neutron diffraction method to measure the through-thickness distribution of welding residual stresses. The model was fabricated from 25.4 mm thick BS 4360 grade 50D steel plate.

The neutron diffraction measurement technique was applied by Holden et al. [25] to assess the residual strains present in a 25 mm thick T-plate welded joint. The residual stresses were then calculated from the measured strains. The T-plate welded joint was used as a laboratory-scale model representing a small angular segment of a complete weld of the type frequently used in typical offshore tubular joints. Welding was carried out with the vertical rolled plate having no restraints and with the use of a balanced welding technique. The average heat input was 1.4 kJ/mm and no post-weld heat treatment was applied. It was noted that there was a high tri-axial stress state close to the toe of the weld. The through- thickness longitudinal stress decreased to zero half way through the plate, and was compressive in the back half of the plate.

The transverse stress was found to be compressive in the middle of the plate and tensile at the front and back surfaces.

Holden et al [25] made a comparison of their own results and those by Allen et al. [38]. In both cases, multi-pass weldments were made, except that, in the tests by Allen et al., the cross-piece was restrained during welding and the measurements were made after the restraints were released. The results for longitudinal and normal strains were quite similar, however, the transverse strains obtained by Holden et al. were higher near to the toe of the weld. The suggested reason for this was that in the constrained weld there would be high tensile strains at the front of the plate and high compressive strains at the back. On removing the restraint, the cross-piece would unload, thus reducing the tensile effect at the front of the plate and compressive stresses at the back of the plate.

Residual welding stresses present in four T-plate joints from BS 4360 grade 50D steel were studied by Morgan and Gardner [36] who applied the air-abrasive hole drilling technique. Two of the joints were evaluated in the as-welded state, and two were post-weld heat treated. Residual stress measurements were made both along the specimen centre line, near the weld toe, and on the specimen side faces immediately below the weld toe on stress-relieved and as welded joints. Strain measurement by three axis strain gauges allowed the calculation of the angular displacement of the maximum principal stress from the longitudinal axis of the specimen - the same methodology as applied by Holden et al. [25].

The geometry tested by Holden et al. [25] was used as the basis for a finite element study by Mok and Pick [28]. This FE investigation is shown in Table 2. The transverse and longitudinal residual stresses obtained in the plate below the toe of the weld for the experimental results and the FE results are shown in Figure 9. The surface residual stresses along the top and bottom surfaces as derived from the FE analysis by Mok and Pick are shown in Figures 10 and 11.

Altogether, the as-welded specimens showed that the tensile residual stress rise rapidly towards the weld and indicated that stresses approaching the yield strength of the material had developed a few millimetres from the weld toe. It was also noted that measurements made beyond 10 mm from the weld resulted in lower longitudinal stresses than those measured on the plate 180 mm from the weld (thought to be induced by the plate rolling and cooling during manufacture). The joints that had PWHT were found to have stresses of a much lower magnitude than the as-welded specimens but there was no clear pattern of stress orientation.

4.3.2 Pipe-on-Plate Welded Joints

Eight test results were found to relate to the evaluation of residual stresses in pipe-on-plate welded joints, with one result derived from a finite element analysis.

Porter Goff et al. [31 & 35] experimentally determined the residual stress distributions in six pipe-on-plate specimens. Three of the joints were evaluated in the as-welded condition, and the remainder were post-weld heat treated before the stresses were measured. None of the joints were restrained during the welding process, in which a mean heat input of between 1.41 and 1.98 kJ/mm was used. The residual stresses were determined by stress relaxation methods, i.e. surface stresses were obtained by abrasive air-jet centre hole drilling, whilst the through-thickness stress distributions were determined using an adaptation of the Rosenthal/Norton block sectioning method. However, the results for the surface stresses were restricted to areas of secondary interest due to the physical interference between the drilling head and the brace pipe.

The distributions of residual stress from all specimens in the as-welded condition showed that the most critical tensile stress state within 2-3 mm of the welded surface. This transverse stress was noted to fall rapidly to half yield tension within 10 mm of the surface in the trans direction. The most compressive through-thickness stresses were found to be at the mid-thickness of the member. It was also observed that the range of stress as in the distribution increased with increasing thickness of the plate. The authors suggested that the weld toe results obtained experimentally from the pipe-on-plate specimens appeared to be typical of true tubular joints. The transverse and longitudinal through-thickness residual stresses at the weld toe are shown for those specimens in the as-welded condition in Figure 12.

Zlochevskii et al. [26] studied the distribution of residual stresses (by a hole drilling technique) as applied to multi-pass welding of shell structures. The joint investigated was a 180 mm diameter solid cylinder 150 mm long welded to an aperture in a 40 mm thick plate. It was found that the magnitude of both transverse and longitudinal residual stresses in the parent metal reached the yield stress in the regions where the weld met the parent metal, while at depths of 2 mm in the weld the yield stress was found to be exceeded by 10-20%.

Leggatt [17] presented results from an investigation undertaken in collaboration with AEA Canada Ltd. One pipe-on-plate result was presented for a pipe of outside diameter of 76.2 mm and thickness of 9.5 mm welded to a plate 130 mm thick. The measurement method used was neutron diffraction. The maximum measured radial stress was 300 MPa, and was located in the weld metal 5 mm below the top surface and 5 mm from the interface with the tube. The maximum measured hoop stress was 350 MPa, at the same location as the maximum radial stress. The maximum axial stress was 50 MPa and was found in the pipe at 2 mm below the top surface, 5 mm from the interface with the weld.

Finch and Burdekin [33] employed the data presented previously (by Free) to specify residual stress distributions for FE analysis of a pipe-on-plate model, using the FE package ABAQUS. The dimensions of the experimental model and the test results obtained are shown in Table 2. The experiment showed that near to the weld toe, the transverse stresses reached a peak tensile yield at about 2 mm below the top surface, and reduced sharply from there downwards to a minimum value close to zero at just below the mid-point of the thickness. The stresses then increased to about one third of the yield strength at the bottom surface of the plate. Near to the weld toe, the longitudinal stresses were noted to reach a peak yield tensile at about 2 mm below the top surface, and reduced sharply from there to a minimum value. They then increased to about half of the yield strength at the bottom surface of the plate. Both the transverse and the longitudinal stresses were noted to become more uniformly distributed through the thickness from approximately 3 mm either side of the weld toe.

4.3.3 Tubular Welded Joints

A total of seven results relating to the residual stresses in tubular joints were found. Five of these were for T joints, and two were for Y (70° and 45°) joints.

Payne and Porter Goff [30] presented results for three T joints. Surface measurements of residual stresses were obtained by abrasive air-jet centre hole drilling, however, as also reported by Porter Goff et al. [31 & 35] the results for the surface stresses were restricted to areas of secondary interest due to the physical interference between the drilling head and the brace pipe, and could only be determined at the weld inner surface below the weld toe. The specimens were welded with a linear weld heat input being limited to about 0.6 kJ/mm per

pass. The through-thickness residual stress results were obtained by block sectioning. Two different chord thicknesses were used, 22 and 36 mm, and it was found that in the thicker chord the critical through-thicknesses stresses were more tensile in the transverse direction, but less tensile in the longitudinal direction. The stresses are presented normalised to the material yield strength, 488, 491 and 365 MPa, and chord thickness 22, 22 and 36 mm respectively, in Figure 13.

A study of the stress distribution in the two Y tubular joints [31 and 35] derived the through-thickness distributions in the transverse and longitudinal directions as shown in Figures 15 and 16 at the positions of the crown and saddle respectively. The results show a tensile stress near to the weld toe, at a value almost equalling the yield stress.

Figure 17 shows the transverse and longitudinal stresses through the thickness of the chord for each of the tubular joints referred to above [27] that had a chord wall thickness of 22 mm. One result for a pipe-on-plate joint is also shown for comparison purposes. It can be seen that all stresses are tensile near to the surface of the weld toe and that stresses are mainly compressive at mid-thickness (except for pipe-on-plate specimen, P1). Stresses are tensile at the opposite surface in order to maintain a self balancing distribution through the thickness.

Machida et al [32] carried out brittle fracture tests on two T type tubular joint model specimens to study the effect of residual stress on the fracture strength. The tests were carried out for as-welded and PWHT (625°C for 2 hours) specimens. The welding residual stresses were calculated from measurements made using the local stress relief method. Figure 14 shows the stress distributions at the chord for two specimens. It should be noted, however, that the residual stresses apparently exceed the yield stress of the material, which is thought to be either an overestimation caused by the stress measurement technique or misquoted residual stress values in the reference.

It may be concluded that the through-thickness stresses show a fairly consistent trend for the pipe on plate, tubular T node and tubular Y node which could be attributed to the self-constraining nature of these joint types.

4.4 PIPE BUTT WELDS

A survey of test data and prediction methods on residual stresses in pipe butt (cylindrical girth) welds [49] was presented in 1989 where stress distributions through the wall thickness and on the outer and inner surfaces were given. Experimental measurements were compared with the analytical model of Scaramangas, as presented by Scaramangas and Porter Goff [47]. The data obtained from these and other test results on pipe butt welds are shown in Table 3 [40 to 51].

The data obtained relating to pipe butt welds [47] were found to exhibit a number of trends useful in understanding the overall behaviour of cylinder girth welds. "The molten weld pool, when it solidifies and shrinks, imposes a circumferential tendon force on the cylinder which is analogous to a tourniquet. However, the longitudinal stresses along the axis of the cylinder due to this effect are compression on the outer surface and tension on the inside surface, at the girth weld centre-line. Away from the girth weld the stresses decay rapidly. In the longitudinal direction of the cylinder, if the cylinder is restrained, though thickness tensile residual stresses are developed due to the different amounts of shrinkage throughout the thickness of the weld. This latter effect induces tension stresses on the outside surface and compression stresses on the inside surface of the cylinder wall." [47].

Leggatt [43, 46] made measurements on a pipe with an outer diameter of 610 mm and with a wall thickness of 15.5 mm. The parent material had a typical yield stress of 510 MPa and the weld metal 540 MPa. Measurement of the through-wall thickness distribution of axial stresses in the weld by the layering method showed that the stresses were compressive on the outer surface, had a peak tensile value of 200 MPa below the surface and were zero at the inner surface. Holden et al. [44] measured the axial strains at a girth weld in a 914 mm diameter line-pipe using neutron diffraction. The pipe had a 16 mm wall thickness. Through-wall variations of the axial residual stress at the weld centre-line were determined by layering methods, and show similar trends to those observed by Leggatt [43, 46].

Jonsson and Josefson [45] determined the stresses during and after single pass butt welding of a pipe with an outer diameter of 203 mm and a wall thickness of 8.8 mm. The residual stresses were obtained around the circumference of the pipe at the weld centre-line and two other axial positions. The residual stress field was found to be rotationally symmetric despite the rapid cooling induced after welding. The hoop stress was observed not to change during the final cooling and was found to exhibit almost no variation in the circumferential direction. In further work by Jonsson et al. [50], residual stress measurements were made for two multi-pass butt welded pipes with an outer diameter of 350 mm and a wall thickness of 20 mm. The pipes had differing weld preparation, the first a single-U groove and the second a narrow-gap. Residual stress measurements were obtained around the circumference at three different axial positions. The residual stress state was found to be rotationally non-symmetric at the weld centre, but approximately symmetric away from the weld. The measured narrow gap groove residual stresses, and radial deflections on the outer surface, were larger than those on the single U groove. The total circumferential variation for both axial and hoop stresses in the single pass butt welded pipe was found to be somewhat smaller than the corresponding variation measured for a multi-pass butt welded pipe.

The work by Scaramangas and Porter Goff [47] considered the through-thickness distributions for three butt welded cylinders in 1 metre diameter pipe with wall thicknesses of 9.1, 15.0 and 19.5 mm from grade 50D BS 4360 steel. These experimental results were then used as the basis for the validation of an analytical model used to predict residual stresses. From these investigations it was found that the primary parameter that determined the residual stress magnitude and through-thickness distribution was the net linear heat input per pass per unit wall thickness. A secondary parameter was identified as being the geometrical ratio of mean cylinder radius to wall thickness (as shown in Table 3 as "R/t").

Residual stresses obtained for thicker butt welded pipes were obtained from the work by Ritchie and Leggatt [40] and Fidler [41, 42]. Ritchie and Leggatt measured the through-thickness variation of axial residual stress in the circumferential weld of a cylinder, outer diameter 761 mm and wall thickness 25.4 mm. The stresses were measured at three locations and were found to be predominantly tensile, with peak values at the toe of the weld root in the range 90 to 250 MPa. These were significantly lower than the weld metal yield stress of 430 MPa. Fidler [41] determined the residual stress distribution in a CrMoV-2CrMo pipe butt weld of 230 mm bore and 84 mm wall thickness. The method of residual stress measurement was by the trepanning technique. The results of the analysis showed that, in general, the residual hoop stresses over the outer two-thirds of the weld were tensile, and were compressive over the inner third. Axial stresses were tensile over the outer third and compressive over the inner two thirds of the weld.

Bonner and Smith [48] measured the residual strains in butt welded pipe using a variety of measuring techniques, including gun-drilling, hole diameter measurement, electro-chemical

machining and hole diameter re-measurement. They presented results of the residual stresses measured in a pipe butt weld for a pipe with a wall thickness of 85 mm using a deep hole technique. This specimen was made from carbon steel pipe with a single-V type weld preparation were used to manufacture the specimen. It was found that the residual stress on the interior surface was compressive, becoming tensile at 9-17mm from this surface. The axial stress was noted to return to compression on the exterior, while the hoop stress magnitude was seen to fall, as in Figure 18.

The through-thickness distributions in the work referred to above are shown in Figures 19 and 20 in the axial and hoop directions respectively. Surface stress distributions measured by Fidler [41, 42] and Leggatt [43] are shown in Figures 21 and 22 respectively. Ueda and Nakacho [14] presented residual stress results for an investigation using a large size penstock model in which a circumferential butt weld was fabricated. Surface residual stress distributions are shown in Figure 23.

It may be concluded that the axial through-thickness stress distribution (Figure 19) is divided approximately between through-thickness bending and through-thickness self-balancing with a tendency towards higher bending stress for thinner walls and towards higher self-balancing stress for thicker walls. The hoop through-thickness stress distribution (Figure 20) is dominated by the tourniquet effect to produce a large membrane stress and small self-balancing stress for all wall thicknesses. The hoop surface stresses are approximately yield stress at the position of the weld and rapidly reduce to about one quarter of the yield stress at a distance of approximately one plate thickness from the weld (Figures 19 and 20). Axial surface stresses reach a maximum of almost half yield at one to two plate thicknesses from the weld and can be much lower, almost zero to 20% yield at the weld itself (Figures 21 and 22).

4.5 PIPE SEAM WELDS

Data from the available literature on pipe seam welds are shown in Table 4. Only two tests were found to relate to the assessment of residual stresses in pipe seam welds. Figure 24 shows the through-thickness residual stresses for the two tests, and Figure 25 shows the surface residual stresses for these tests. Although data are scarce, the two results present similar overall trends, in the distribution of residual stresses due to pipe seam welds.

Ueda et al [51] measured the residual stresses in pipe seam welds for a large penstock model of 780 MPa high strength steel plate, diameter 1400mm, and wall thickness 50 mm. The maximum residual stress perpendicular to the weld line was found to be almost 590 MPa in tension on the inner surface, which was considerably larger than that of almost 200 MPa in the butt welded pipe. This was thought to be due to the fact that the bending restraint in the longitudinal joint was smaller than that in the pipe butt joint. The residual stresses along the weld line were found to be at a maximum tensile stress in the pipe seam welded joint at a magnitude of almost 400 MPa.

Mitchell [52] made residual stress measurements using the deep-hole method on A533B steel pipe (with a nominal yield stress of 345 MPa) with a diameter 1180 mm and a wall thickness of 85 mm. Peak hoop stress values of 350 MPa were measured approximately 10-12 mm below the outer surface of the weld. Compressive stress values of 250 MPa were measured on its inner surface. The axial and through-thickness stress distributions were similar, but found to be slightly lower in magnitude. Stresses in the parent plate were found to be low, and mainly compressive, ranging from about 60 MPa in the hoop direction at the outer surface to near zero

at the inner surface. In the axial and through-thickness directions, both surface values were near zero, but compresses stresses of 30 - 50 MPa were measured at mid-wall thickness.

Pipe seam welds are generally thought to be less constrained than pipe butt welds, with the constraint being dependent on the radius to thickness ratio. However insufficient data are available for any firm conclusions to be drawn regarding the trends.

4.6 REPAIR WELDS

A total of twenty tests relating to the residual stresses in repair welds have been collated, as shown in Table 5.

Hepworth [53] reported on residual stresses measured in ½Cr½Mo¼V weld metal repair welds. Two of the repair welds were made in material cut from a closed die forging and a further two were made on sections cut from a casting of nominal 1Cr½Mo¼V composition. The residual stresses were measured using the hole drilling method. Surface residual stresses were measured along lines parallel and normal to the welding direction. These are shown in Figures 26 and 27 across the weld for two of the tests (R1 and R2). The stresses have been normalised against the weld metal yield stress in the as-welded condition of 650 MPa. Although the figures would seem to indicate that the longitudinal stresses of a magnitude equal to or greater than the weld metal yield stress, it should be noted that the high stresses derived from the hole drilling technique are known be an over-estimate of residual stress, which could be as high as 25%. The stresses measured in the tests indicate that the transverse stress is about two thirds of the longitudinal stress. At the end of the weld the stresses decrease with increasing distance from the HAZ.

Ueda et al. [57] used thermal elastic-plastic stress analysis to predict residual stresses in a mild steel plate, 90 mm thick. All the residual stress components calculated in the weld metal were tensile, the longitudinal stresses being greater than the transverse stresses, which is similar to the findings of Hepworth [53].

Leggatt [54] made residual stress measurements at repair welds in pressure vessel steels in the as-welded condition. The measurements were made in seven panels and, with the exception of one test, strong-backs (sb) were attached prior to repair welding and remained in place until completion of the measurements. Surface residual stresses were measured using the centre hole rosette gauge technique. Internal stresses were measured in one of the panels using a two stage relaxation technique of block removal and layering - a simplified version of the Rosenthal and Norton method. The surface residual stresses in the repair welds and adjacent HAZ were extremely variable, with maximum values similar in magnitude to the repair weld metal yield stress, and minimum values which in some cases were compressive. Maximum values tended to occur at the centre of repair beads, or in the repair/parent HAZ. Internal longitudinal stresses were tensile and approaching yield magnitude throughout the repair weld and decreased rapidly with distance outside it, becoming compressive at a distance of 15 to 30 mm from the fusion boundary.

Further work by Leggatt [55,56] was undertaken on a theoretical investigation into the effects of structural restraint, repair depth and wall thickness on the distribution of transverse residual stresses at repair welds in heavy section plates [54] and cylindrical structures. He concluded that longitudinal stresses in repair welds are tensile and near yield magnitude throughout the

cross section of the repair. Transverse stresses are of near-yield magnitude at the surface, but decrease with depth from the surface, the rate of decrease depending on the restraint acting at the repair, as in Figure 27.

Bryan et al [58] presented residual stresses measured in heavy section steel test vessels, 152 mm thick and fabricated from A533, grade B, class 1 steel. The repair welding followed the ASME XI (ASME boiler and pressure vessel code) half-bead procedure, with no subsequent heat treatment. Residual stresses were determined from pre-weld and post-weld strain gauge measurements and from using a hole-drilling technique. Four specimens were tested with full penetration repair welds, and two were tested with partial penetration welds. In general, measurements of residual stress levels in the vicinity of the half-bead weld repairs showed that comparatively low tensile and compressive circumferential and axial residual stresses were present in the weld metal. However, in the base metal adjacent to the weld repairs and up to 25-50 mm from the heat affected zone (HAZ), peak tensile stresses were close to yield magnitude, depending upon the depth in the base metal.

Lidbury [21] made reference to these tests and others with relation to a study on repair welding procedures. It was noted that repair welds made without PWHT may be expected to contain longitudinal residual stresses which are large and tensile throughout the thickness. Associated values of transverse stress could also be large and tensile at the surface of the repair, but may decrease with distance below the surface, depending on the restraint.

4.7 CLOSURE WELDS

The term closure weld is used to describe a weld which is made from one side only, and is usually as a result of restricted access to one side of the weld e.g. inside a tubular. They often occur offshore where man-ways are replaced in a chord member by re-welding a curved section of plate into the hole. As a result of the application of these closure welds, they are frequently made under more adverse conditions of tolerance with a significant degree of mismatch with differing root gaps and are often performed under temporary weather protection in a number of different welding positions.

An experimental test programme was undertaken by Jones et al. [59] in which forty-four small-scale and nine full-scale tubular closure welded joints were fatigue tested. It was found that the stress distribution observed on the tapered side of the welded joint exhibited a rapid increase in stress along the taper, as well as significant hoop strain being present at both sides of the joint. The results of this experimental programme were also presented by Andrews and Jones [61].

Finite element analyses were conducted on pipe butt welds by King and Foroughi [60] which were used to show that a typical closure weld had high stresses at the root associated with the stress concentrating effect of the root geometry, and secondary stresses due to the fabrication and misalignment and changes in thickness from the stud to the brace. It was also concluded that the greater the difference in wall thickness between the plates the closure weld was used to join, the greater the magnitude of the residual stress.

The residual stresses caused by single-sided closure welds in pipe butt joints are generally compressive at the outer surface and tensile at the bore due to the circumferential force caused by the solidification and shrinkage of the weld. However, the results contrast those for single-

sided closure welds in plates. Tensile residual stresses equal to the yield stress occur at the outer surface since the reaction force does not produce bending stresses which in a cylinder are of opposite sign to the shrinkage stresses transverse to the weld.

5. FACTORS AFFECTING RESIDUAL STRESS DISTRIBUTIONS

5.1 RESIDUAL STRESS DIRECTION RELATIVE TO THE WELD BEAD

For each of the geometries discussed in the preceding sections, the residual stress distributions have been presented longitudinal (parallel) and transverse (normal) to the weld bead, at the surface and through the thickness.

The residual stresses measured in plate butt welds are shown in Figure 2. The transverse stresses in plate butt welds were tensile at the surfaces with the maximum appearing at or a short distance below the top surface for thicknesses of 200-300 mm. The stress was a minimum (most compressive) at mid-thickness. There were insufficient data for comparison of longitudinal through-thickness stresses, but the data from Leggatt [17] shown in Figure 3, indicates that longitudinal stresses were tensile through the thickness, of greater magnitude than the transverse stress and equal to the material yield stress at the surfaces. Stresses at the surface of the butt weld are shown in Figures 4-7. For comparison, the stresses shown in Figures 4, 5 and 6 are at the top surface, transverse to the weld line. They each show that the longitudinal stresses are greater and are at a maximum at the weld. The magnitude at the weld can be up to the yield stress of the material.

In tubular joints, the transverse and longitudinal through-thickness stresses show similar trends (Figure 17). For transverse through-thickness stresses, the maximum residual stress occurs at the weld toe and the minimum value, which is generally compressive, at mid-thickness. The stresses were tensile on the opposite surface to achieve a self-balancing distribution through the thickness. The surface stresses were predicted by Mok and Pick [28] for the T tubular joint specimen (Figure 11) which also indicated a maximum stress at the weld toe. The stresses measured by Machida et al. [32] (Figure 14) at the surface of a T tubular were noted, however, to apparently exceed the yield stress of the material, which is thought to be either an overestimation caused by the stress measurement technique. Stresses measured in the chord weld line were maximum at the saddle.

5.2 THICKNESS

In pipe butt welds, both the axial and hoop stress through-thickness distributions indicated an effect of thickness. At the outer surface, the hoop stresses (parallel to weld) showed a similar trend to longitudinal stresses in plate butt welds for thicknesses up to 20 mm.

The effect of thickness was considered for tubular joints (see Figure 13). The transverse residual stresses measured through the chord thickness at the crown were found to be more tensile for those joints with thicker chords and it was noted that the effect was greater at the surface.

Figure 12, which presents the results obtained for three pipe on plate specimens, shows that as the plate thickness is increased, the stresses at the toe of the weld are apparently not affected and are of similar magnitude. However, the compressive stresses at the mid-thickness and the tensile stresses at the opposite surface are found to increase with increasing thickness in order to maintain the equilibrium through the thickness.

The literature review suggests that the effect of thickness on the residual stress distribution in plate butt welds has not been investigated. The results presented in Figure 2 however, indicate that the stresses are of a greater magnitude in thicker plates (almost yield for thicknesses of 200 mm and over). The effect on longitudinal stresses cannot be substantiated due to the lack of data.

For pipe butt welds, Leggatt [46] observed that axial stresses at the weld were primarily a function of the pipe wall thickness and noted that they showed a clear trend from tensile stresses at the inner surface in thin walled pipes (below 16 mm) to compressive stresses in thick walled pipes (above 25 mm). The data shown in Figure 19 for through-thickness transverse (axial) stress distribution supports this observation - for thicknesses up to 16 mm the distributions indicate that the stresses through the weld are compressive at the outer surface and tensile on the inner surface. For thicknesses greater than 25 mm, compressive stresses were observed from the results from Ritchie and Leggatt [40] and Bonner and Smith [48].

The through-wall hoop residual stresses are compared in Figure 20. For the large thickness pipes, the hoop stress can be seen to be compressive at the inner surface, whereas for the pipe of thickness less than 20 mm, the stresses are noted to be tensile through the thickness of the pipe.

5.3 BOUNDARY RESTRAINT

The data presented in Tables 1-5 indicate whether or not information relating to the boundary restraint was available. Restraint is defined as an externally applied fixed displacement at the geometry boundary. No significant investigation into the effect of boundary restraint on residual stresses was evident from the literature studied.

The stresses in a multi-pass butt welded joint of 50 mm thickness were derived by Ueda and Nakacho [14] in order to consider the effect of restraint on the joint by theoretical analysis. Two extreme restraint conditions were assumed; a condition under which longitudinal deformation and angular distortion occurred freely (restraint condition A) and one under which both deformations were restricted (restraint condition B). The stresses measured at the top surface are shown in Figure 28. The results showed that the effect of the restraint condition on the top surface was relatively small. This was thought to be due to the fact that as the plate thickness increased, deformations were restrained internally when the finishing bead was applied because the previously deposited weld metal recovered rigidity. Ueda and Nakacho [14] concluded that the distribution of residual stress near the finishing bead may be characterised by the fact that the maximum tensile stresses appear not on the finishing bead but several layers below, in this case at approximately 25% of the wall thickness.

5.4 HEAT INPUT

The effect of heat input on residual stress patterns in pipe girth welds was presented by the UEG Tubular Joints Group in 1989 [49]. The findings stated that for thin-walled tubes in which the heat input per unit wall thickness was high (>100J/mm^2), the axial through-thickness residual stress was compressive at the external surface but tensile at the internal surface. For thicker walled tubes and tubes where the heat input per unit wall thickness was low (<70 J/mm^2), the external surface had a residual stress between 60% and 100% of the compressive

yield strength. The tensile stress at the internal surface was less than approximately 50% of the yield strength and in some cases it was compressive.

No comparative investigation was found for T-butt welds, but BS PD6493:1991 [1] provides an idealised distribution of the transverse residual stresses at the toe of a fillet or T-butt weld as a function of the heat input (Figure 32).

Karthick and Radhakrishnan [12] found in their analysis of residual stresses in butt welded mild steel plates that as the heat input increased, the extent of the tensile stress across the plate from the fusion line increased but its magnitude decreased.

5.5 POST-WELD HEAT TREATMENT

Lidbury [21] and Leggatt [16] reviewed the effect of PWHT on residual stresses in heavy section weldments for plate butt welded specimens. The results obtained by Porter Goff et al. [31,35] on the effect of PWHT on pipe on plate welded specimens are shown in Figures 29 and 30.

The work by Leggatt [16] was carried out on submerged-arc welds in 50 mm thick C-Mn-Al-Nb steel test panels subjected to a range of seven different PWHT conditions. Leggatt [16] looked at the effect of restraint on the residual stresses in T-butt welds and found that the maximum residual stresses in the welds always lay in the longitudinal direction parallel to the weld. The transverse stresses were in general much lower and were found to be relatively insensitive to heat treatment conditions. The maximum measured residual stresses in the test panels were up to 50 MPa greater than the upper bound of the stress relaxation data for corresponding PWHT temperatures and hold times. The higher stress level in the test panels was attributed to stress recovery during cooling after PWHT. It was also found that the predicted maximum residual stress after heat treatment (in accordance with BS5500:1976) represented 30% of the typical room temperature yield stress of the weld metal in the as-welded condition, or 36% of the minimum weld metal yield stress after PWHT.

Zhou et al. [10] studied plate butt welds in A737 steel with a yield stress of 511 MPa. The stress relief applied was a two hour treatment at 550°C. The PWHT was found to reduce the residual stresses to relatively low tensile values, generally in the range 35-70 MPa. The results were used to demonstrate that the stress relief operation was effective and that even high tensile or compressive stresses could be reduced to modest levels in steel through standard stress relief treatments.

The investigation by Fidler [15] into the residual stresses in plate butt welds in CrMoV steel (yield stress 310 MPa) found that the maximum residual stresses measured in the weld metal in the as-welded condition were high (in excess of 300 MPa for the weave weld and 500 MPa for the stringer and horizontal/vertical welds). However, the standard stress relief procedure of one hour per 25mm thickness was sufficient to reduce residual stresses to less than 50 MPa for both the weave and stringer welds and less than 103 MPa for the horizontal/vertical weld.

The results from Porter Goff et al. [31,35] are shown in Figures 29 and 30 for three pipe on plate specimens, of BS 4360 Grade 50 steel. The PWHT cycles for specimens P1 (yield stress 420 MPa) and P3 (yield stress 360 MPa) satisfied the requirements of BS 5500 under the concession clause for hold temperatures in the range 550 to 580°C. However, specimen P2 (yield = 375 MPa) failed to meet the requirements. The results for specimen P2 showed

stresses at the weld toe in excess of 30% of the room temperature yield stress. This result indicates that the BS 5500 concession clause should be used with care. Further tests were carried out by Porter Goff et al. [35] with a series of tests on welded plates in Grade 50D steel with two different filler materials, and PWHT in the range 450 to 550°C. These results confirmed Leggatt's finding that residual stresses vary considerably with the filler wire used. The PWHT concession equivalent time formula was broadly supported by the results of a simplified creep model.

Morgan and Gardner [36] studied residual stresses in T-plate butt welds in steel with a yield stress of 376 MPa. It was found that in the longitudinal direction, residual welding stresses were generally tensile in as-welded specimens with values at the weld toe being of yield stress magnitude. However, after stress relieving at 600°C for four hours, the residual stresses were reduced to below 55 MPa even near the weld toe.

5.6 STRESS REDISTRIBUTION EFFECTS

5.6.1 General Principles

A number of reports refer to redistribution of residual stress, particularly with respect to crack growth. The superposition theorem can be used to define the effect on stress intensity factor which may be expected.

Figure 31a shows a plate of elastic material with an applied tensile stress, but no crack. Therefore the stress intensity factor is zero. Introducing a crack as in Figure 31b introduces the Mode I stress intensity factor K. If the same stress σ is applied to the crack face as well to the remote boundary, as shown in Figure 31c, the stress field in the plate will be the same as that for the uncracked plate for which the Mode I stress intensity factor is zero. Since the superposition theorem applies to the total stress intensity factor from combined loading, then the stress intensity factor for the crack with the remote stress σ applied alone must be equal and opposite to the stress intensity factor for the crack with the crack face stress σ applied alone. Thus the superposition theorem leads to a very convenient method for calculating stress intensity factor as follows. The stress intensity factor of a crack with a remote load distribution can be calculated by applying a stress distribution to the crack faces, equal to the stress distribution at the position of the crack but without the crack present. This is shown in Figure 31d.

The theorem is general and applies to both non-uniform, self-balancing, stress distributions and displacement-controlled conditions which are characteristic of residual stress distributions. Although residual stresses will redistribute as the crack increases in length, the theorem demonstrates that there is no redistribution effect on the value of stress intensity factor, since its value for all crack lengths can be determined from a single, uncracked plate, residual stress distribution. Mixed mode loading involving Mode II and Mode III stress intensity factors can also be considered in the same way.

5.6.2 Fatigue Crack Growth

Fatigue crack growth is dependent on stress intensity factor in two ways. Primarily, the applied range of stress intensity factor ΔK influences the crack growth rate through the Paris law. Since residual stress is not cyclic it does not contribute to ΔK. However, crack closure effects

are important since a fatigue crack will only grow due to that part of the cycle which produces crack tip tensile stresses. Thus the R ratio, expressed as K_{min}/K_{max}, influences crack growth rate.

Two reports are identified in the literature [62, 63] which partly attribute experimentally observed crack growth rates to redistribution of residual stress with crack growth. An effect of residual stress redistribution on stress intensity factor is implied by Shi et al. [62] and specifically stated by Lam and Lian [63]. These observed effects are considered here to be due either to crack closure effects or to an incorrect technique for calculating the stress intensity factor due to residual stress [62]. These conclusions are therefore considered to be spurious. Two reports in the literature, Todoroki and Kabayashi [64] and EPRI [65], consider residual stress redistribution with crack growth. These reports both concluded that the effect of redistribution is fully accounted for by the superposition theorem.

5.6.3 Plasticity

As described in Section 2.1, fracture assessment procedures such as that incorporated into BS PD 6493:1991 require the calculation of two parameters: Kr and Lr (or Sr). Stresses are categorised as primary or secondary, depending on whether they are reacted externally to the structure (e.g. pressure, dead-weight) or internally through the surrounding material (e.g. thermal stress, residual stress). Primary stresses contribute to both the Kr and Lr (or Sr) parameters. Secondary stresses contribute to the Kr parameter only.

Experimental work by Sharples et al [8] has considered the role of residual stress in the context of the Lr parameter. Where primary stress is large, it was demonstrated that plastic flow can largely eliminate a self-balancing residual stress distribution, in effect by mechanical stress relief. Under such circumstances it is not necessary to include residual stress in the calculation of the Kr parameter. Sharples has suggested an Lr cut-off value of approximately 1.0, beyond which residual stress need not be considered. Further work may identify a progressive reduction in the residual stress contribution for Lr values up to 1.0.

To some extent this effect is recognised in the fracture procedure of BS PD 6493:1991 where the ρ factor, which accounts for the influence of plasticity on secondary stress, reduces to zero as the Lr value approaches 1.05.

6. CHARACTERISATION OF RESIDUAL STRESS PROFILES AND COMPARISON WITH CURRENTLY RECOMMENDED PROFILES

6.1 INTRODUCTION

The data obtained from this survey has been compared with the stress profiles recommended in BS PD 6493:1991 [1] and the Nuclear Electric (NE) compendium of as-welded residual stress profiles [66]. The comparison has enabled revised guidance to be formulated on best upper bound profiles.

6.2 PLATE BUTT WELDS

6.2.1 Transverse

The distribution of residual stresses transverse to the weld of a plate butt weld is dependent upon the restraint at the joint. BS PD 6493 provides an illustration of residual stress distributions subject to membrane and bending restraint (Figure 32). The trends illustrated in Figure 32 are partly reflected by the data obtained in this survey. A self balancing distribution (Figure 32c) is shown by Stout [22] in Figure 2. This shows a balanced distribution between compression and tensile with maximum stresses approaching yield strength at the surface. The effects of restraint are shown in Figures 32d and 32e and through the results obtained by Ueda et al. [51] (Figure 28). The results this investigation show that the residual stresses at the root of the weld become compressive when the plate is restrained from bending. An upper bound profile for transverse fractional residual stress ($\sigma_f = \sigma^s/\sigma_y$), for the case of minimum restraint, is provided in the NE compendium [66] of the form:

$$\sigma_f = 1.0 - 0.917(z/t) - 14.533(z/t)^2 + 83.115(z/t)^3 - 215.45(z/t)^4 + 244.16(z/t)^5 - 96.36(z/t)^6 \quad (8)$$

Data obtained from Leggatt [17] infer that the idealised profile is not conservative in the mid-thickness region (Figure 33a). However the data of Leggatt are inconsistent with that found previously and therefore no corrections to the Nuclear Electric profiles are suggested.

There are insufficient available data to draw any firm conclusions on the effect of restraint on the residual stress distribution.

6.2.2 Longitudinal

A typical distribution of stresses parallel to the weld at a butt weld is also illustrated in PD 6493 (Figure 32). For longitudinal stresses an upper bound profile of the form:

$$\sigma_f = 0.82 + 2.892(z/t) - 11.316(z/t)^2 + 10.545(z/t)^3 - 1.846(z/t)^4 \quad (9)$$

is given in the NE compendium [66] for ferritic steels. Figure 33b compares this profile with the additional data of Leggatt [17]. Due to the inconsistency of these data with that found previously no modification of the above profile is suggested.

6.3 T-BUTT WELDS

6.3.1 Transverse

The BS PD 6493 recommended profile for transverse residual stresses is:

$$\text{if } z \le z_0, \qquad \sigma_f = \sigma_y\left(1 - z/z_o\right)$$

$$\text{if } z > z_0, \qquad \sigma_f = 0 \quad (10)$$

where $z_o = \sqrt{\frac{122}{\sigma_y}\left(\frac{q}{v}\right)}$.

$\left(\frac{q}{v}\right)$ is defined in J/mm, σ_y in MPa, z and z_0 are in mm and z is the distance below the weld toe. This profile is also recommended for residual stresses in the transverse direction in T-butt weldments in the NE compendium.

Figures 34a-c compare the PD 6493 distribution with those measured in tubular joints. For each of the figures, it can be seen that the idealised distribution is conservative at the mid-thickness. However, where self balancing residual stress distributions are evident, the recommendations of PD 6493 do not give tensile stresses at the surface opposite to the weld toe.

Stacey [27] noted that the data available were limited to joints of low plate thickness and low to medium rates of heat input, i.e. the BS PD 6493 approach could be less conservative for thicker joints and higher input rates. Figure 34a shows the distributions for three tubular-T node specimens, which were prepared with a heat input of 600 J/mm. It shows that for greater chord thickness (i.e. specimen T3, see Figure 13) the idealised stress distribution becomes less conservative. Figure 34c shows the distribution for three pipe on plate specimens (see also Figure 12) which vary in thickness and also in heat input. The distribution reduces in conservatism again as thickness increases.

Although this report is primarily concerned with through-thickness residual stress profiles, for completeness some information has been included for surface profiles. Figure 35 shows comparisons of surface residual stress profiles as calculated by Mok and Pick [28] with those of the NE compendium.

Figure 36 shows the transverse data for each of the T-butt geometries and Figure 37 compares the derived upper bound profiles. In this case the profile derived from all the data is an upper bound to everything apart from surface stresses for T-plate geometries. As an alternative to the PD 6493 equation (Equation 10), a profile defined by the following expression has been derived for T-butt welded joints:

$$\sigma_f = 0.97 + 2.327(z/t) - 24.125(z/t)^2 + 42.485(z/t)^3 - 21.087(z/t)^4 \qquad (11)$$

This profile is plotted in comparison with data obtained from a plate T-butt weld and a pipe-on-plate weld in Figure 38.

A new equation was also derived for the transverse residual stresses present in tubular T and Y joints, and this profile is shown with data from tubular T and Y joints in Figure 40.

$$\sigma_f = 0.96 - 2.48(z/t) - 7.942(z/t)^2 + 21.687(z/t)^3 - 12..101(z/t)^4 \quad (11b)$$

6.3.2 Longitudinal

The NE compendium recommends a stress profile for longitudinal through-thickness residual stresses in T-butt welded plates in the form:

$$\sigma_f = 0.75 + 4.766(z/t) - 26.696(z/t)^2 + 38.11(z/t)^3 - 16.82(z/t)^4 \quad (12)$$

Figure 40 compares the recommended profile for through-thickness longitudinal residual stresses with the measured data of Holden et. al. [44]. For completeness, Figure 41 shows comparisons of surface residual stress profiles as calculated by Mok and Pick [28] with those recommended in the NE compendium in the longitudinal direction.

The profile defined by Equation 12 was compared with the data obtained for other T-butt geometries and it was shown that for tubular T-butt geometries, the recommended profile for plate T-butt welds given in the NE compendium was not conservative. A new upper bound polynomial fit to data specific to tubular node weld geometries was therefore derived.

Figure 42 shows the normalised longitudinal stress data for each of the tubular T-butt geometries. For each of these sets, an upper bound curve was obtained based on confidence limits. Figure 43 shows these curves and it can be seen that the pipe on plate profile provides an upper bound to all the tubular T-butt data. The upper bound to the pipe on plate data is thus recommended for use as a conservative residual stress profile for all tubular T-butt ferritic weldments. This is represented by the equation:

$$\sigma_f(z/t) = 0.977 - 1.234(z/t) - 7.601(z/t)^2 + 16.075(z/t)^3 - 8.226(z/t)^4 \quad (13)$$

This profile has been plotted in comparison with the measured data in Figures 44 to 46 and is shown to be generally conservative.

For T-butt welds in plates the existing profile in the NE compendium (Equation 12) specific to T-plate geometries is still recommended.

6.4 PIPE BUTT WELDS

6.4.1 Transverse

For ferritic pipe butt weld transverse residual stresses, the NE compendium recommends a fourth order polynomial of the form:

$$\sigma_f = \sigma_{f\_outer}\left(1.0 - 3.29(z/t) - 26.09(z/t)^2 + 73.16(z/t)^3 - 45.72(z/t)^4\right)$$

where

$$\sigma_{f\_outer} = 0.3515 - 0.00878(R/t) + 0.00419(R/t)^2 - 7.129x10^{-5}(R/t)^3 \quad (14)$$

where R is the mean radius and t is the wall thickness

The recommended transverse profiles from the NE compendium have been compared with data obtained from work by Scaramangas and Goff [47] and Bonner and Smith [48] in Figure 47. For values of R/t = 24.1 and 30, the NE compendium predicts the residual stress profile quite well, but for a higher value of R/t (49.6) the NE compendium does not predict the measured profile very well. It should be noted that this value of R/t is actually outside the range of the NE compendium recommendations. At these very high values of R/t (t=9.1mm) it is suggested that a 1/2 cosine profile be adopted. This is in broad agreement with Scaramangas and Goff who suggest that both heat input and the value of displacement-controlled play a significant role in determining the residual stress profile of a plate butt weld. Scaramangas suggested that the heat input is the more influential factor (Figure 48). A programme of experimental and analytical work showed that for high input, a 1/2 cosine wave profile of transverse residual stress is observed in pipe butt welds. The 1/2 cosine wave tends towards a more linear (through-wall bending) distribution for higher values of R/t. At lower values of heat input, a single or multiple 'S' profile is observed which is attributed to the fact that the effect of the last weld pass does not completely swamp out the effects of previous weld passes. On the basis of these experimental results and a literature survey, Stacey [27] recommends that the 1/2 cosine profile for transverse residual stresses in ferritic pipe butt welds should be adopted. This recommended distribution is represented by the form

$$\sigma_{res.}[x] = \sigma_0 \cos.(\pi x/T) \qquad (15)$$

where x is measured from the weld root. σ_0 attains a value of σ_y for high heat inputs (>60J/mm^2) and does not exceed 0.5 σ_y for lower values (<60J/mm^2).

To summarise, it is recommended that:

a) for R/t <40 the NE compendium should be used

b) for R/t >40 and heat input <60J/mm^2 a ½ cosine profile should be used with σ_o=1/2σ_y

c) for R/t >40 and heat input >60J/mm^2 a ½ cosine profile should be used with σ_o=σ_y

This review was aimed at residual stress profiles for defect assessment in offshore structures. Consequently, the literature review only involved references pertaining to ferritic weldments. However, for the sake of completeness, the profiles for austenitic pipe butt welds are given below [66].

If t≥25mm, $\sigma_f = \sigma_{f\_bore}\left(0.27 - 0.91(z/t) - 4.93(z/t)^2 + 8.60(z/t)^3 - 2.03(z/t)^4\right)$

and σ_{f_bore} is determined from

For $R/t \leq 8.5$, $\sigma_{f\_bore} = 0.118(R/t)$

For $R/t > 8.5$, $\sigma_{f\_bore} = 1.0$

If t <25mm, $\sigma_f = \left(\sigma_{outer}/\sigma_y\right)\left(1 + (z/t)(\sigma_{bore}/\sigma_{outer} - 1)\right)$ (16)

where $\sigma_{bore} = \sigma_{f\_bore}\sigma_y$

For $R/t \leq 10$, $\sigma_{outer} = \sigma_y$

For $R/t > 10$, $\sigma_{outer} = \sigma_y\left(1 - 0.07\left[\left(R/t\right) - 10\right]\right)$

6.4.2 Longitudinal

For longitudinal through-thickness stresses, a linear profile defined by a stress equal to yield, σ_y at the outer surface and σ_S at the bore is given in the NE compendium as:

$$\sigma_{s\_bore}/\sigma_y = 1 + (z/t)\left(\sigma_{s\_bore}/\sigma_y - 1\right) \qquad (17)$$

where, $\sigma_{s\_bore}/\sigma_y = 1$ $\quad t \le 15mm$

and $\sigma_{s\_bore}/\sigma_y = 1 - 0.014(t - 15)$ $\quad t > 15mm$

and z is measured from the outer surface in mm. No additional data have been found for this case.

6.5 PIPE SEAM WELDS

6.5.1 Transverse

No further data have been obtained for pipe seam welds, therefore the recommended profiles are as suggested by the NE compendium. That is, for transverse residual stresses, the recommended through-thickness stress profile is the same as that for plate butt welds

$$\sigma_f = 1.0 - 0.917(z/t) - 14.533(z/t)^2 + 83.115(z/t)^3 \qquad (18)$$
$$-215.45(z/t)^4 + 244.16(z/t)^5 - 96.36(z/t)^6$$

6.5.2 Longitudinal

For the longitudinal residual stresses, Devonshire [68] recommends that a through-wall tensile residual stress field be assumed i.e.

$$\sigma_f = \sigma_y \qquad (19)$$

The recommended profiles for pipe seam welds are illustrated in Figure 49.

6.6 REPAIR WELDS

For repair welds insufficient new experimental data was obtained and therefore the profiles given in the NE compendium are recommended (Figure 50).

6.6.1 Transverse

For transverse residual stresses, the stress profile is defined by the fourth order polynomial

$$\sigma_f(z/t) = 0.75 - 2.265(z/t) - 3.557(z/t)^2 + 9.989(z/t)^3 - 4.634(z/t)^4 \qquad (20)$$

6.6.2 Longitudinal

The longitudinal profile is defined by

$$\sigma_f(z/t) = 0.75 - 4.766(z/t) - 26.696(z/t)^2 + 38.11(z/t)^3 - 16.82(z/t)^4; (z/t) \le 0.65$$

$$\text{For } (z/t) > 0.65, \sigma_f = 0. \qquad (21)$$

7. CONCLUSIONS AND RECOMMENDATIONS

The information reviewed in this report shows that residual stress distributions in welded joints can be categorised by the weld geometry. The nature of the residual stress distribution depends on the geometrical constraint or the restraint imposed during welding. Where structures are self-constraining, such as girth welds in pipes, the through-thickness residual stress distributions can be well defined. The residual stress then depends on the inherent stiffness of the structure which in the case of the pipe girth weld is the radius to thickness ratio. Where the structure is not self-restraining and the applied restraint is unknown, such as flat plate butt welds, the measured residual stress distributions can be variable.

The information from the literature review has been used to derive upper bound stress profiles [67] which provide users with a better estimate than the over-conservative assumption that they are equal to the yield stress throughout the section. The following conclusions have been derived:

- A shortage of data available from tests on T-butt welds has been identified. It is therefore recommended that future work should be carried out to establish the effects of thickness and/or heat input which are evident in plate and pipe butt welds. Similar considerations may be given to closure welds.

- The available data for structural steels relevant to BS 7191 [3] and BS 4360 [4] are also limited. It is recommended that future test programs use offshore representative grades of steel so that any differences with other ferritic steels can be quantified, particularly with those of pressure vessel steels which have formed the bulk of available data.

However, in order to reduce the conservatism of using upper bound profiles which allow for the influence of other factors on the residual stress distribution, it is recommended that further work should be carried out to establish the effects of the following:

- restraint on flat plate geometries.

- heat input on all geometries. This has been established to some extent by Scaramangas and Goff [47] for though wall transverse stresses in pipe butt geometries. There is a lack of data for heat inputs of more than 2kJ/mm.

- weld preparation, particularly for pipe and plate butt geometries.

REFERENCES

[1] BS PD6493:1991, Guidance on methods for assessing the acceptability of flaws in fusion welded structures, British Standards Institution, London, 1991

[2] Milne, I., Ainsworth, R.A., Dowling, A.R. and Stewart, A.T., Assessment of the integrity of structures containing defects, CEGB report R/H/R6 rev. 3, May 1991

[3] BS 7191:1989, Weldable structural steels for fixed offshore structures, British Standards Institute, London, September 1991

[4] BS 4360:1990, Weldable structural steels, British Standards Institute, London, December 1991

[5] Offshore Installations: Guidance on design, construction and certification, Fourth edition, UK Department of Energy, London, July 1993

[6] Green, D. and Knowles, J., The treatment of residual stress in fracture, Assessment of Pressure Vessels, ASME PSV, Volume 233, 1992

[7] Green, D., Sharples, J.K. and Stewart, G., Experimental evidence in support of proposal for the treatment of residual stress in fracture assessment of pressure vessels, ASME PSV Volume 250, 1993

[8] Sharples, J.K, Harrison, M., May, K.A., Chivers, T.C. and Smith, E., The effect of residual stress on fracture behaviour. ASME PSV Volume 250, 1993

[9] AEA internal document

Plate Butt Welds

[10] Zhou, R.J., Pense, A.W., Basehore, M.L. and Lyons, D.H. A study of residual stress in pressure vessel steels. Welding Research Council Bulletin 302, p23-32, February 1985

[11] Ruud, C.O. and Dimascio, P.S. A prediction of residual stress in heavy plate butt welds. Journal of materials for energy systems, American Society for Metals, Volume 3, p62-65, June 1981

[12] Karthick, V.G., Radhakrishnan. Analysis of heat affected zone and residual stresses in welds. Scandinavian journal of metallurgy Volume 16, p262-266, 1987

[13] Sandstrom, R., Larsson, L.E., and Gott, K. Evaluation of the 3D residual stress field from x-ray diffraction measurements on weldments of A533 heavy plate. Nuclear Engineering & Design, Amsterdam, Volume 86, p315-325, 1985

[14] Ueda, Y. and Nakacho, K. Distributions of welding residual stresses in various welded joints of thick plates., Transactions of Japanese Welding Research Institute, Volume 15, Number 1, 1986

[15] Fidler, R. An investigation into the effect of some welding variables on residual stresses. CEGB R/M/N874

[16] Leggatt, R.H. Relaxation of residual stresses during post-weld heat treatment of submerged-arc welds in a C-Mn-Nb-Al steel. TWI Research Report No.288/1985, October 1985

[17] Leggatt, R.H. Measurement of residual stresses in complex welded components. 5585/12A/91, TWI, June 1991

[18] Edited by Wohlfahrt, H. Residual stresses as a consequence of welding. From Advances in surface treatments - technology, applications and effects. Edited by Niku-Lari. International guidebook on residual stresses Volume 4, Pergamon Press, 1987

[19] Ueda, Y., Fukuda, K. and Nakacho, K. Basic procedures in analysis and measurement of welding residual stresses by the finite element method. From the International Conference on Residual stresses in welded construction and their effects . Organised by The Welding Institute, Paper No.3, p27-37, November 1977

[20] Porter Goff, and Tsiagbe, W. Residual stress in welds: effect of PWHT, SERC GR/E/74977, Cambridge University Engineering Dept. Final Report, Issued September 1989, Revised August 1990

[21] Lidbury, D. The significance of residual stresses in relation to the integrity of LWR pressure vessels. International Journal of pressure vessels and piping, Volume 17 No 4, p197-328, 1984

[22] Stout, R.D. Post-weld heat treatment of pressure vessel steels. Research Council Bulletin No.302, February 1985

[23] Wu, X.R. and Carlsson, J. Welding residual stress intensity factors for welding half-elliptical surface cracks in thin and thick plates. Engineering Fracture Mechanics Volume 19, No3 p407-426, 1984

[24] Ueda, Y. and Kim, Y.C. New measuring method of three-dimensional residual stresses using effective inherent strains as parameters. From Residual Stresses in Science and Technology, Volume 1, Published by DGM Information Gesell-Schaft, Edited by Macherauch E. & Hauk V, 1987

T-Butt Welded Joints

[25] Holden, T.M., Root J.H., Holt, R.A. and Roy G. Neutron diffraction measurements of the residual strain state of a tubular T-joint. Proceeding of the 7th International Conference on Offshore Mechanics And Arctic Engineering, p127-131, February 1988

[26] Zlochevskii, A.B., Shuvalov, A.N., Leonov, V.P., Margolin, B.Z., Rybin, Yu.I. and Stakonov, V.I. Distribution of residual stresses in the components of shell structures after multi-pass welding and hydraulic tests. Automatic Welding, (Avt. Svarka) No.4, p11-16, April 1984

[27] Stacey, A. The significance of residual stresses in the defect assessment of offshore structures. Materials engineering OMAE - Volume III-B. From international conference on offshore mechanics and arctic engineering, p729-739, 1993

[28] Mok, D. and Pick, R. Finite element study of residual stresses in a plate T-joint fatigue specimen. Proc. Institute Mechanical Engineers Volume 204, p127-134, 1990

[29] Tsiagbe, W. and Porter Goff, R.F.D. The effect of PWHT on residual stress in tubular joints. 2nd International offshore and polar engineering conference, San Francisco, Volume IV p342-346, June 1992

[30] Payne, J. and Porter Goff, R.F.D. Experimental residual stress distributions in welded tubular T-nodes. Fatigue and crack growth in offshore structures, C134/86, Proceedings of Institute Mechanical Engineers, p109-116, IMechE 1986

[31] Porter Goff, R.F.D., Free, J.A. and Tsiagbe, W. Residual stresses in welded tubular nodes. Conference Proceedings of Fatigue of offshore structures, p285-295, London 1988

[32] Machida, S., Hagiwara Y. and Kajimoto, K. Evaluation of brittle fracture strength of tubular joints of offshore structures, 6th Int. OMAE Offshore mechanics and arctic engineering, p231-237, 1987

[33] Finch, D. and Burdekin, F. Effects of welding residual stresses on significance of defects in various types of welded joint. Eng. Fracture Mechanics, Volume 41, No 5, p721-735, 1992

[34] White, J. Residual stresses in large stiffened tubulars used in offshore structures civil engineering transactions, the institution of engineers, Australia, p98-103, 1979

[35] Porter, Goff, R.F.D., Free, J.A. and Tsiagbe, W. Residual stresses in Y-nodes and PWHT joints, OTH 89 315, 1989

[36] Morgan, H. and Gardner, L. The influence of post-weld heat treatment on the fatigue performance of 'T' butt welded joints tested at low stress levels, Volume 1 - Report on Department of Energy project 887, OTN 92-161, Commercial in Confidence, Sept. 1991

[37] Bonner, N.W. Measurement of residual stresses in thick-section steel welds, SERC/ERCOS Project, University of Bristol, End of year Report, November 1991

[38] Allen, A.J., Hutchings, M.T. and Rainey V. Measurement of through-thickness residual stress in offshore steels using the neutron diffraction technique, AERE R 12178, May 1986

[39] Ueda, Y., Nakacho, K. and Moriyama, S. Simple prediction methods for welding deflection and residual stress of stiffened panels, Transactions of Japanese Welding Research Institute, Volume 15, No. 2, p197-204, 1986.

Pipe Butt Welds

[40] Ritchie, D. and Leggatt, R.H. The measurement of the distribution of residual stresses through the thickness of a welded joint. From "Strain", UDC:539.319, p 61-70, May 1987

[41] Fidler, R. Residual stresses in a ½Cr½Mo¼V-2CrMo pipe weld: Part 1 -The as-welded condition. International Journal Pressure Vessels & Piping. Volume 14, p35-62, 1983

[42] Fidler, R. Residual stresses in a $^1/_2Cr^1/_2Mo^1/_4V$ butt weld, CEGB Research Dept. R/M/N621, January 1972

[43] Leggatt, R.H. Residual stresses at circumferential welds in pipes, The Welding Institute Research Bulletin, p181-188, June 1982

[44] Holden, T., Powell, B., MacEwen, S. and Lazor, R. Axial strains at a girth weld in a 914 mm linepipe. 2nd Int. Symposium on non destructive characterisation of materials, p625-631, July 1986

[45] Jonsson, M. and Josefson, R. Experimentally determined transient and residual stresses in a butt-welded pipe. Journal of strain analysis Volume 23 No 1, Published by IMechE, 1988

[46] Leggatt, R. Residual stresses at girth welds in pipes. Welding Institute of Canada, Welding in energy-related projects. Pergamon Press, p429-440

[47] Scaramangas, A. and Porter Goff, R. Residual stresses in cylinder girth butt welds. 17th Offshore Technology Conference, OTC5024, p25-30, May 1985

[48] Bonner, N. and Smith, D. Measurement of residual stresses in a thick-section steel weld. 2nd Int. conference on engineering integrity assessment, Glasgow, May 1994

[49] UEG Tubular joints Group (TJG), Newsletter supplement 12 Appendix A, p24-35, Sept. 1989

[50] Jonsson, M., Josefson, B. and Nasstrom, M. Experimentally determined deformations and stresses in narrow-gap and single-U multi-pass butt welded pipes, Journal of offshore mechanics and arctic engineering, Volume 115, p116-122, May 1993

[51] Ueda, Y., Fukuda, K., Nishimura, I., Hideaki, I., Chiba, N. and Fukuda, M. Three dimensional cold bending and welding residual stresses in Penstock of 80 kgf/mm^2 class high strength steel plate, Transactions of Japanese Welding Research Institute. Volume 12, No.2, p117-126, 1983

Pipe Seam welds

[52] Mitchell, D. R6 validation exercise - through-thickness residual stress measurement son an experiment test vessel rig, CEGB, Research Report RD/B/6088/R88, June 1988

Repair welds

[53] Hepworth, J.K. Surface residual stress in repair welds made without preheat or post-weld heat treatment, CEGB TPRD/M/1427/R84, CEGB Confidential, July 1984

[54] Leggatt, R. Residual stress measurements at repair welds in pressure vessel steels in the as-welded condition, TWI report 315/1986, October 1986

[55] Leggatt, R. Computer modelling of transverse residual stresses in repair welds, IIW Document No. X-1176-88, May 1988

[56] Leggatt, R. Residual stresses at repair welds without PWHT, TWI seminar 'Repair welding without post-weld heat treatment - Problems and solutions', Institute of Materials, London, Lecture No.4, December 1993

[57] Ueda, Y., Kim, Y.C., Garatini, K., Yamakita, T., Bang, H. Mechanical characteristics of repair welds in thick plate, (Report I), Transactions of Japanese Welding Research Institute, Volume 15 No.2, 1986

[58] Bryan, R.H., Merkle, J.G., Iskander, S.K., Whitman, G.D. and Holz, P.P. Test of a thick vessel with a flaw in residual stress field, Proc. Conf. on pressure vessels and piping, San Francisco, June 1979, published by ASME, 1979

Closure welds

[59] Jones, R L, Andrews, R M and Forshaw, M E. Single sided welding of closure joints in large tubular fabrications, OTH 90 335, Prepared by TWI for the Department of Energy - Offshore Technology report, 1991

[60] King, R and Foroughi, R. The application of influence function methods to the estimation of fatigue performance in closure welds, Conference on Fatigue of welded constructions, Brighton, session IV, paper 33, p241-250, April 1987

[61] Andrews, R M. and Jones, R L. The fatigue performance of single sided closure welds in offshore structures, 1991 OMAE-Volume III-B, Materials Engineering, ASME, 1991

Other aspects

[62] Shi, Y.W., Chen, B.Y., and Zhang, J.X. Effects of welding residual stresses on fatigue crack growth behaviour in butt welds of a pipeline steel. Engineering fracture Mechanics. Volume 36, No.6, p893-902, 1990

[63] Lam, Y.C. and Lian, K.S. The effect of residual stress and its redistribution on fatigue crack growth. Theoretical and Applied Fracture Mechanics 12, p59-66, 1989

[64] Todoroki, A. and Kabayashi, H. Prediction of fatigue crack growth rates in residual stress fields. Fracture and Strength '90 - Key Engineering Materials V. p367-372, Published by Trans. Tech. Pub., Zurich, Switzerland, 1990

[65] Weld residual stress redistribution near growing cracks, EPRI NP-2964, Project 606-3, March 1983

[66] Mathieson, P.A.R., A compendium of as-welded residual stress profiles. Nuclear Electric, Technology Division, RD/SIB/MEM/02333, Internal Document, September 1991

[67] Bate, S.K. and Green, D. Summary of report of guidance on residual stress profiles for use in fracture mechanics, AEA-TSD-0064, May 1994

[68] Devonshire, H., Suggested as-welded residual stress profiles. AEA Reactor Services report, AEA-RS-4325, May 1994

Reference	Measurement Method	Plate thickness (mm)	Heat treatment		Proof stress (MPa)	Boundary Restraint		Heat input (KJ/mm)	Residual stress direction relative to weld bead			
			Yes	No		Yes	No		Surface Parallel	Surface Transverse	Thro' Thickness Parallel	Thro' Thickness Transverse
Wohlfahrt (18)	X-ray diffraction	10			StE 690*			1.19	x	x		
Karthick & Radhakrishnan (12)	X-ray diffraction	12		x	250-300			7.92	x			
Karthick & Radhakrishnan (12)	X-ray diffraction	12		x	250-300			3.96	x			
Karthick & Radhakrishnan (12)	X-ray diffraction	12		x	250-300			1.32	x			
Porter Goff & Tsiagbe (20)	Hole drilling	12	x		680			2.2	x	x		
Porter Goff & Tsiagbe (20)	Hole drilling	12	x		480			2.2	x	x		
Porter Goff & Tsiagbe (20)	Hole drilling	12	x		420			2.9	x	x		
Stout (22)		24			375		x				x	x
Wu & Carlsson (23)		25							x	x		
Leggatt (17)	Neutron diffraction	25.4			368		x	1.6-1.8			x	x
Leggatt (17)	Neutron diffraction	25.4			368		x	1.6-1.8			x	x
Ueda & Nakacho (14)		50		x	SS41 m s*		x	SAW	x	x		
Leggatt (16)	Hole drilling & block removal	50	x		362-440	sb		3.5			x	x
Leggatt (16)	Hole drilling & block removal	50	x		362-440	sb		3.5			x	
Leggatt (16)	Hole drilling & block removal	50	x		362-440	sb		3.5			x	x
Leggatt (16)	Hole drilling & block removal	50	x		362-440	sb		3.5			x	x
Leggatt (16)	Hole drilling & block removal	50	x		362-440	sb		3.5			x	x
Leggatt (16)	Hole drilling & block removal	50	x		362-440	sb		3.5			x	x
Leggatt (16)	Hole drilling & block removal	50	x		362-440	sb		3.5			x	x
Zhou et al.(10)	Hole drilling & Battelle chip	76		x	511			2.77			x	x
Zhou et al.(10)	Hole drilling & Battelle chip	76	x		511			2.77			x	x
Fidler (15)	Trepanning & hole drilling	76	x		310	sb		1.3-2.5	x	x		
Fidler (15)	Trepanning & hole drilling	76	x		310	sb		0.7-1.4	x	x		
Fidler (15)	Trepanning & hole drilling	76	x		310	sb		1-1.5	x	x		
Ueda & Nakacho (14)		100		x	225-275			Electroslag	x	x		
Wu & Carlsson (23)		100									x	
Zhou et al.(10)	Hole drilling & Battelle chip	103		x	511			2.77			x	x
Zhou et al.(10)	Hole drilling & Battelle chip	103	x		511			2.77			x	x
Sandstrom et al. (13)	X-ray diffraction	130		x	448		x	1.8	x	x		
Sandstrom et al. (13)	X-ray diffraction	130	x		448			1.8	x	x		
Zhou et al.(10)	Hole drilling & Battelle chip	150	x		740			4	x	x		x
Lidbury (21)		150	x		585				x	x		
Rudd & Dimascio (11)	X-ray diffraction	170			310				x	x		
Sandstrom et al. (13)	X-ray diffraction	170	x		448			1.8	x	x		
Lidbury (21)	X-ray diffraction	172	x		345						x	x
Lidbury (21)	Hole drilling	279	x		345		x		x	x	x	x
Ueda & Nakacho (14)		300		x	310			SAW	x	x		
Ueda et al. (19)	FE Results	300		x	310			4.9		x		x
Ueda et al. (19)	FE Results	200		x	310			3.4				x
Ueda et al. (19)	FE Results	200	x		310			3.4				x
Ueda et al. (19)	FE Results	200	x		310			3.4				x
Ueda et al. (19)	FE Results	200	x		310			3.4				x
Ueda et al. (19)	FE Results	200	x		310			3.4				x

Key: * = proof stress not known sb = strong backs attached

Table 1: Plate Butt Welds

Reference	Joint Type	Measurement Method	Plate thickness (mm)	Tau Ratio (brace/chord thickness ratio)	Heat treatment		Proof stress	Boundary Restraint		Heat input	Residual stress direction relative to weld bead			
					Yes	No	(MPa)	Yes	No	(KJ/mm)	Surface Parallel	Surface Transverse	Thro' Thickness Parallel	Thro' Thickness Transverse
Allen et al (38)	T-plate	Neutron diffraction	25											
Holden et al (25)	T-plate	Neutron diffraction	25.4			x	421		x	1.4			x	x
Mok & Pick (28)	T-plate	Neutron diffraction	26			x	421		x		x	x	x	x
Morgan & Gardner (36)	T-plate	Hole drilling	100		x		376	x			x		x	
Morgan & Gardner (36)	T-plate	Hole drilling	100		x		376	x			x		x	
Morgan & Gardner (36)	T-plate	Hole drilling	100			x	376	x			x		x	
Morgan & Gardner (36)	T-plate	Hole drilling	100			x	376	x			x	x	x	
Leggatt (17)	Pipe/plate	Neutron diffraction	9.5			x					x	x		
Finch & Burdekin (33)	Pipe/plate	Stress relaxation	22										x	x
Porter Goff et al (35)	Pipe/plate	Block removal	22		x		420		x	1.41	x	x	x	x
Porter Goff et al (31)	Pipe/plate	Hole drilling & sectioning	22			x	420		x	1.41			x	x
Porter Goff et al (35)	Pipe/plate	Block removal	40		x		375		x	1.8	x	x	x	x
Porter Goff et al (31)	Pipe/plate	Hole drilling & sectioning	40			x	375		x	1.8			x	x
Zlochevskii et al (26)	Pipe/plate	Hole drilling	40							1	x	x		
Porter Goff et al (35)	Pipe/plate	Block removal	50		x		360		x	1.98	x	x	x	x
Porter Goff et al (31)	Pipe/plate	Hole drilling & sectioning	50			x	360		x	1.98			x	x
Machida et al (32)	Tubular-T	Local stress relief	40 (0.62)	0.75		x	440			GMAW	x	x		
Machida et al (32)	Tubular-T	Local stress relief	40 (0.62)	0.75	x		440			GMAW	x	x		
Payne & Porter Goff (30)	Tubular-T	Hole drilling & sectioning	22 (0.67)	0.75		x	488		x	0.6			x	x
Payne & Porter Goff (30)	Tubular-T	Hole drilling & sectioning	22 (0.5)	0.50		x	491		x	0.6			x	x
Payne & Porter Goff (30)	Tubular-T	Hole drilling & sectioning	36 (0.67)	0.39		x	365		x	0.6			x	x
Porter Goff et al (31)	Tubular-Y	Hole drilling & sectioning	22 (0.62)	0.64		x	430		x	1.83			x	x
Porter Goff et al (31)	Tubular-Y	Hole drilling & sectioning	22 (0.5)	0.50		x	430		x	1.15			x	x

Table 2: T-Butt Welds

Reference	Measurement Method	Plate thickness (mm)	R/t	Heat treatment		Proof stress (MPa)	Heat input (KJ/mm)	Residual stress direction relative to weld bead			
				Yes	No			Surface Parallel	Surface Transverse	Thro' Thickness Parallel	Thro' Thickness Transverse
Jonsson et al. (45)	Hole drilling	8.8	11.53			380	0.73	x	x		
Scaramangas & PG (47) & TJG (49)	Sectioning & hole drilling &EDM	9.1	54.96			520	0.8			x	x
Scaramangas & PG (47) & TJG (49)	Sectioning & hole drilling &EDM	15	33.33			542	0.8			x	x
Leggatt (43, 46)	Sectioning & hole drilling	15.5	19.70			540	0.56-1.0	x	x		x
Leggatt (43, 46)	Sectioning & hole drilling	15.5	19.70			540	0.56-1.0	x	x		
Holden et al (44)	Neutron diffraction	16	25.56			448					x
Scaramangas & PG (47) & TJG (49)	Sectioning & hole drilling &EDM	19.5	25.64			527	0.8			x	x
Jonsson et al. (50)	Hole drilling	20	8.80			360	1.5-1.88				
Jonsson et al. (50)	Hole drilling	20	8.80			360	0.58-2.99	x	x		
Ritchie & Leggatt (40)	Slotting & hole drilling	25.4	14.98			430	0.35-0.49			x	x
Fidler (42)	Trepanning	33	8.03		x	2¼Cr 1Mo	MMA	x	x		
Fidler (42)	Trepanning	33	8.03	x		2¼Cr 1Mo	MMA	x	x		
Ueda et al. (51)	Sectioning	50	8.75			784		x	x	x	x
Ueda et al. (51)	Sectioning	50	8.75			784		x	x	x	x
Ueda & Nakacho [14]		50			x	225-275	SAW	x	x	x	x
Ueda & Nakacho [14]		50			x	225-275	SAW	x	x	x	x
Fidler (41)	Trepanning	84	2.37			2¼Cr 1Mo	MMA	x	x	x	x
TJG (49) from	FE Result	4.6	34.80			270	0.35			x	
Scaramangas & PG (47)	FE Result	8.6	6.20			270	0.85			x	

Table 3: Pipe-Butt Welds

Reference	Measurement Method	Plate thickness (mm)	R/t	Heat treatment		Proof stress (MPa)	Heat input (KJ/mm)	Residual stress direction relative to weld bead			
				Yes	No			Surface Parallel	Surface Transverse	Thro' Thickness Parallel	Thro' Thickness Transverse
Ueda et al (51)	Sectioning	50	14.00		x	784		x	x	x	x
Mitchell (52)	Hole drilling	85	6.94		x	345		x	x	x	x

Table 4: Pipe-Seam Welds

Reference	Measurement Method	Plate thickness	Heat treatment		Boundary Restraint		Proof stress	Heat input	Residual stress direction relative to weld bead			
		(mm)	Yes	No	Yes	No	(MPa)	(KJ/mm)	Surface Parallel	Surface Transverse	Thro' Thickness Parallel	Thro' Thickness Transverse
Leggatt (54)	Hole drilling & block removal	50		x	sb		515	1.0-1.7	x	x		
Leggatt (54)	Hole drilling & block removal	75		x		x	436	2.3-5.8	x	x		
Leggatt (54)	Hole drilling & block removal	75		x	sb		497	1.2-2.8	x	x		
Leggatt (54)	Hole drilling & block removal	75		x	sb		515	1.2-1.6	x	x	x	x
Leggatt (54)	Hole drilling & block removal	75		x	sb		515	1.3-1.5	x	x		
Lidbury (21) Babcock & Wilcox	X ray diffraction	76.2		x	sb		590				x	
Leggatt (54)	Hole drilling & block removal	95		x	sb		517	1.1-1.6	x	x		
Leggatt (54)	Hole drilling & block removal	105		x	sb		714	1.2-2.0	x	x		
Hepworth (53)	Centre hole drilling	125		x			650		x	x		
Hepworth (53)	Centre hole drilling	125		x			650		x	x		
Hepworth (53)	Centre hole drilling	125		x			650		x	x		
Hepworth (53)	Centre hole drilling	125		x			650		x	x		
Hepworth (53)	Centre hole drilling	125	x				650		x	x		
Hepworth (53)	Centre hole drilling	125	x				650		x	x		
Bryan et al (58)	Hole drilling	152.4 (nom)		x		x	500-570		x	x	x	x
Bryan et al (58)	Hole drilling	152.4 (nom)		x		x	500-570			x		x
Bryan et al (58)	Hole drilling	152.4 (nom)		x		x	500-570					
Bryan et al (58)	Hole drilling	152.4 (nom)		x		x	500-570					
Bryan et al (58)	Hole drilling	152.4 (nom)		x		x	500-570					
Bryan et al (58)	Hole drilling	152.4 (nom)		x		x	500-570					

Table 5: Repair Welds

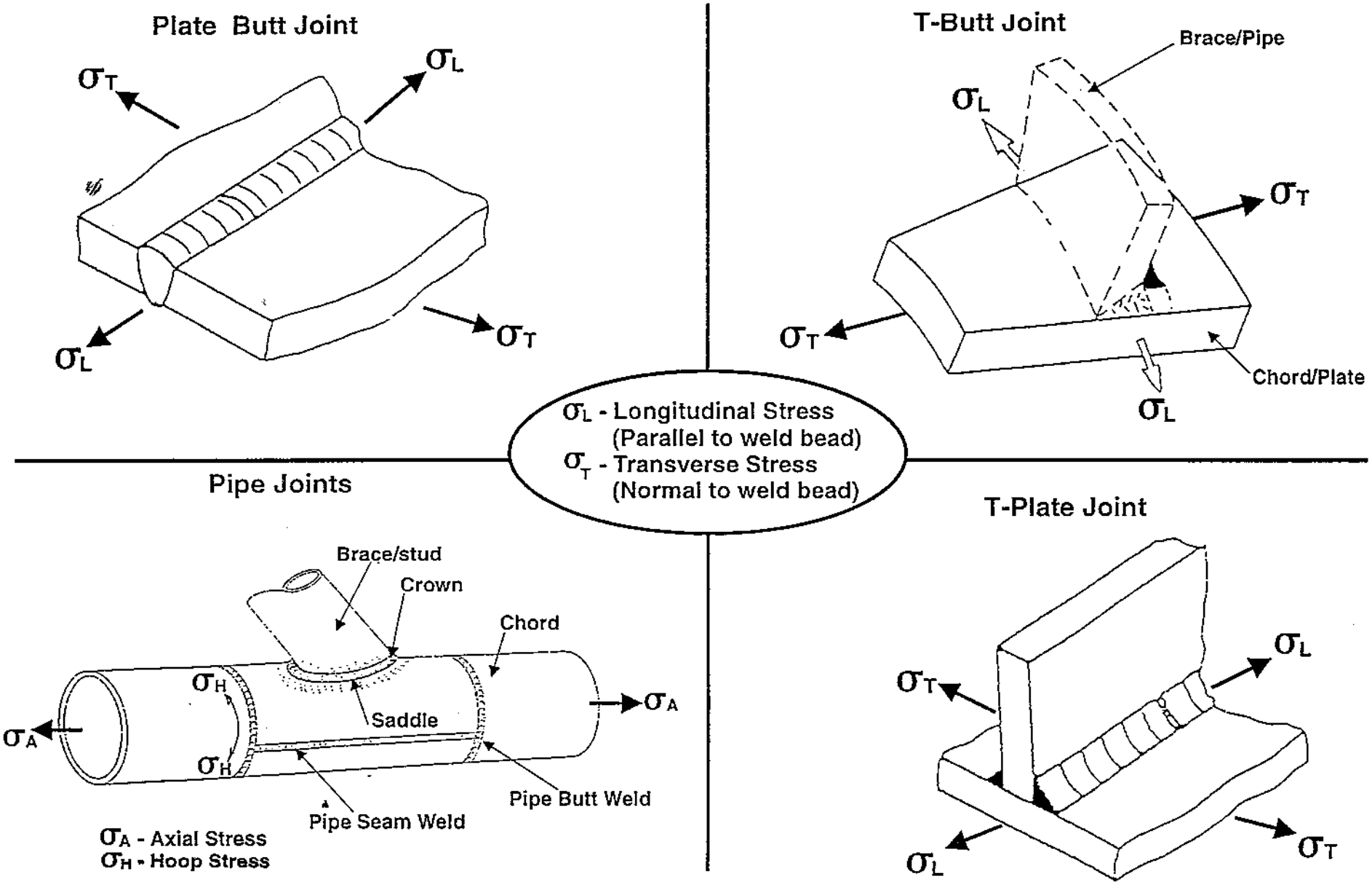

FIGURE 1: Schematic Diagrams of Welded Joint Types Showing Direction of Stresses

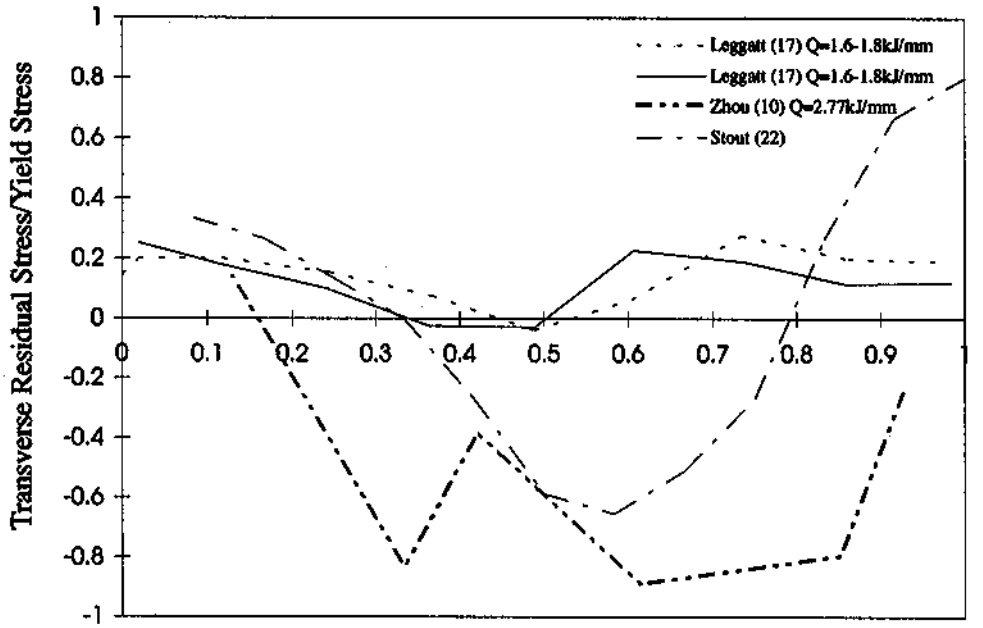

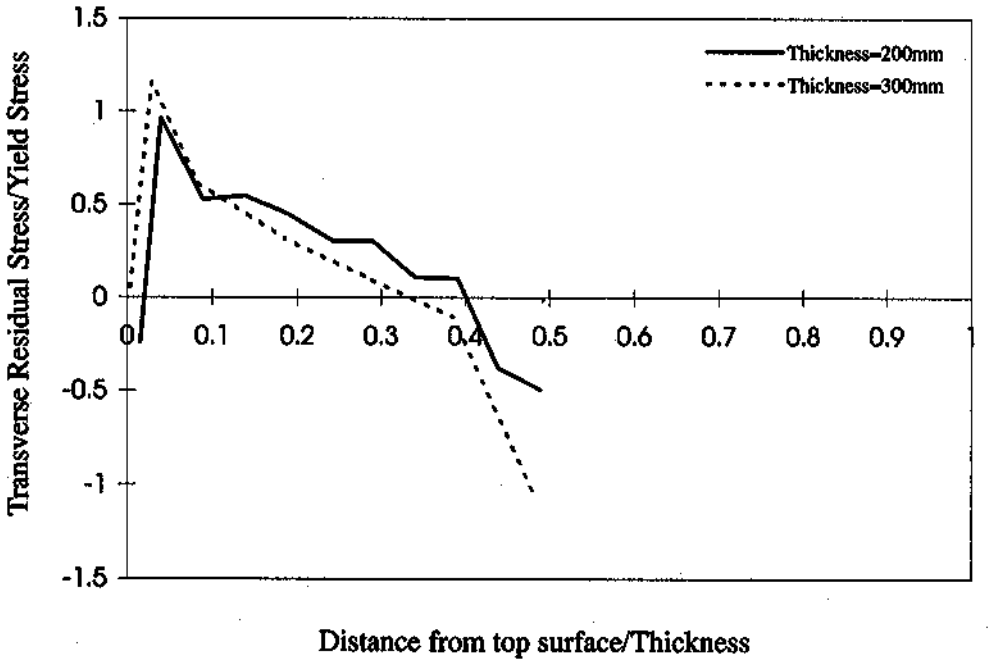

Figure 2 Comparison of through thickness transverse residual stresses in plate butt welds (19)

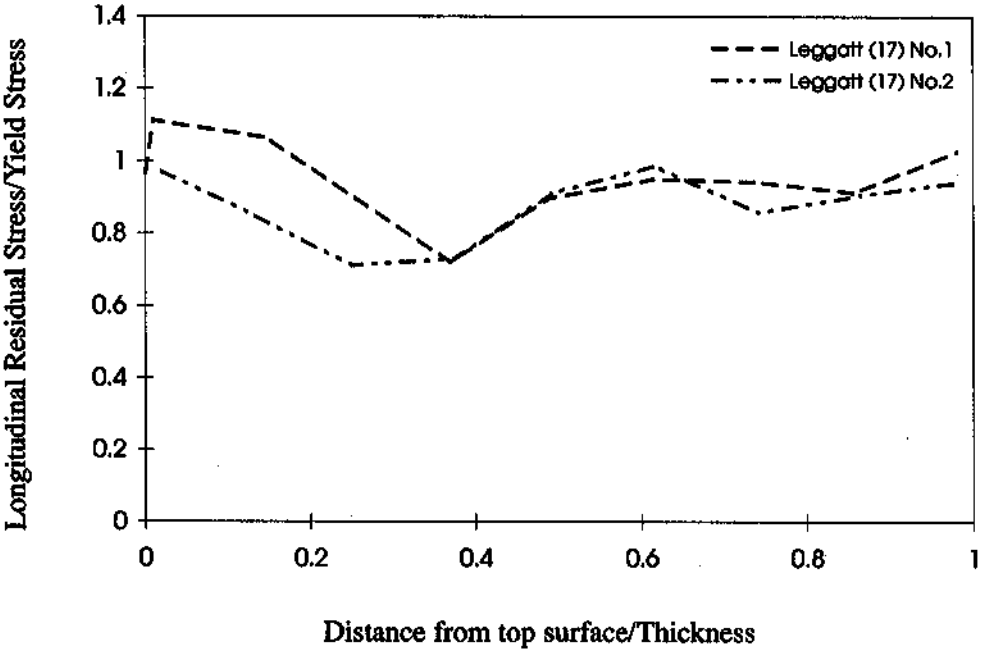

Figure 3 Through thickness longitudinal stresses in plate butt weld (17)

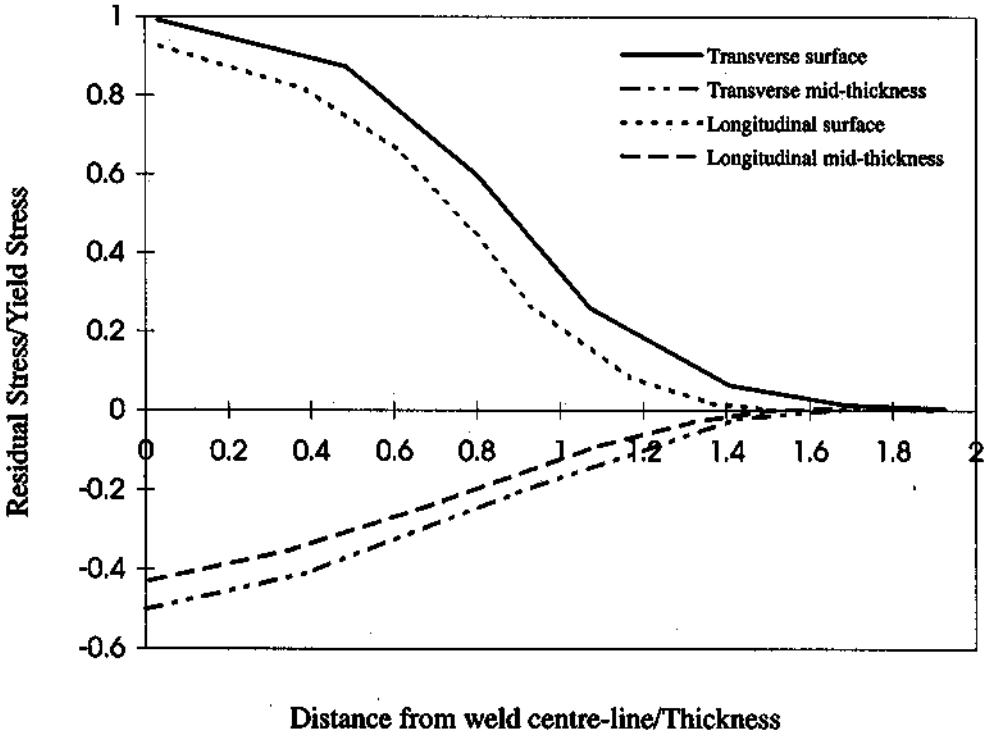

Figure 4 Predicted as-welded stresses for heavy plate butt welds (11)

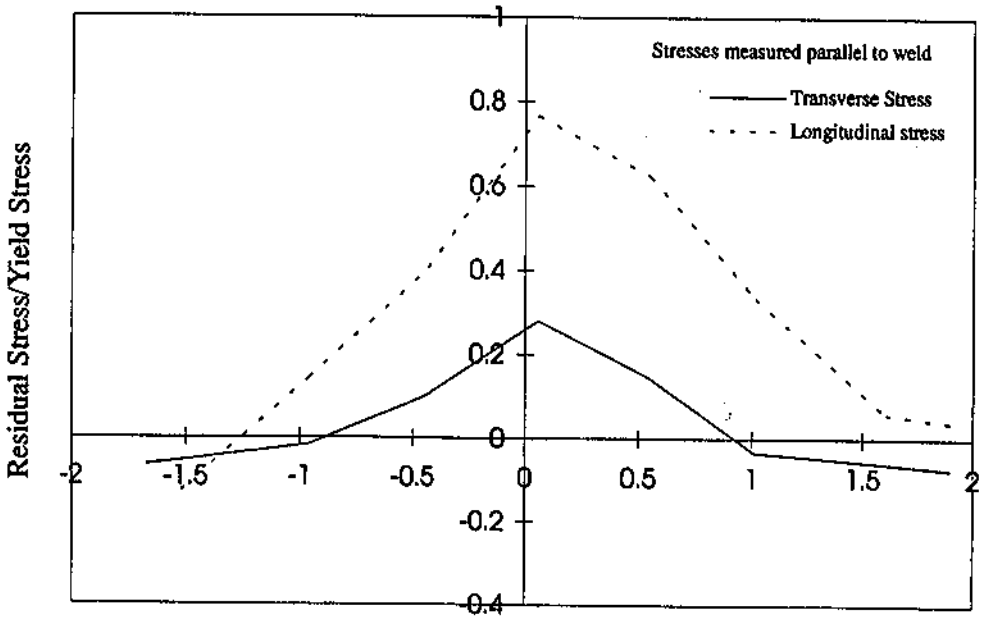

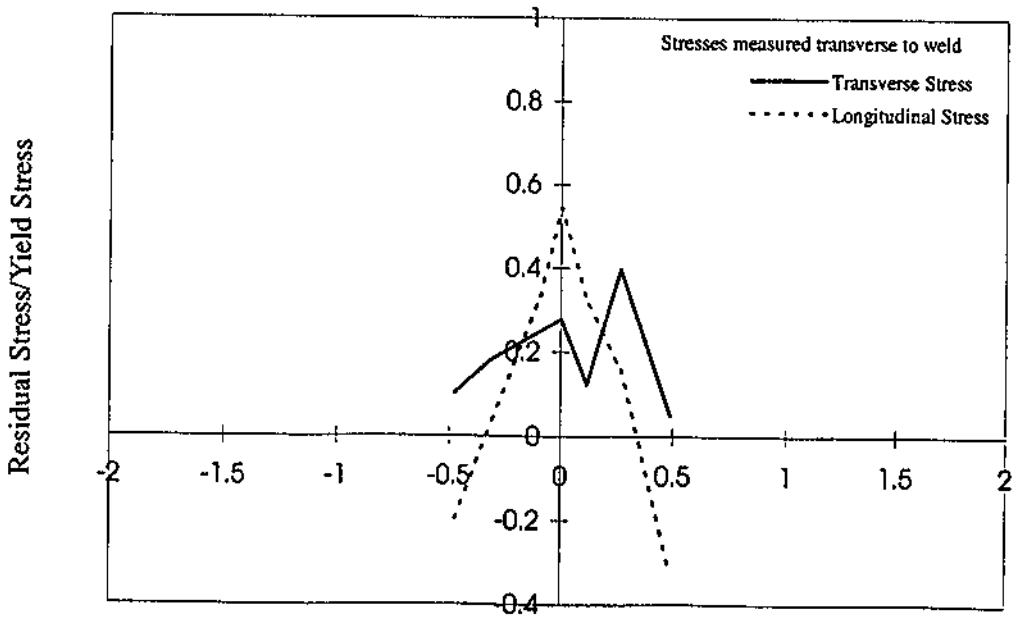

Figure 5 Surface residual stresses measured transverse and parallel to weld bead for A543 pressure vessel steel plate butt welded (10)

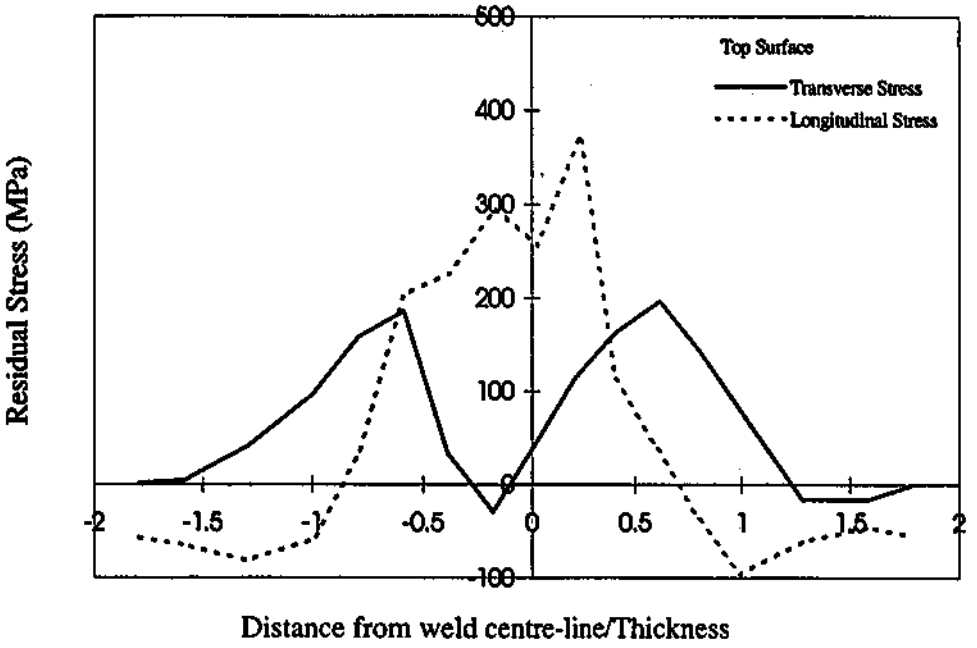

Figure 6 Top surface residual stresses in a multi-pass butt welded plate (SS41, 50mm thick) (14)

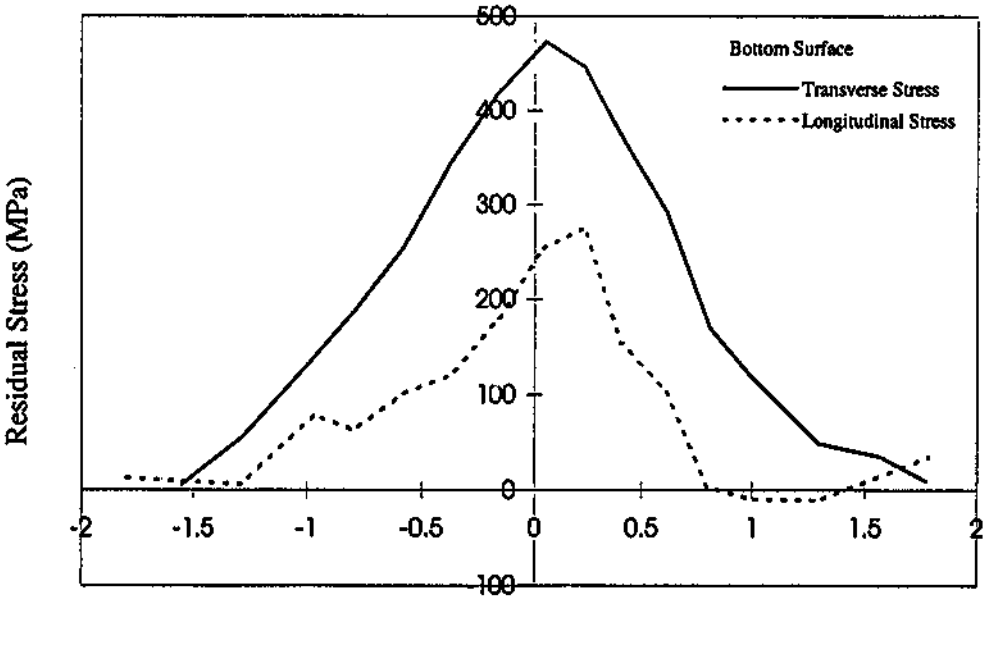

Figure 7 Bottom surface residual stresses in a multi-pass butt welded plate (SS41, 50mm thick) (14)

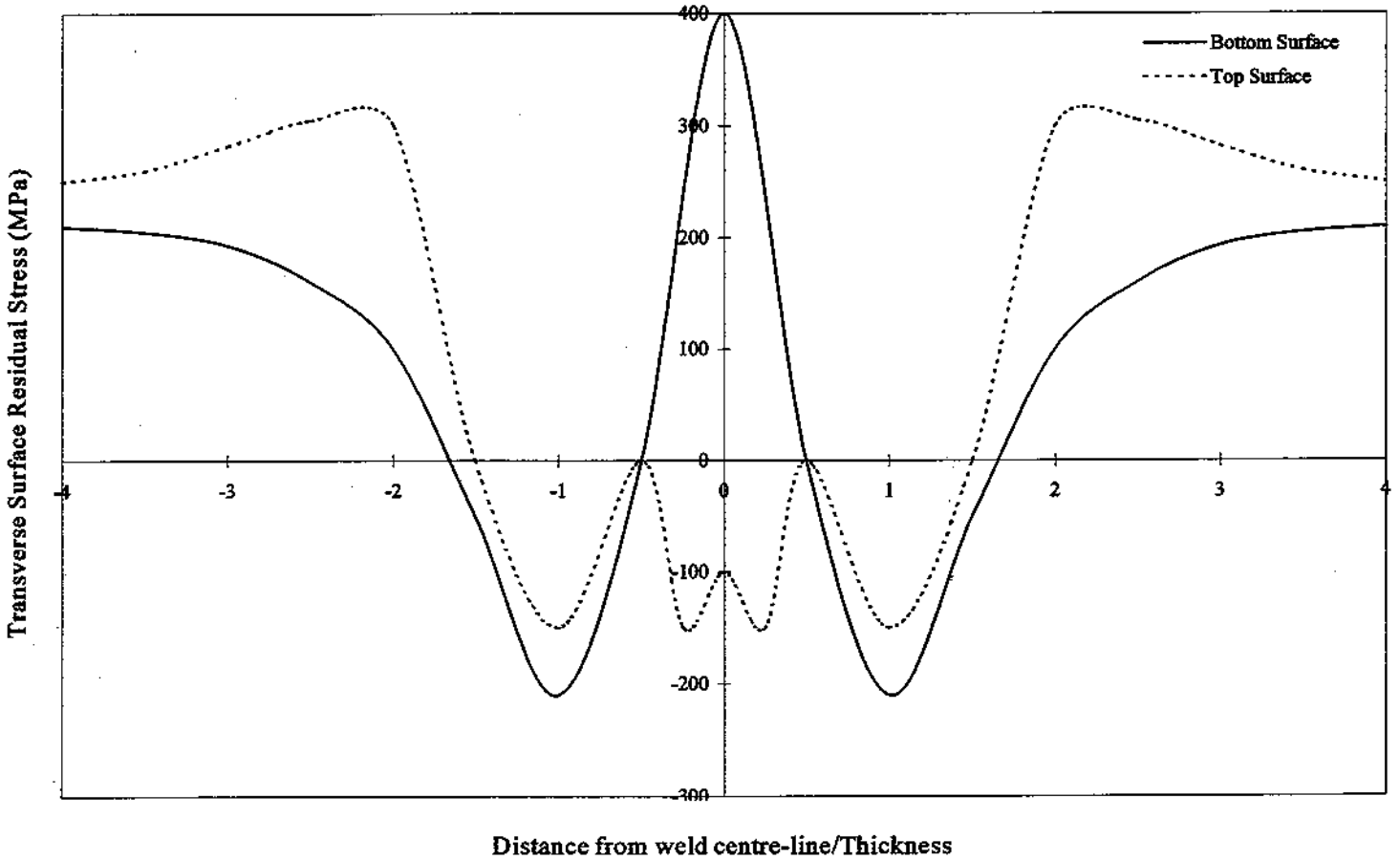

Figure 8 Transverse residual stress distribution for plate welded joint (18)

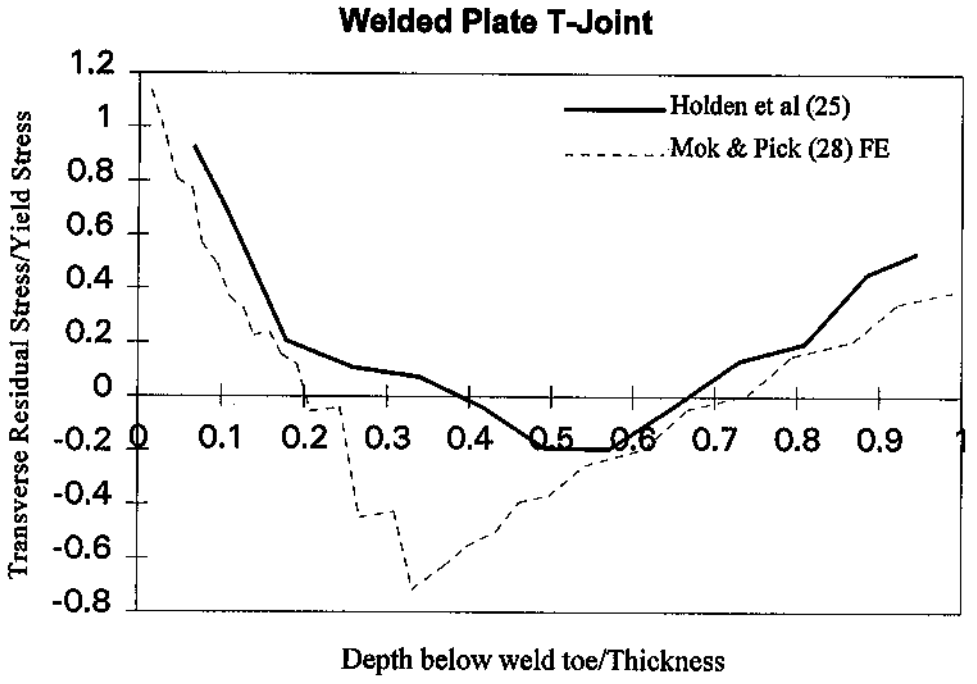

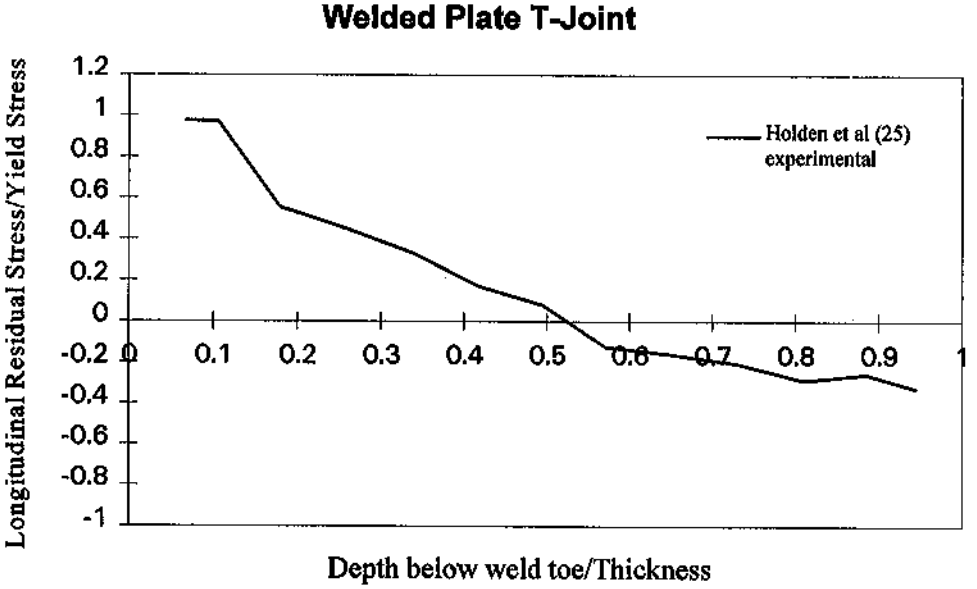

Figure 9 Through thickness residual stresses in T-Butt joint (25 & 28)

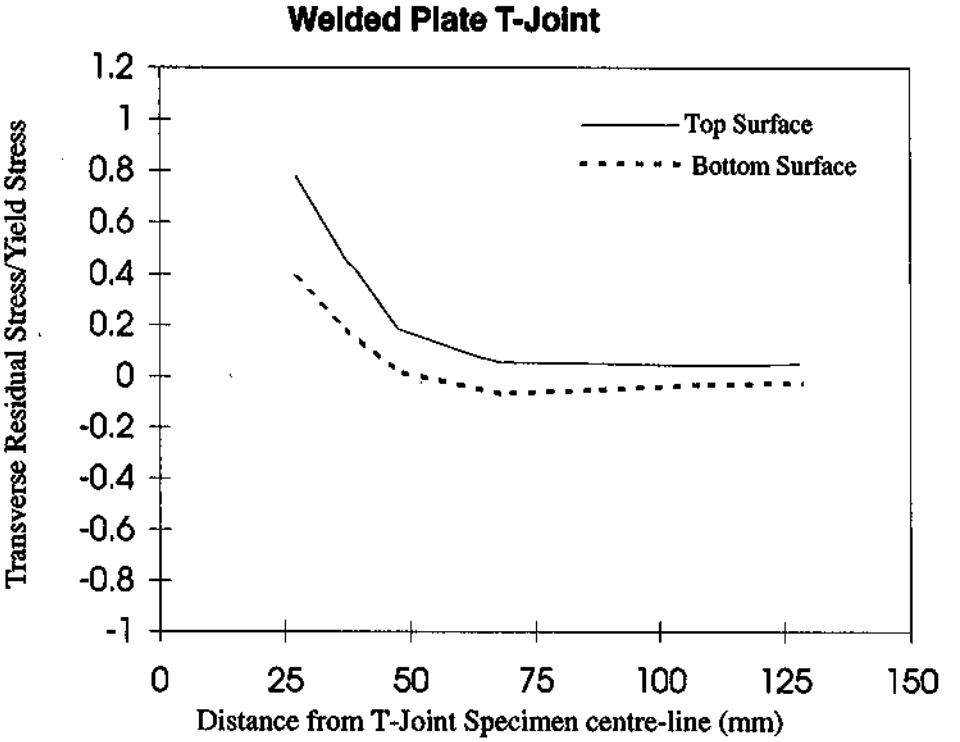

Figure 10 Transverse surface stresses (derived from FE) in T-butt joint (28)

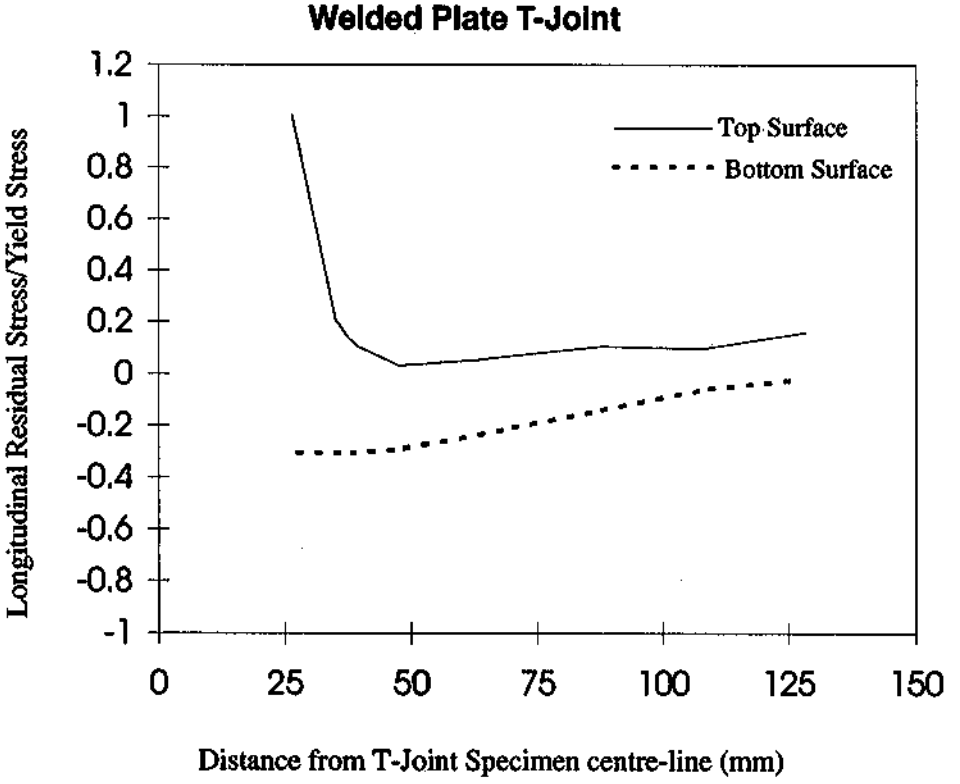

Figure 11 Longitudinal surface stresses (derived from FE) in T-butt joint (28)

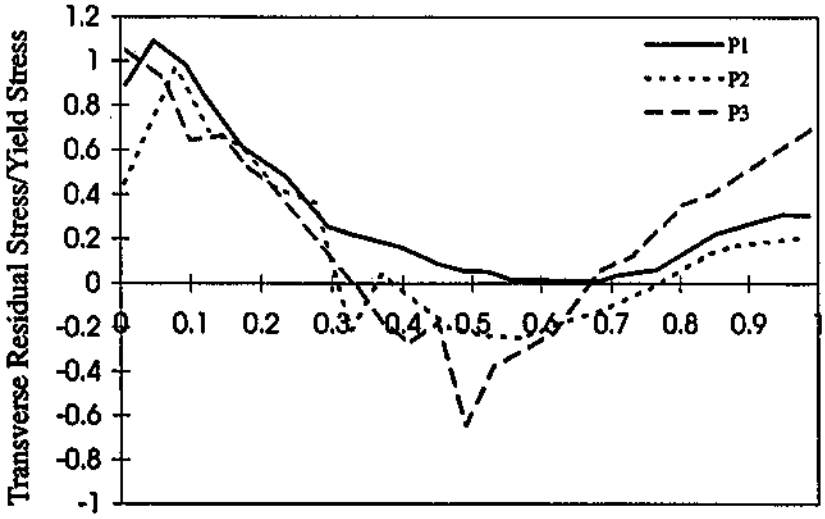

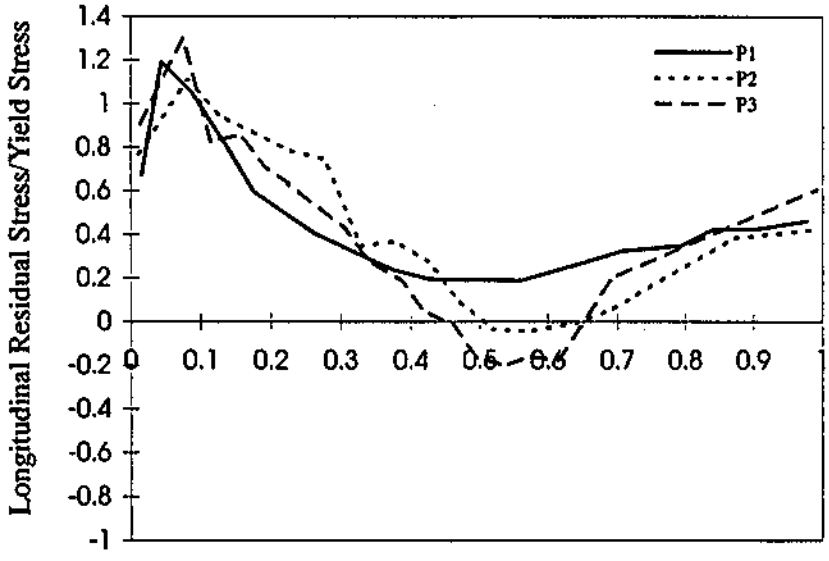

Specimen	Pipe diameter x thickness	Yield Stress (MPa)	Weld	
			Passes	Heat input
P1	1200 x 22 mm	420	7	1.41 KJ/mm
P2	1230 x 40 mm	375	16	1.80 KJ/mm
P3	1230 x 50 mm	360	24	1.98 KJ/mm

Geometry of Pipe on Plate Specimens

Figure 12 Through thickness residual stresses in Pipe on Plate specimens (31)

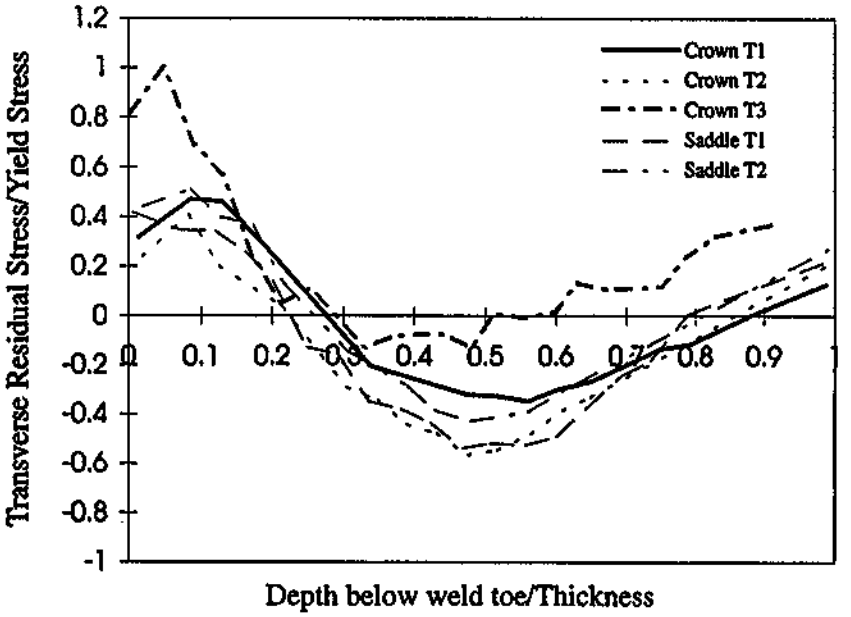

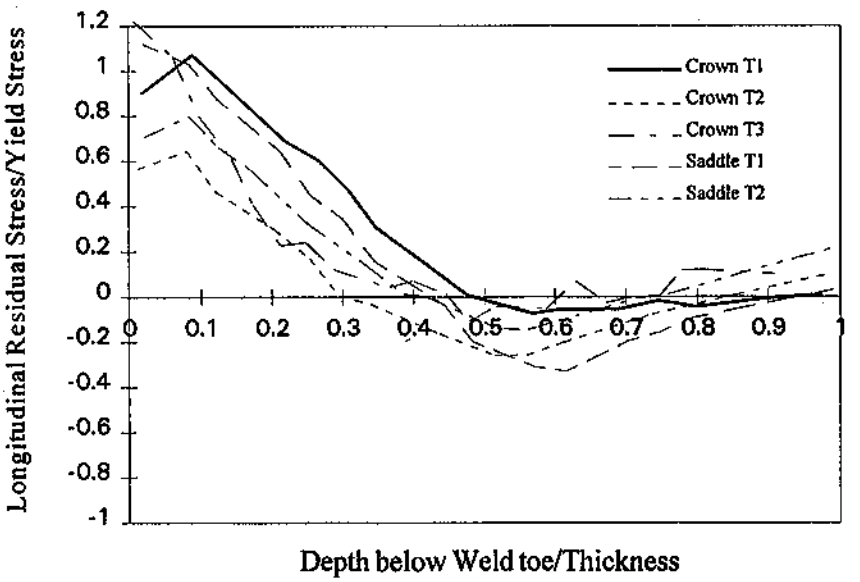

Specimen	Chord Diameter x thickness	Brace Diameter x thickness	Yield Stress MPa
T1	915 x 22 mm	610 x 16 mm	488
T2	915 x 22 mm	455 x 11 mm	491
T3	915 x 36 mm	610 x 14 mm	365

Geometry of T Tubular Joints

Figure 13 Through thickness residual stresses in T Tubular joints (30)

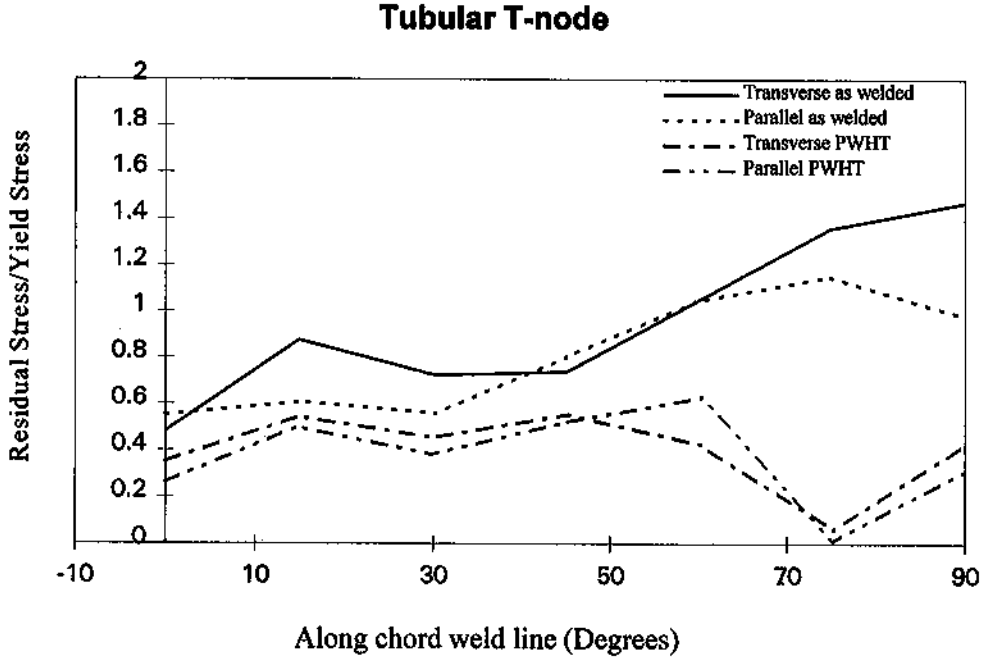

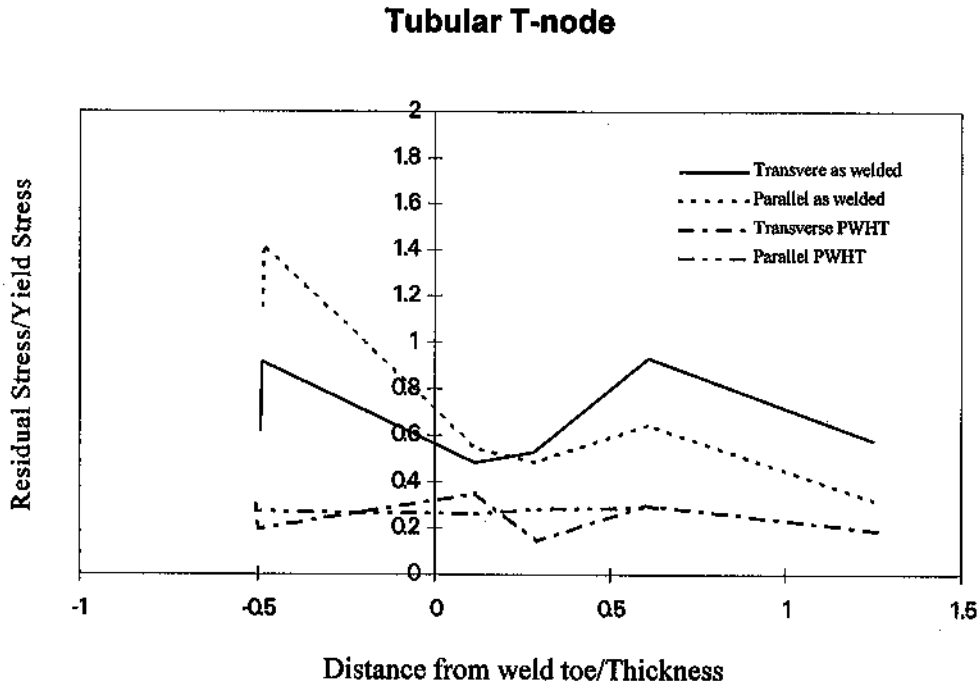

Figure 14 Surface residual stresses measured at chord of a T tubular joint (32)

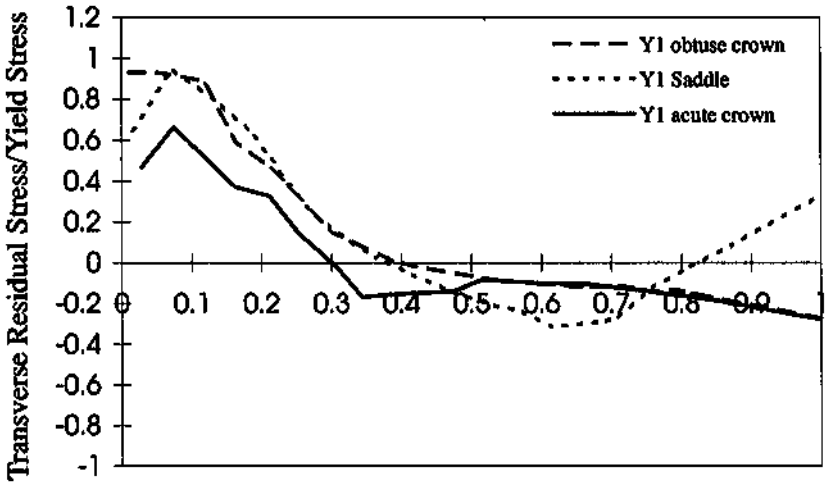

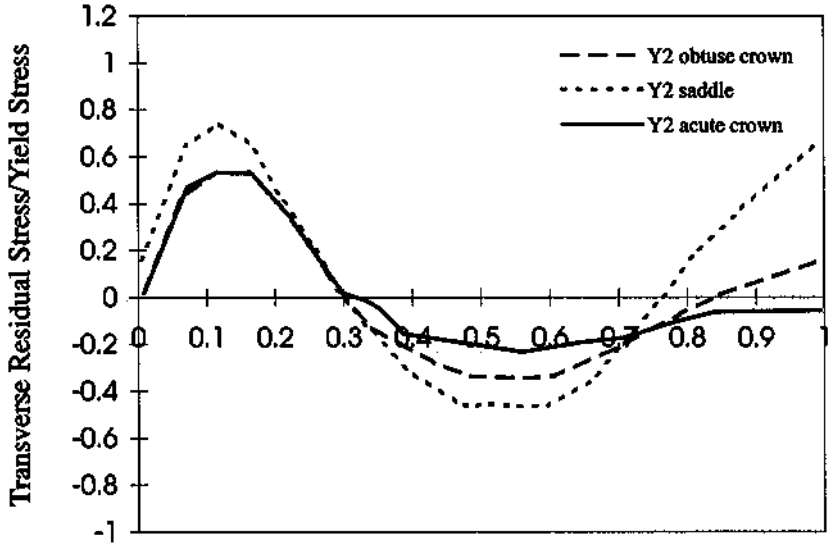

Specimen	Chord diameter x thickness	Brace diameter x thickness	Weld	
			Passes	Heat in KJ/mm
Y1	920 x 22 mm	610 x 14 mm @ 70°	6	1.83
Y2	920 x 22 mm	460 x 11 mm @ 45°	4	1.15

Geometry of Y Tubular joints

Figure 15 Through thickness transverse residual stresses in Y tubular joints (35)

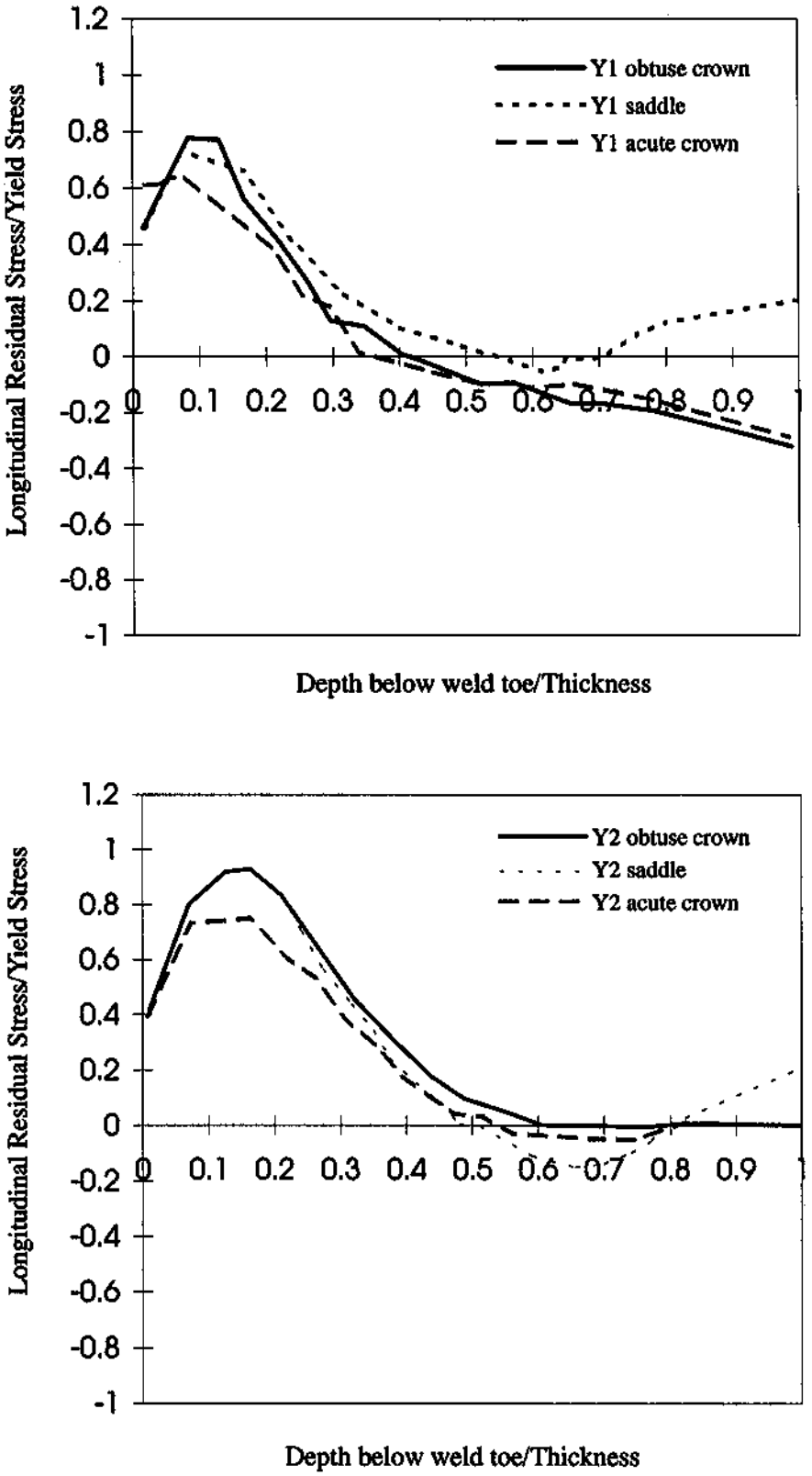

Figure 16 Through thickness longitudinal residual stresses in Y tubular joints (35)

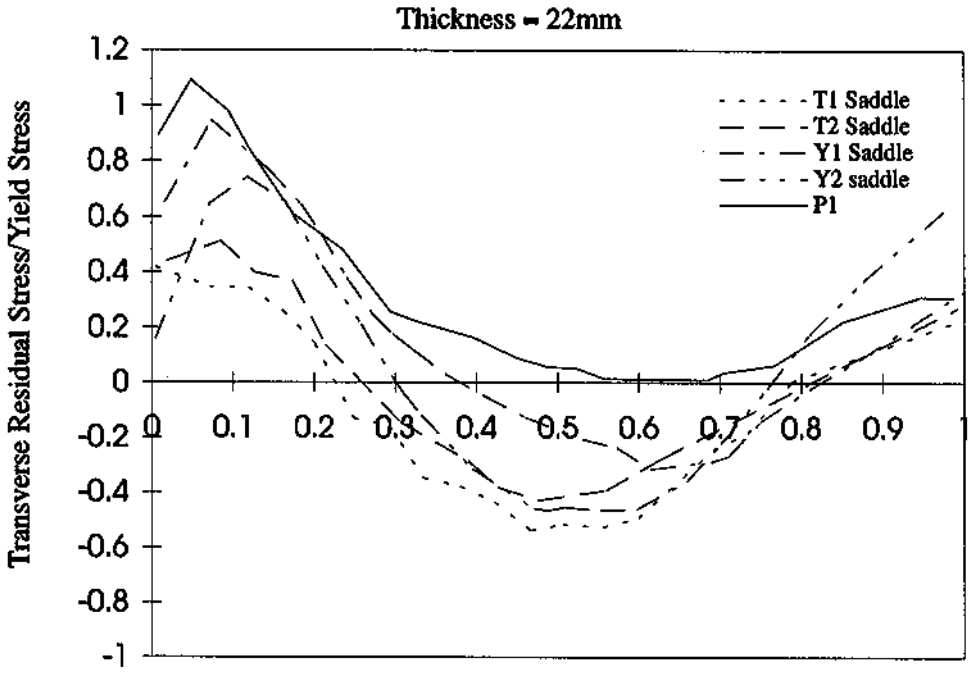

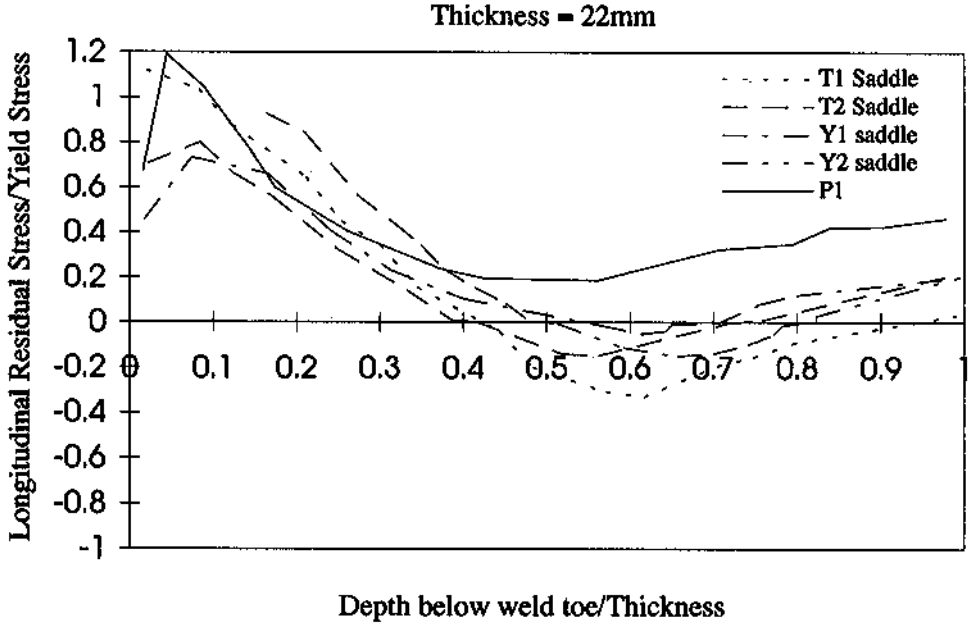

Figure 17 Comparison of through thickness residual stresses in Tubular butt welds (27 & 29)

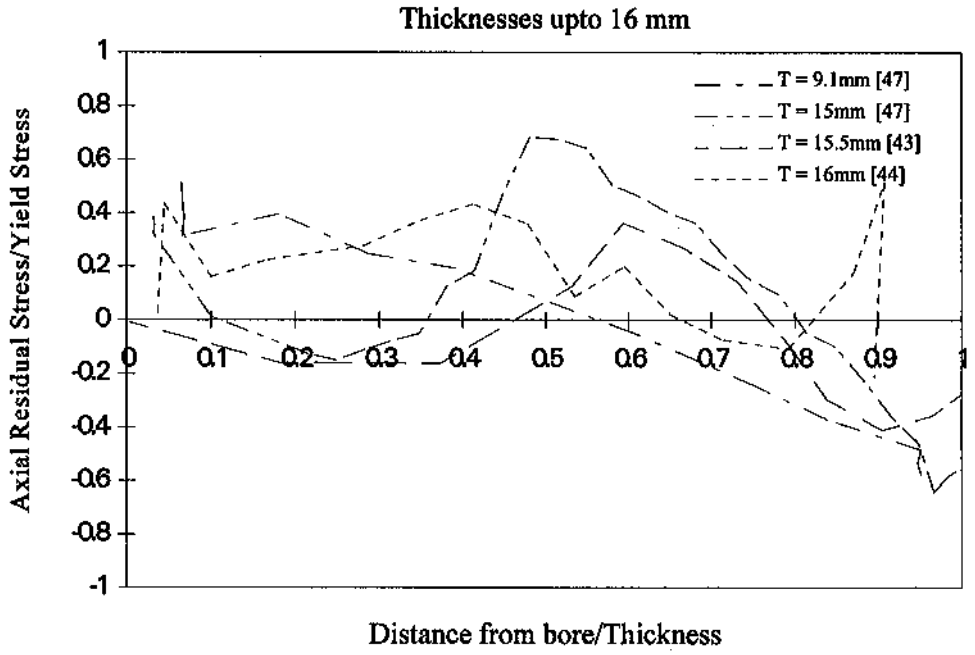

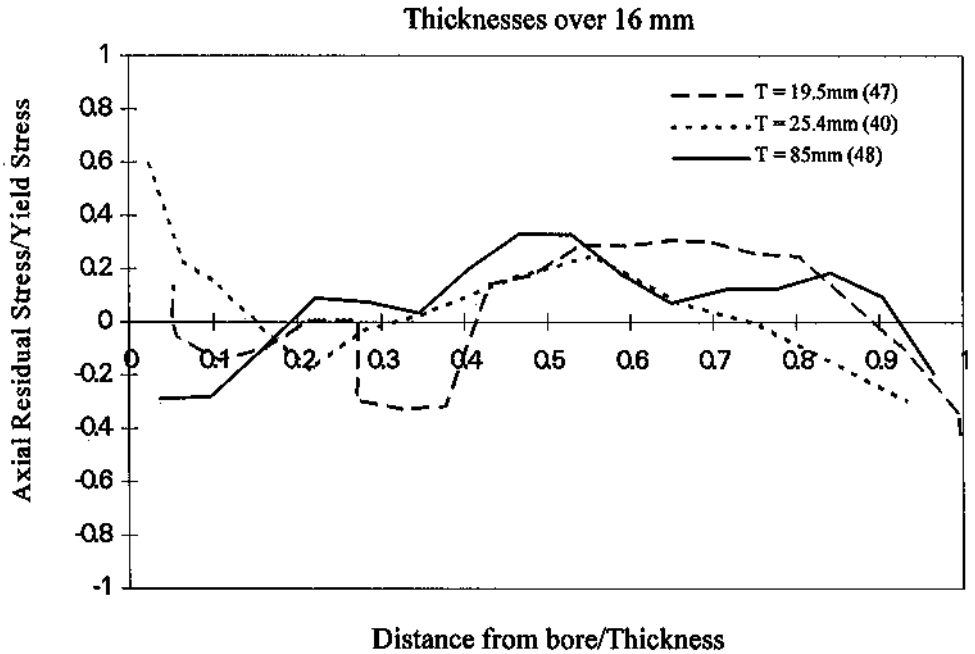

Figure 18 Comparison of through thickness axial residual stress distributions in pipe butt welds

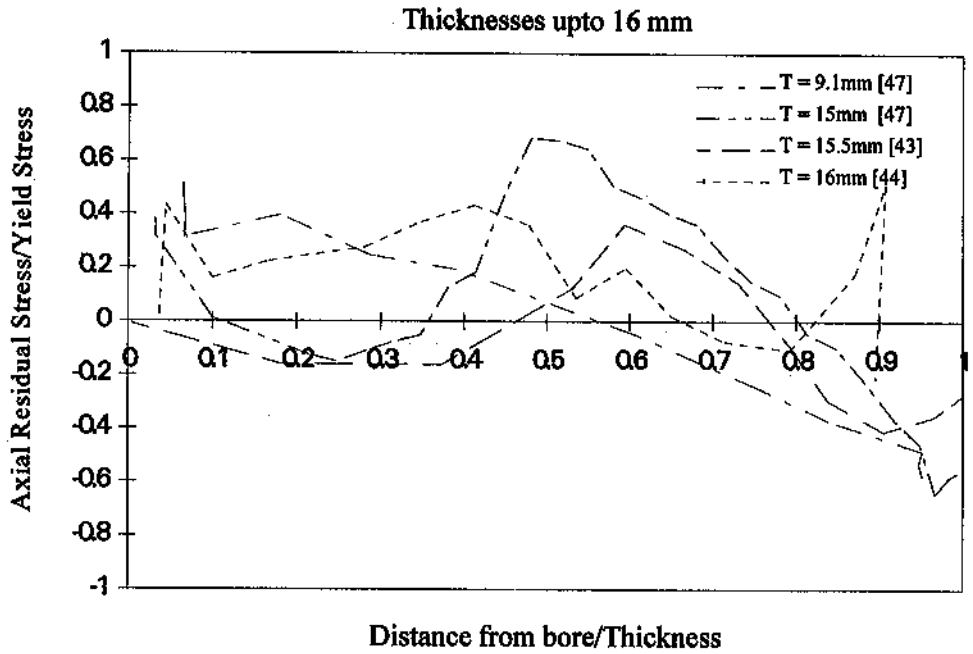

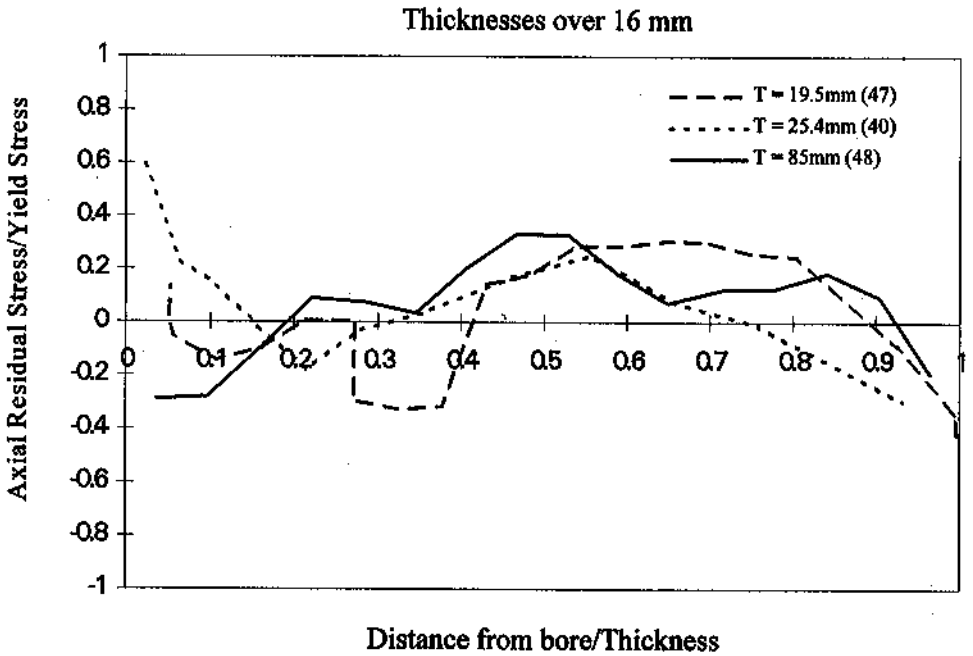

Figure 19 Comparison of through thickness axial residual stress distributions in pipe butt welds

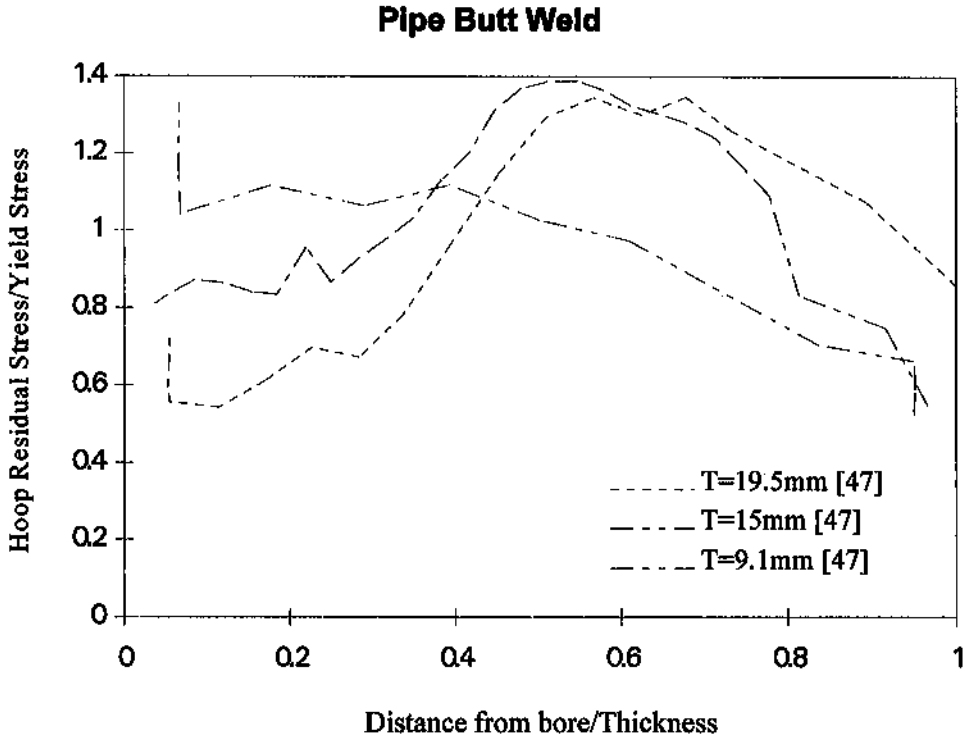

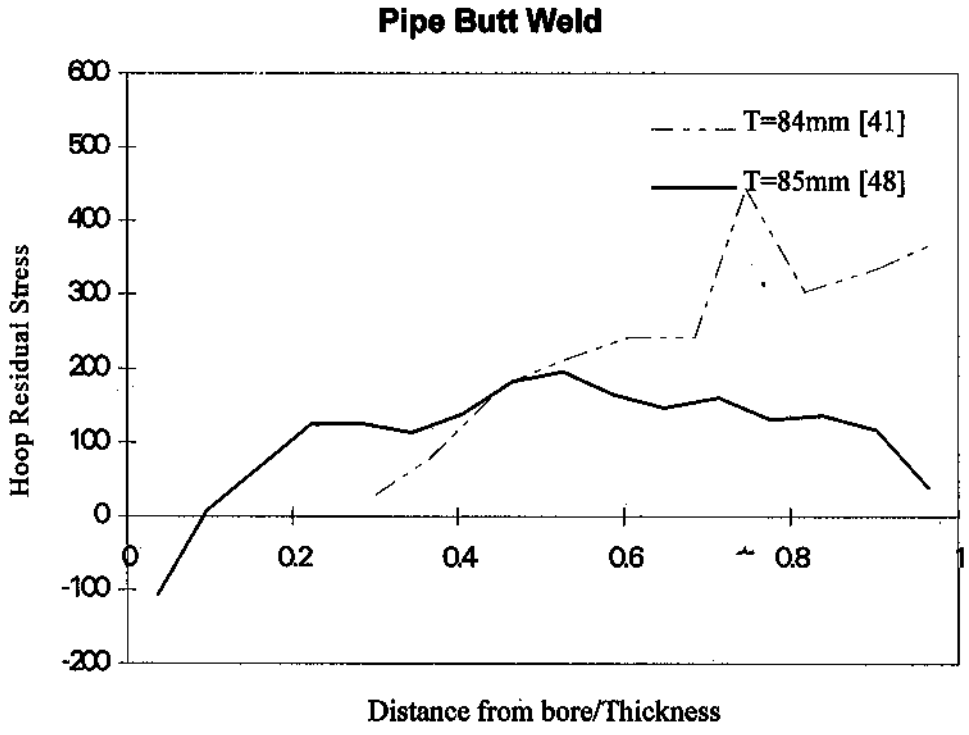

Figure 20 Comparison of through thickness hoop residual stress distributions in pipe butt welds (41 & 48)

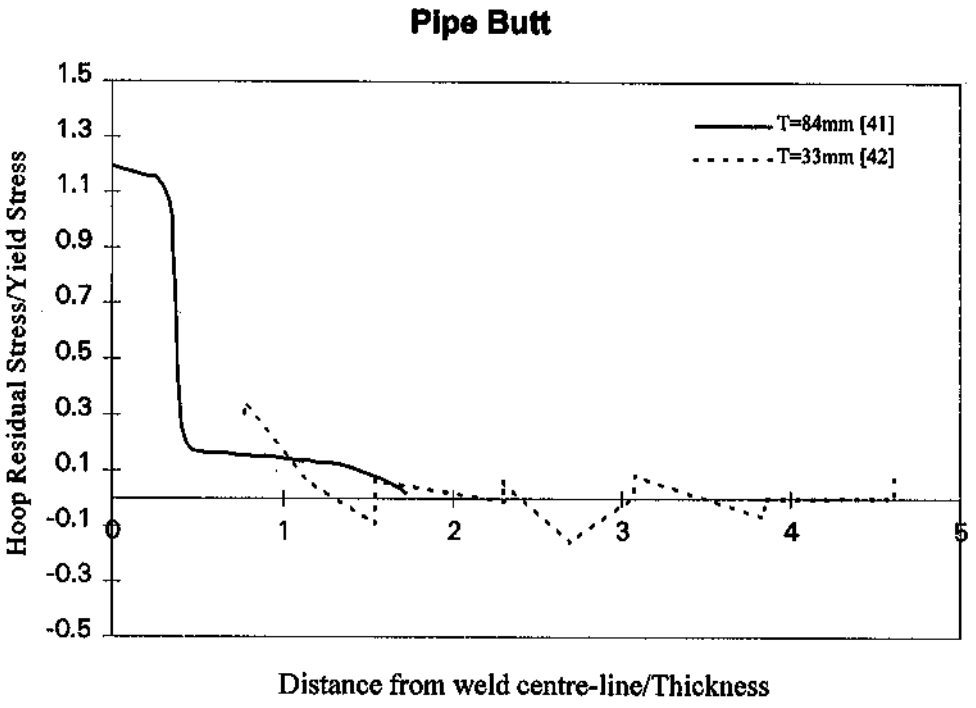

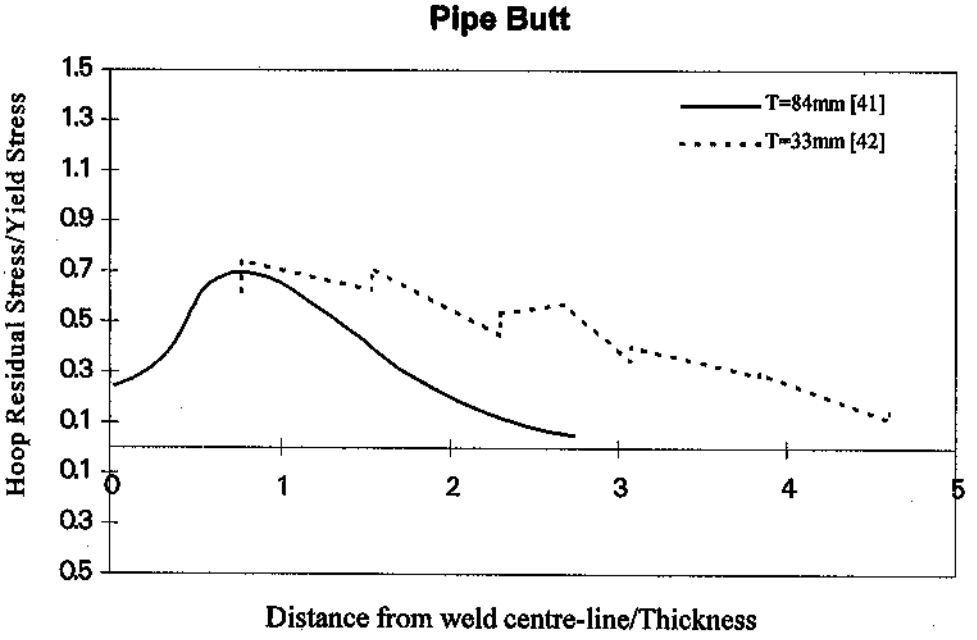

Figure 21 Comparison of surface residual stresses in pipe butt welds (41 & 42)

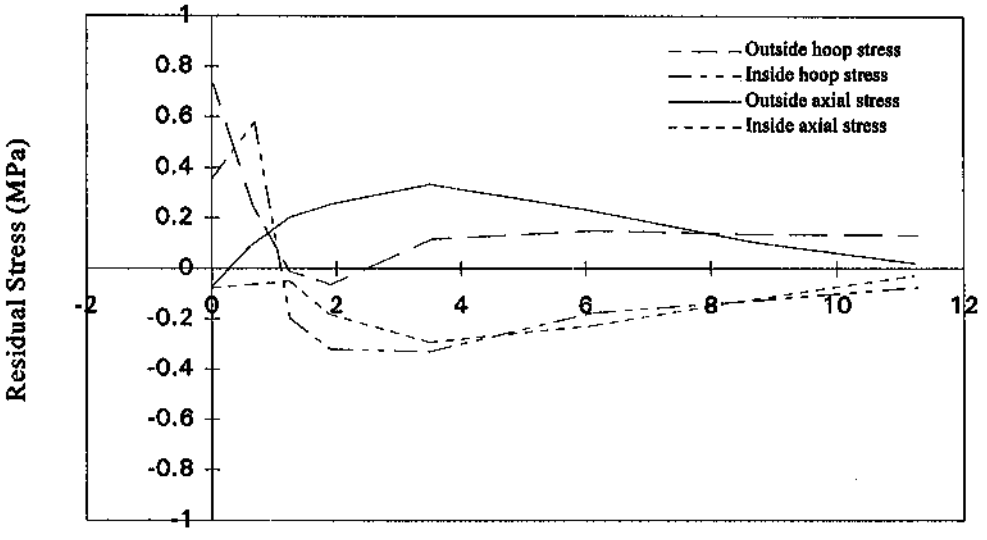

Figure 22 Surface residual Stress in a pipe butt weld (43)

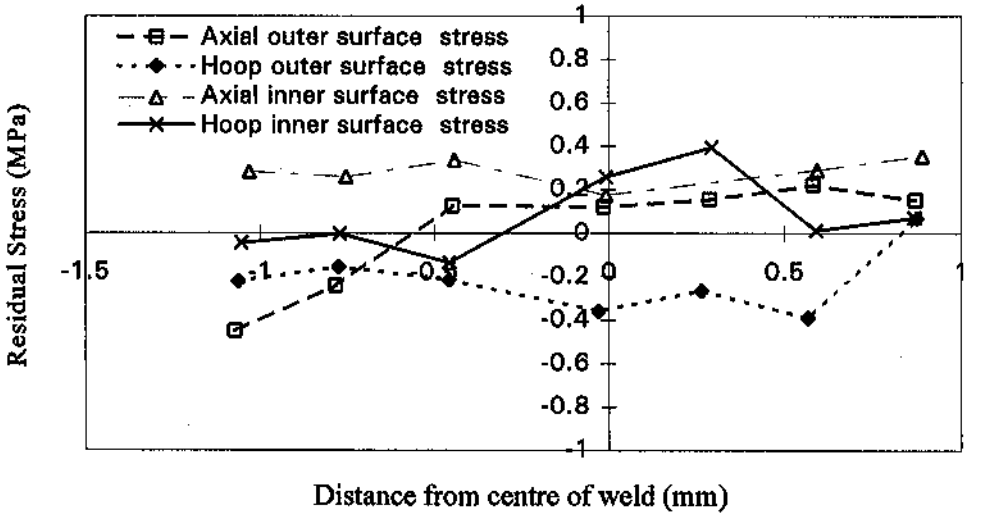

Figure 23 Surface residual stresses in a pipe butt weld (14)

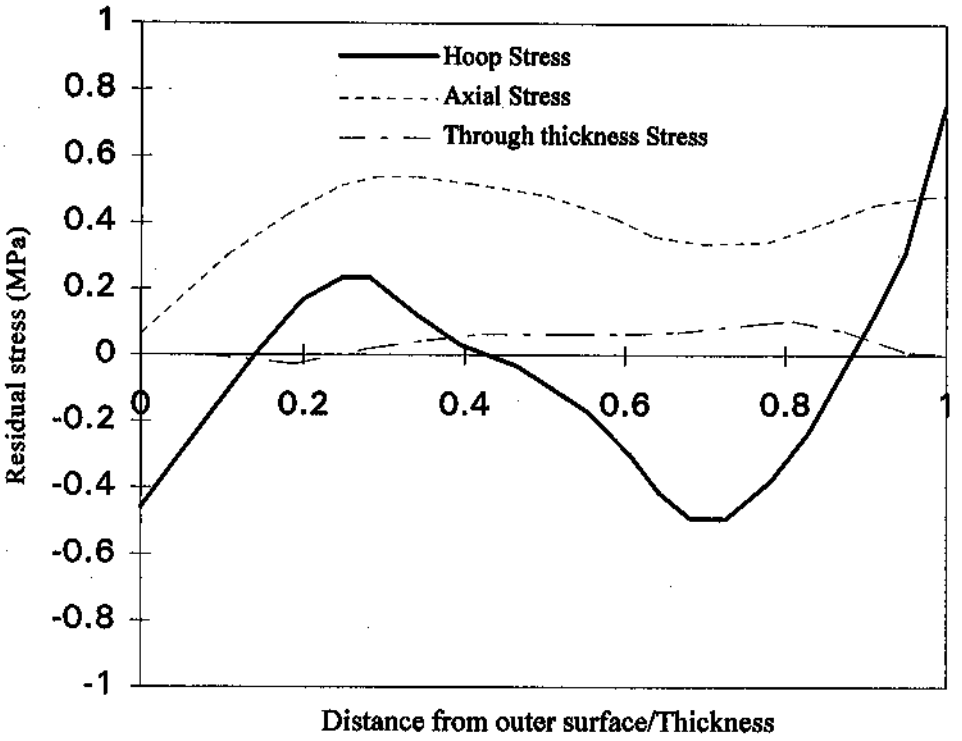

Figure 24a Through thickness residual stresses in longitudinal seam welds (14)

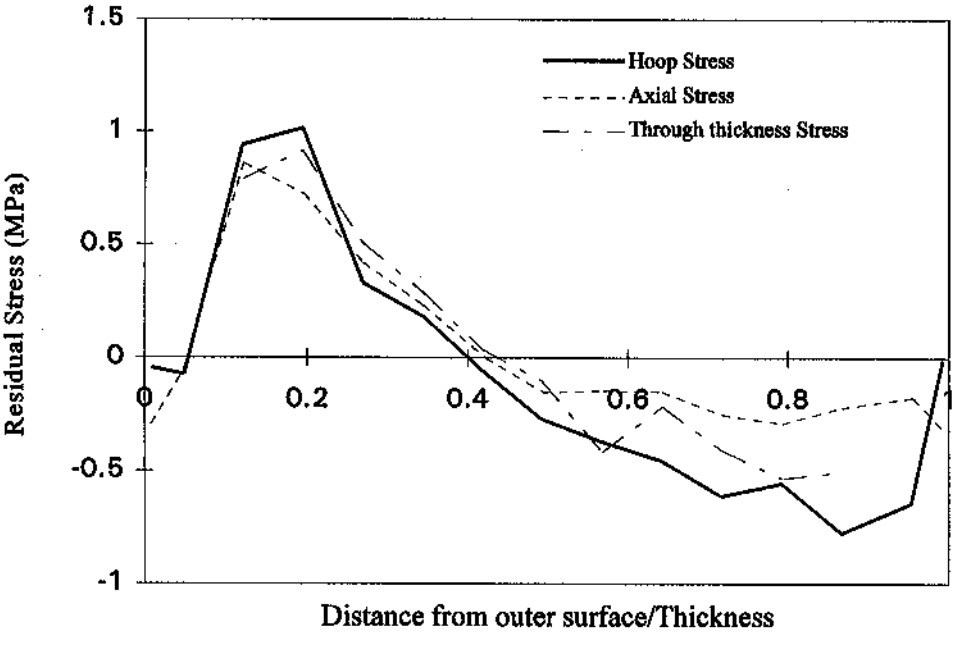

Figure 24b Comparison of through thickness residual stresses in longitudinal (seam) welds (52)

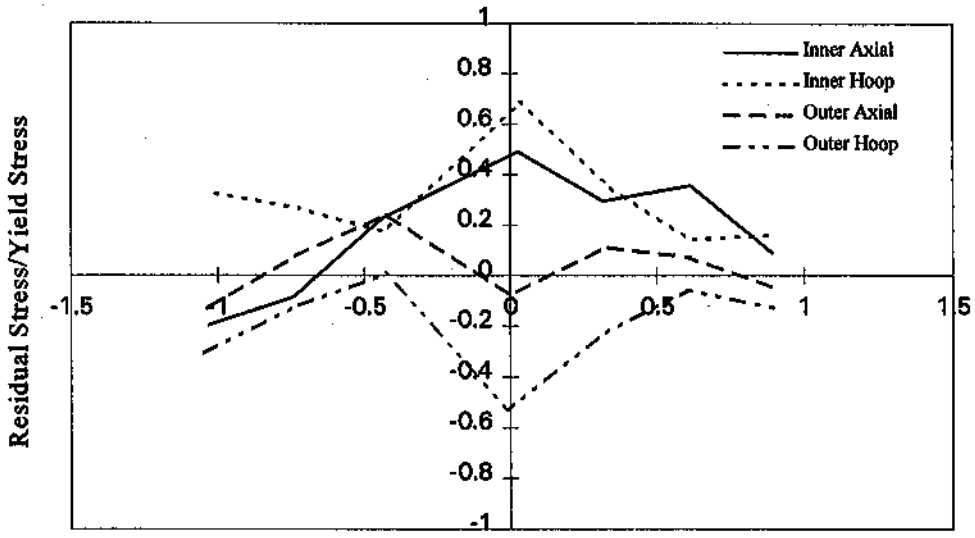

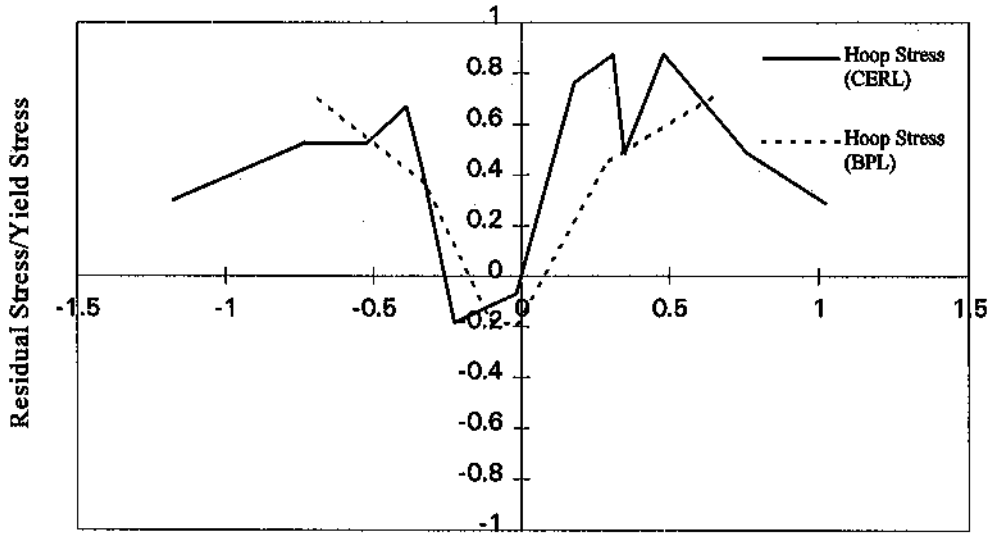

Figure 25 Comparison of surface residual stresses in longitudinal (seam) welds (51)

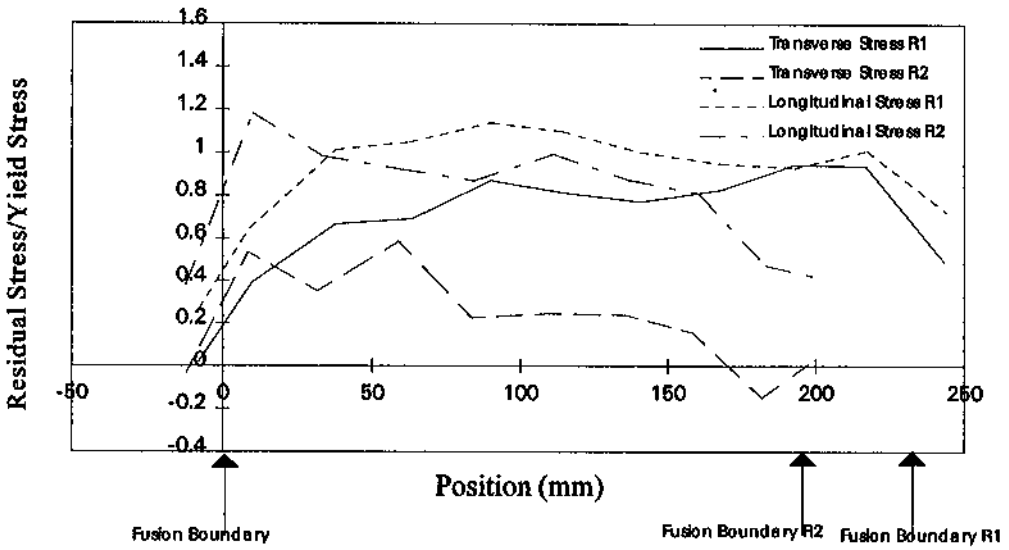

Figure 26 Surface Residual Stresses Measured Parallel to the Welding Direction along the central weld bead (53)

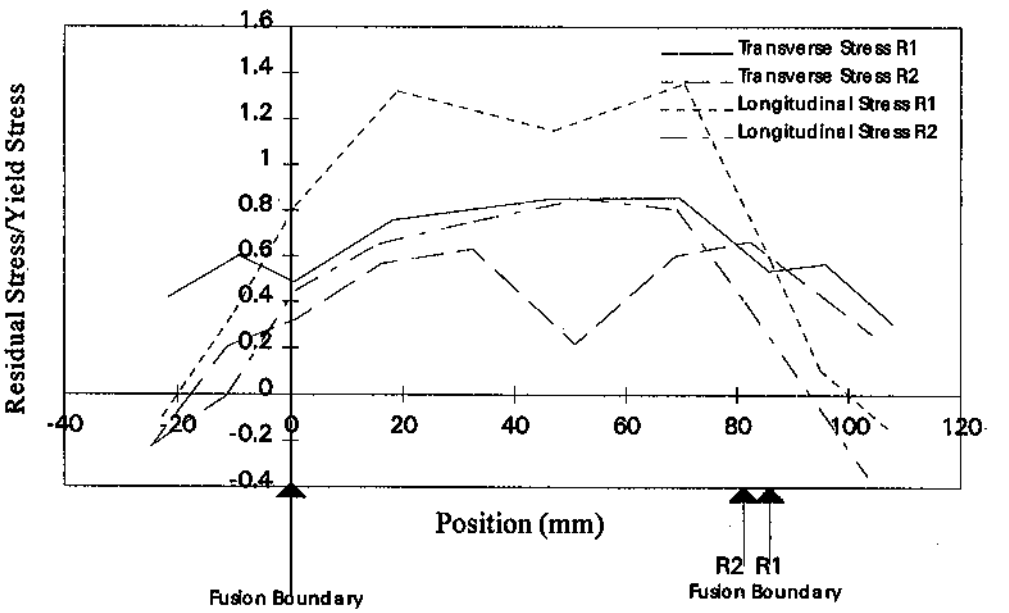

Figure 27 Surface Residual Stresses Measured Normal to the Welding Direction (53)

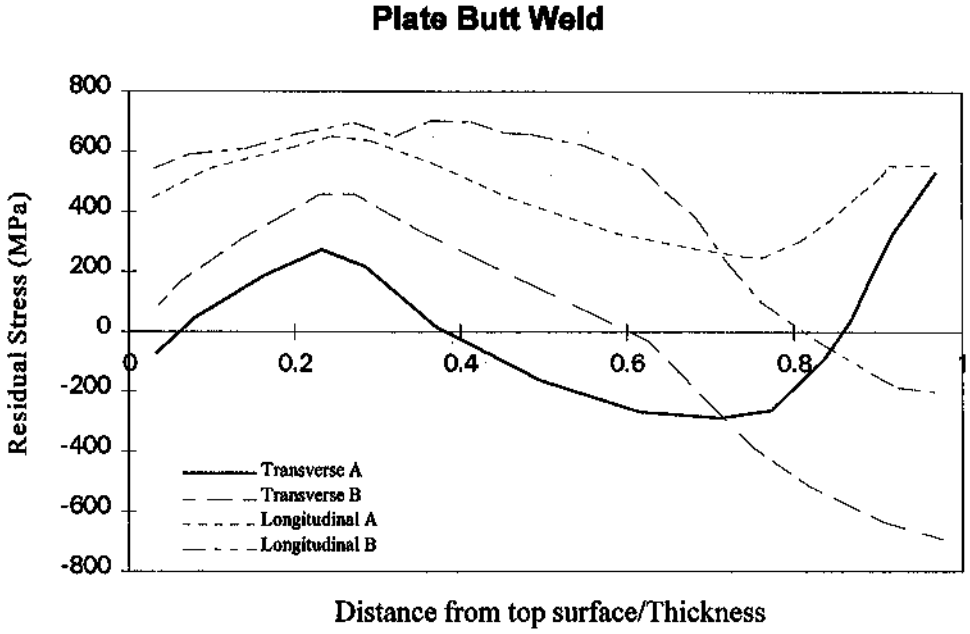

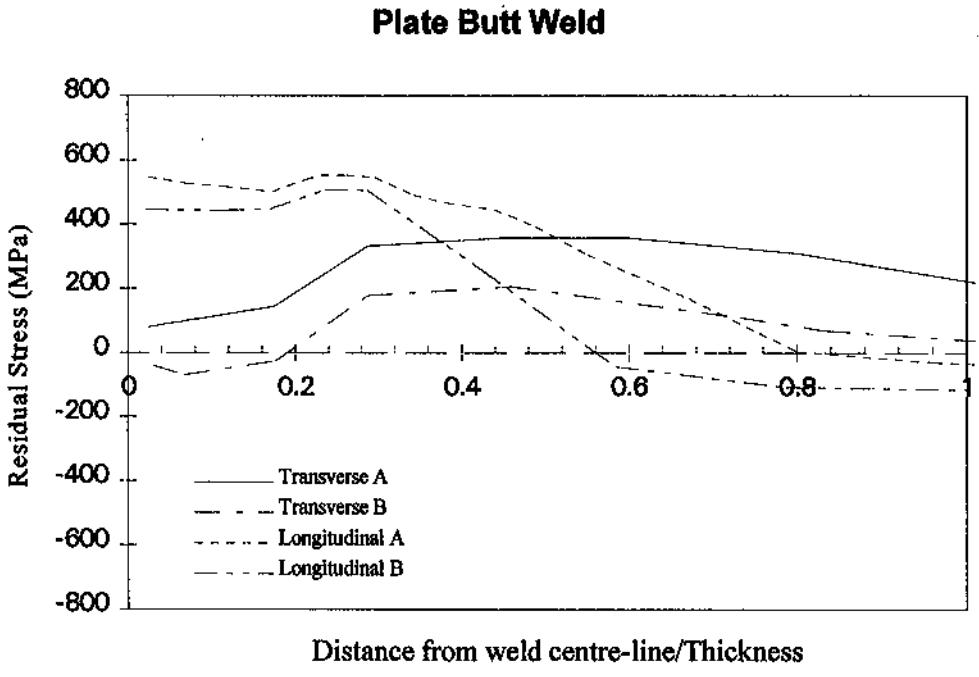

Figure 28 Residual stresses in multi-pass butt welded plate (14) (SM50, 50mm thick)

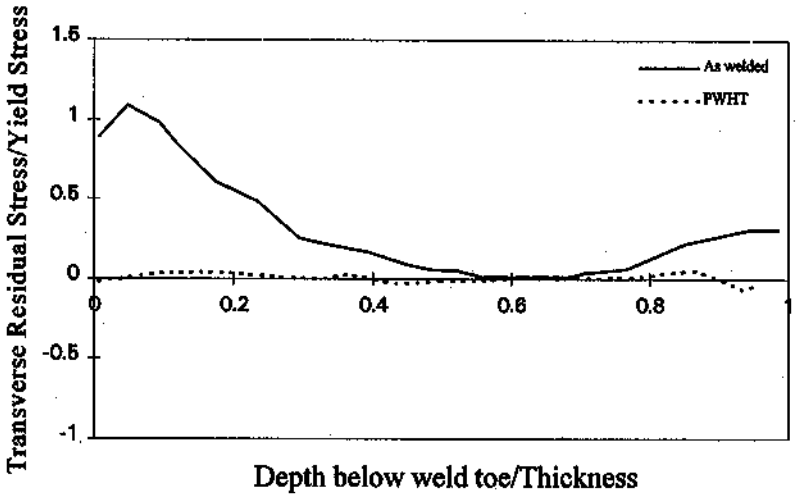

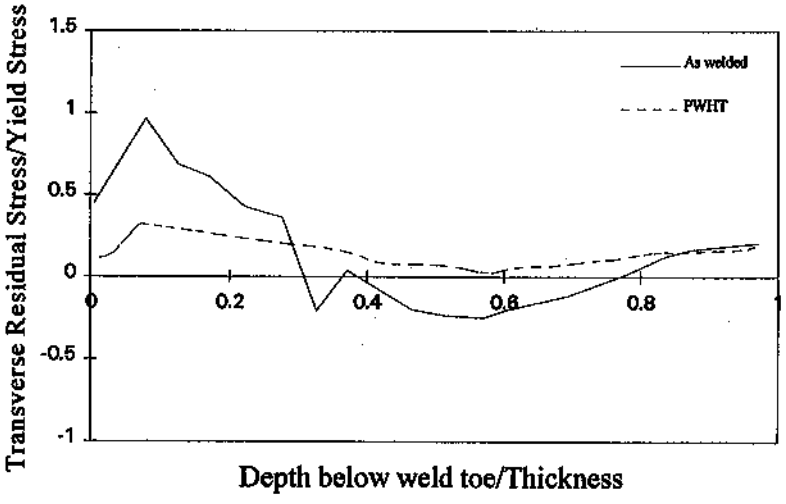

Specimen	Yield (MPa)	Heating rate max °C/hr	Cooling rate max °C/hr	Max Temp °C	Comment
P1	420	60	58	579	226 mins above 550°C
P2	375	138	113	550	112 mins above 545°C
P3	360	150	97	583	184 mins above 550°C

Figure 29a The effect of PWHT on residual stress in pipe on plate joints (35)

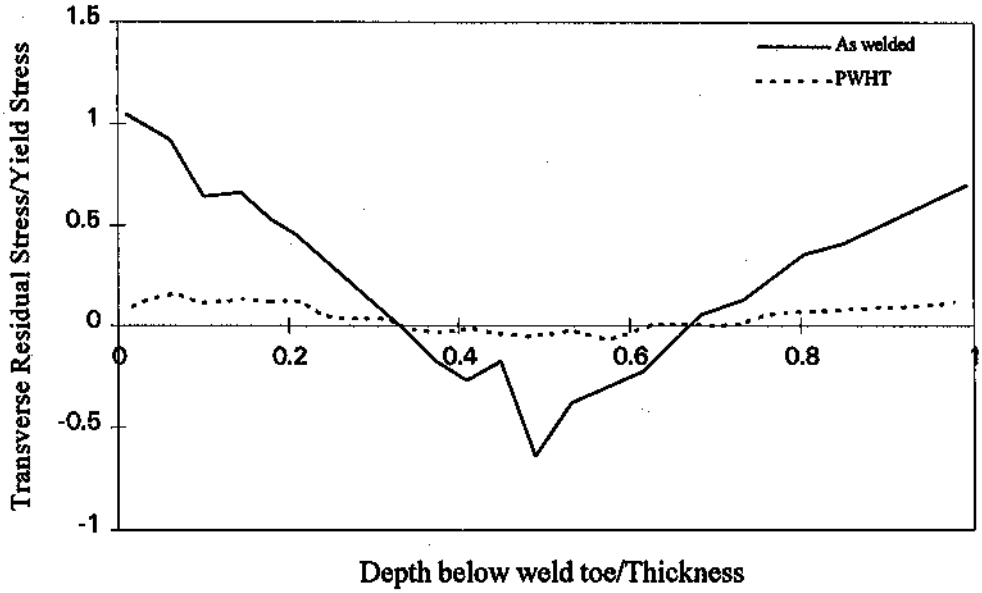

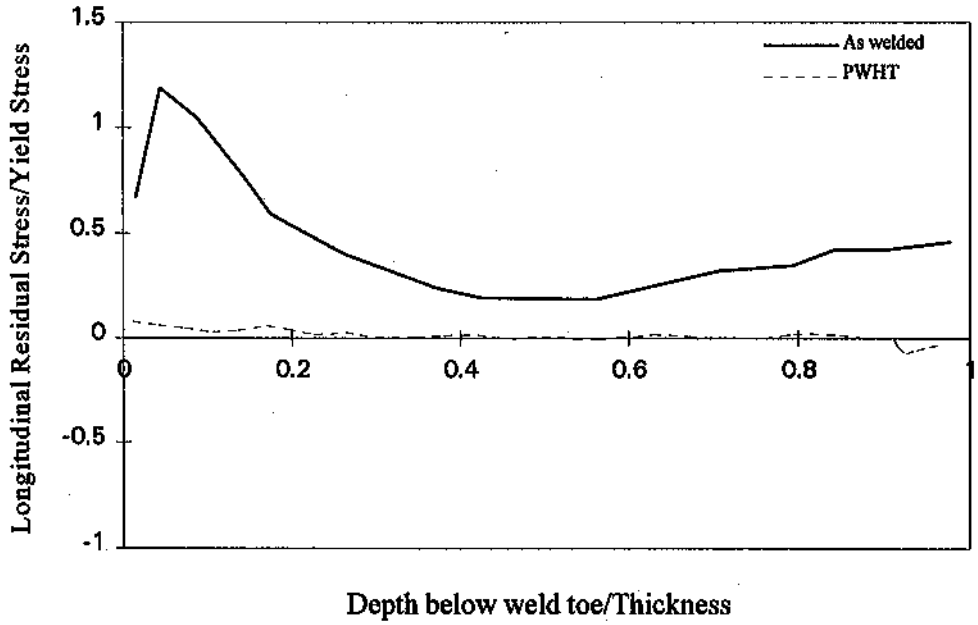

Figure 29b The effect of PWHT on residual stress in pipe on plate joints (35)

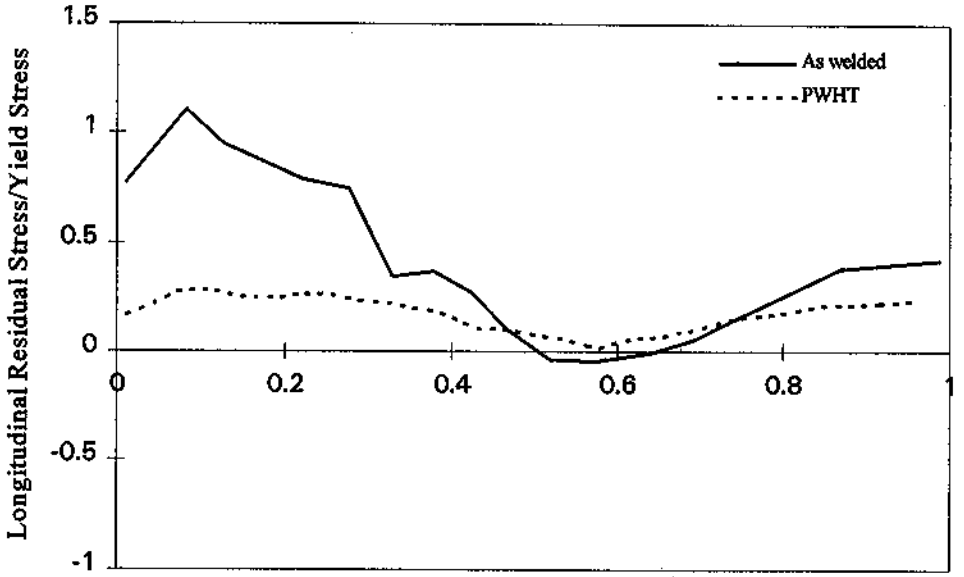

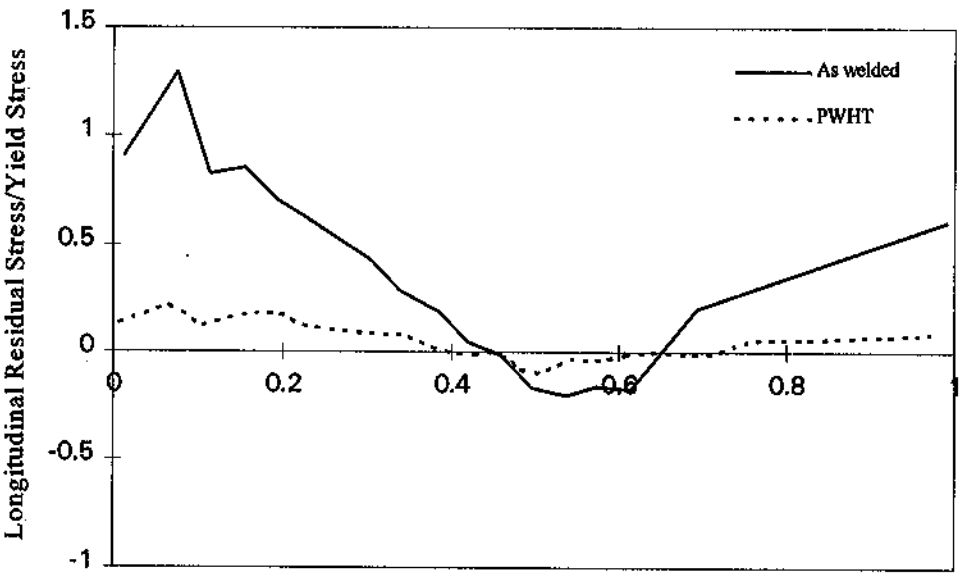

Figure 29c The effect of PWHT on residual stress in pipe on plate joints (35)

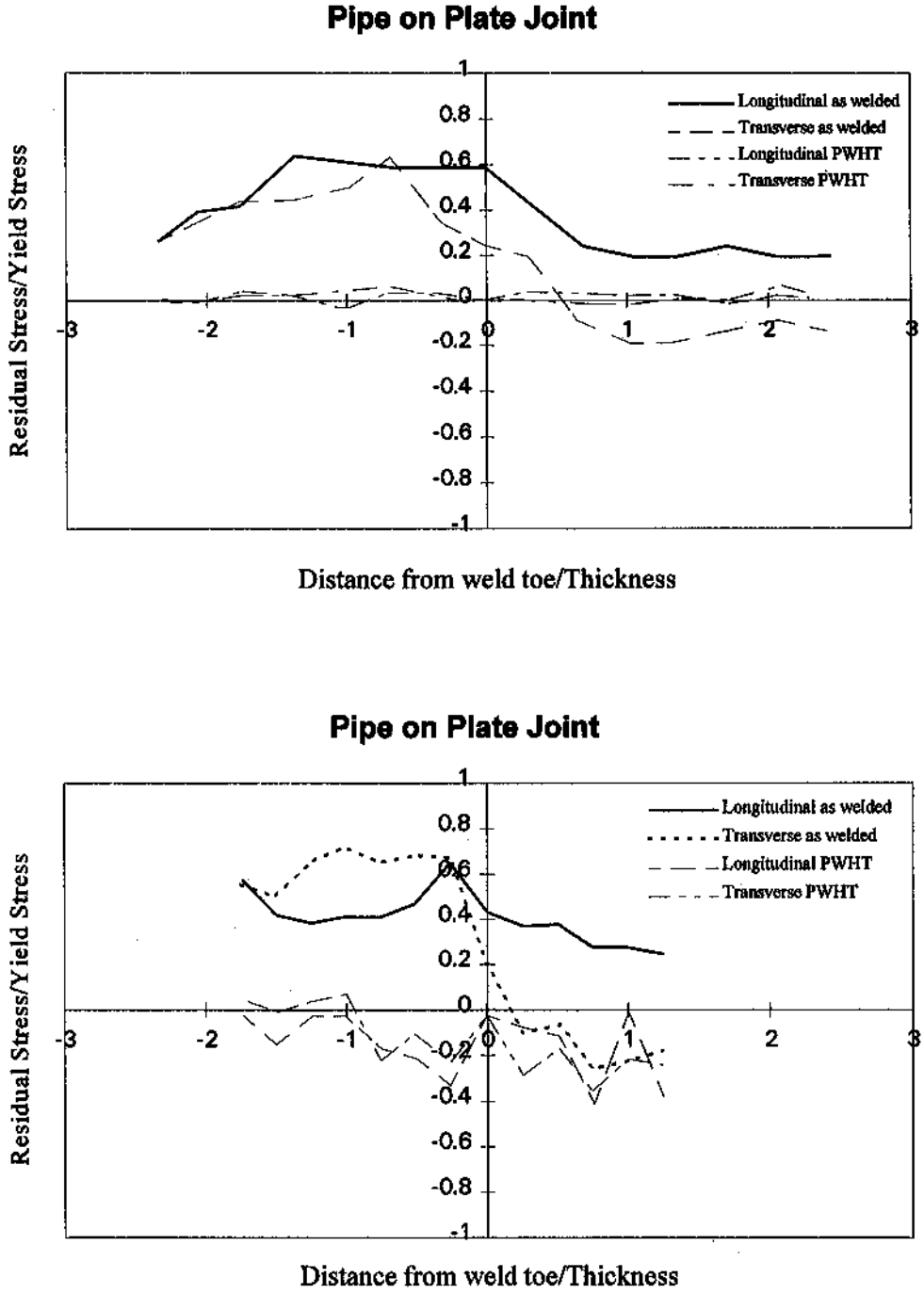

Figure 30a Surface residual stresses in pipe on plate specimens (35)

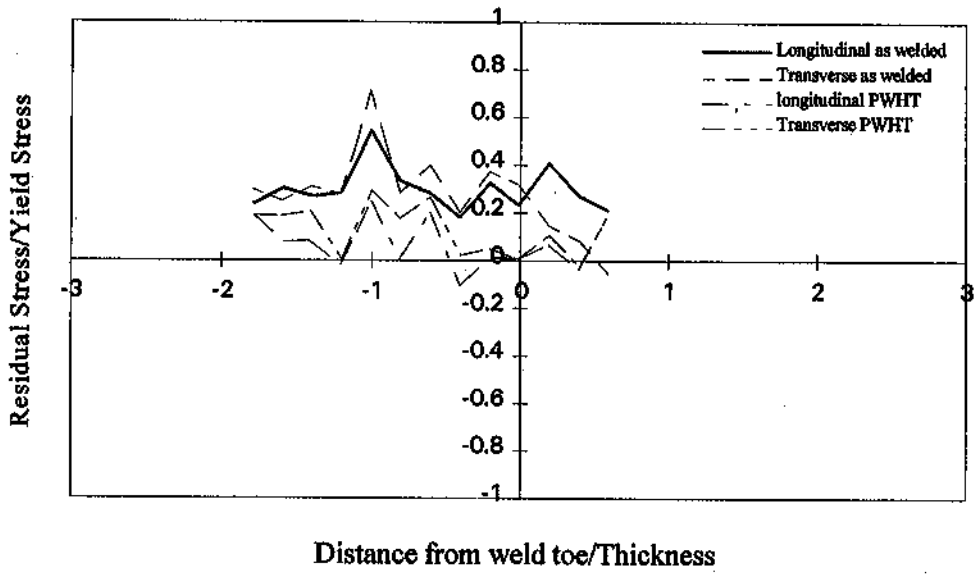

Figure 30b Surface residual stresses in pipe on plate specimens (35)

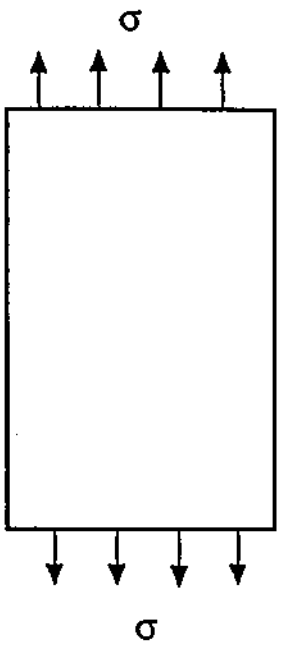

(a) S.I.F = 0

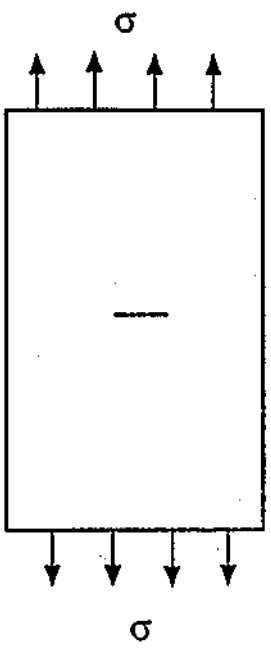

(b) S.I.F = K

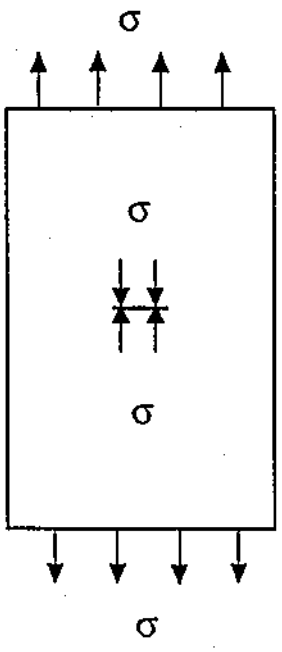

(c) S.I.F = 0

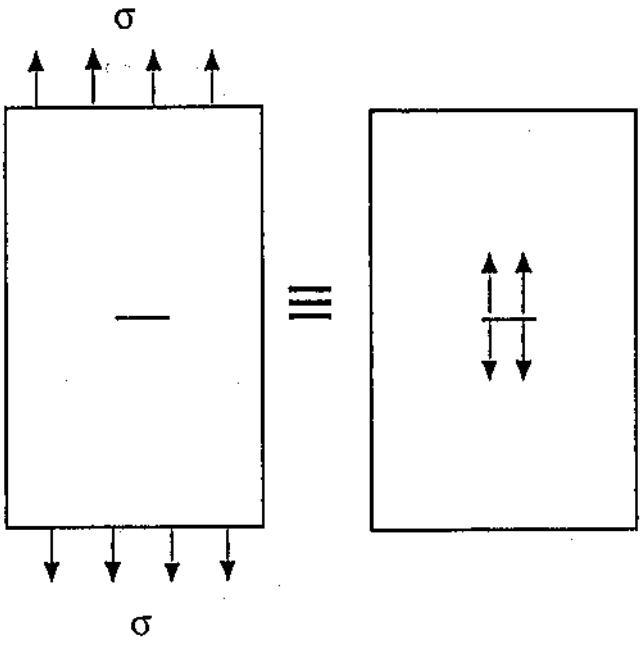

(d) S.I.F = K
Two cases are equivalent

Figure 31: Principle of superpostion

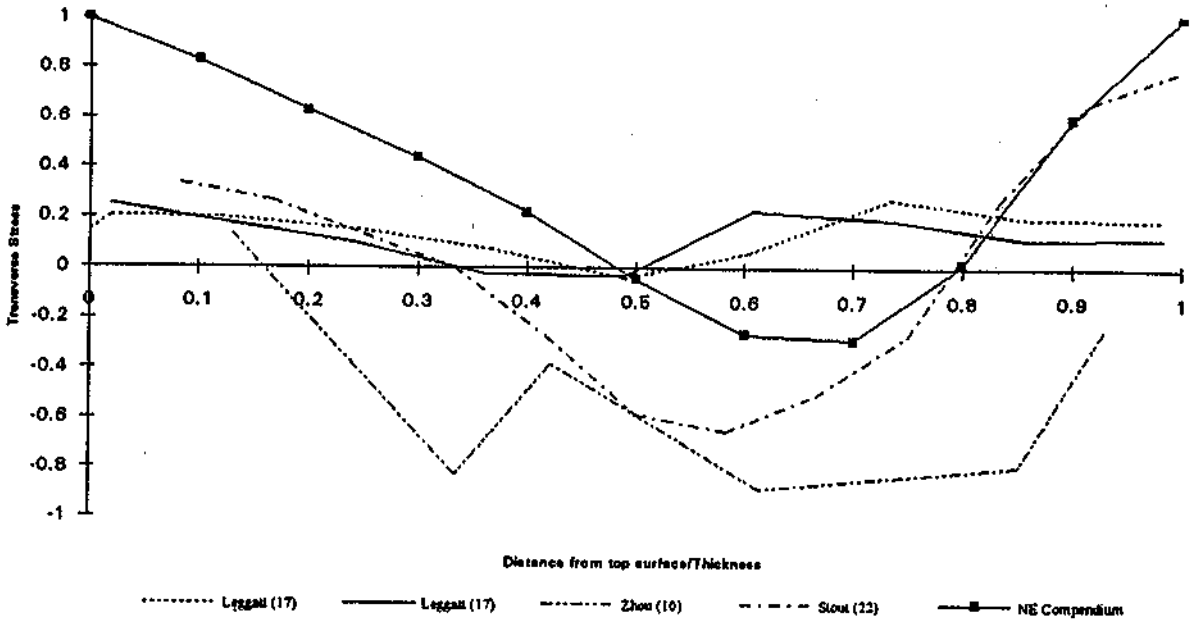

a) Transverse stress

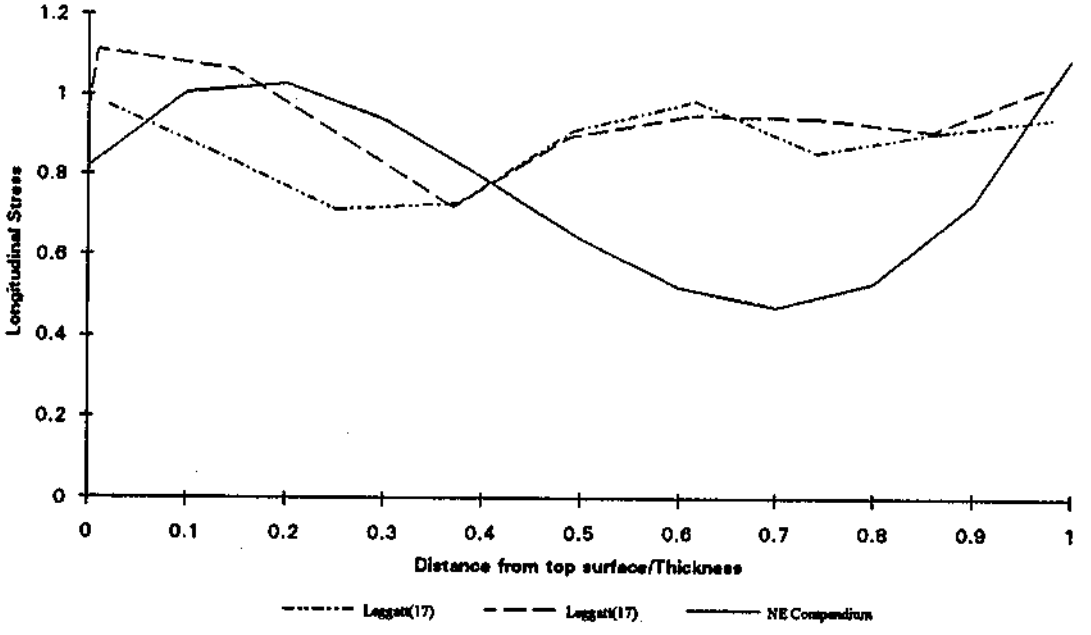

b) Longitudinal stress

Figure 32 Comparison of Nuclear Electric Compendium with plate butt weld residual stress data

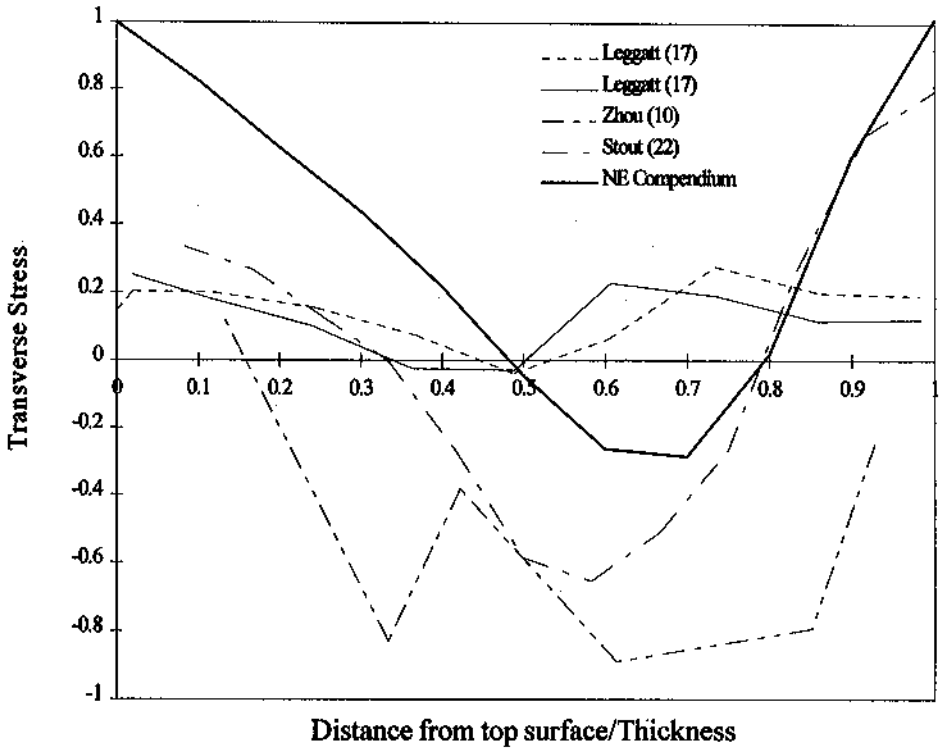

a) Transverse Stress

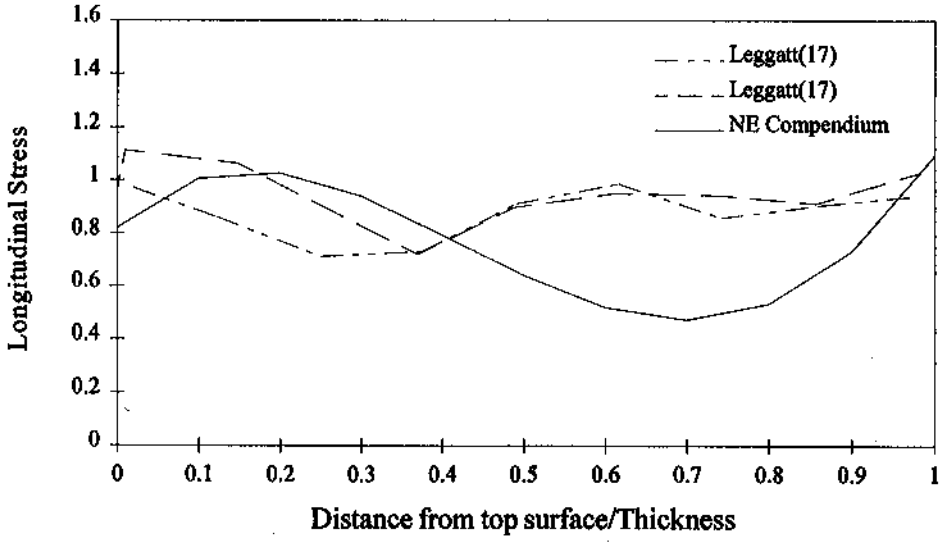

b) Longitudinal Stress

Figure 33 Comparison of Nuclear Electric Compendium with plate butt weld residual stress data

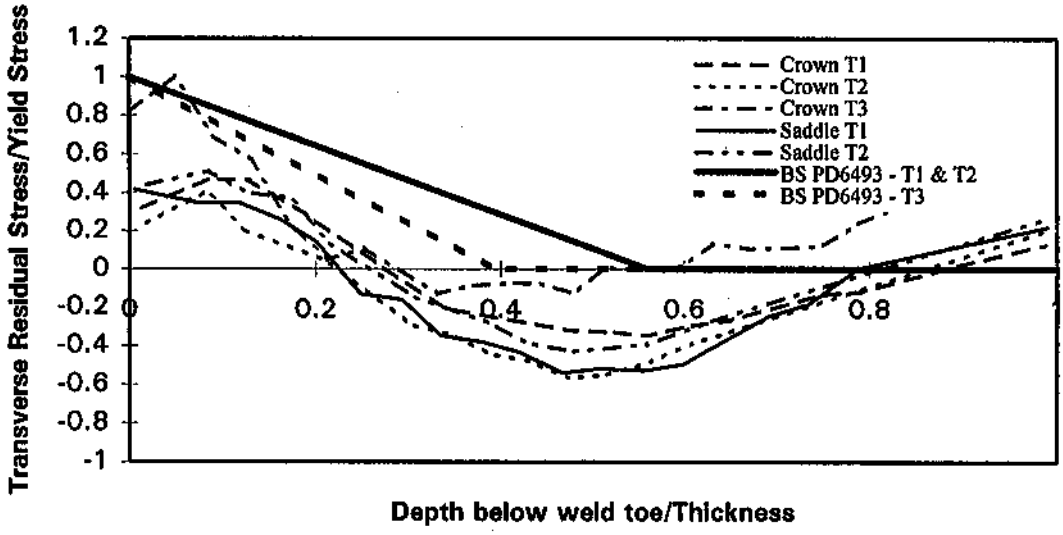

Figure 34a: Comparison of BS PD6493 idealised distribution of transverse residual stresses at toe of weld with measured distributions for tubular nodal welds

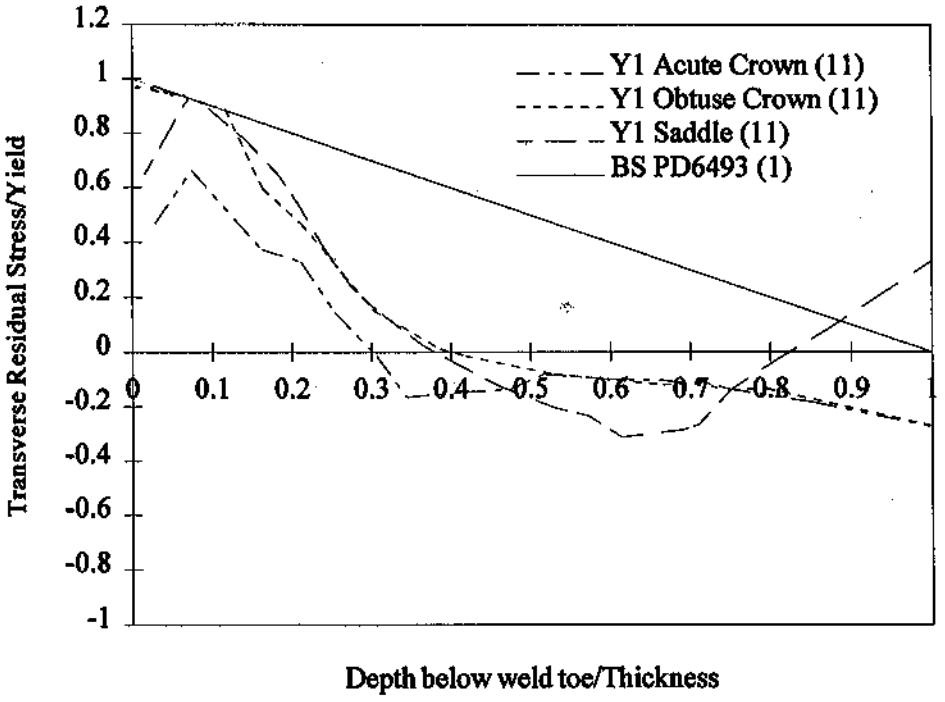

Tubular Y-node

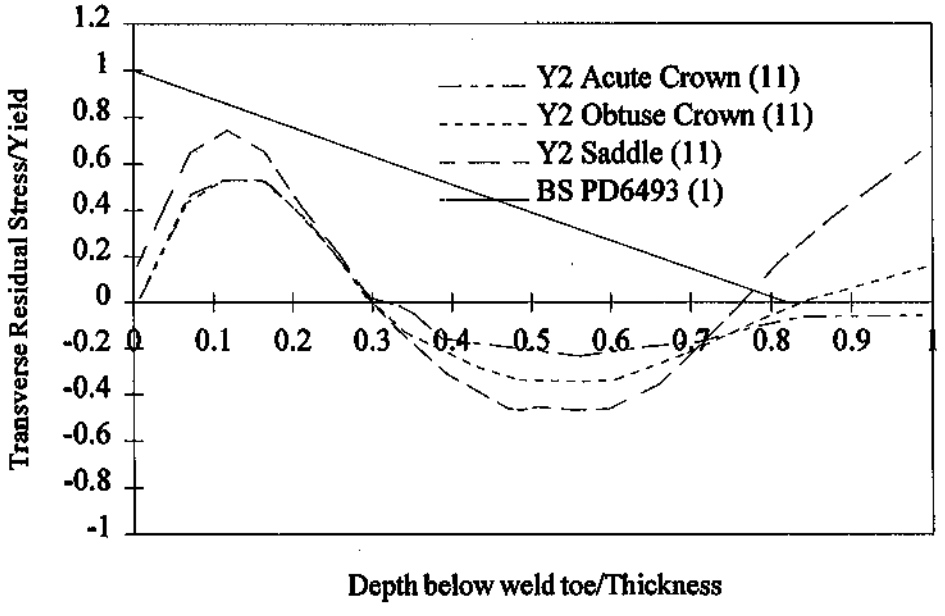

Figure 34b Comparison of BS PD 6493 idealized distribution of transverse residual stresses at weld with measured distributions for tubular nodal welds

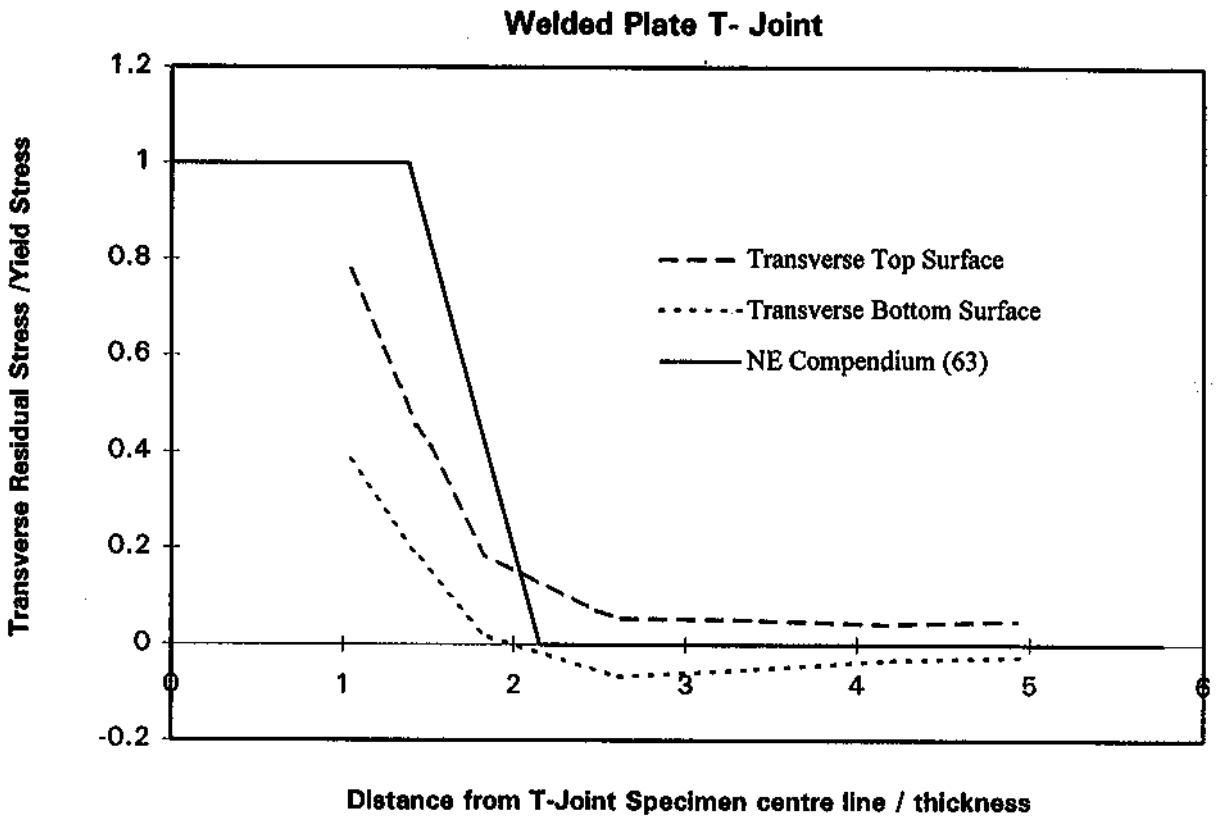

Figure 35: Comparison of Nuclear Electric compendium with FE results obtained by Mok & Pick [28]

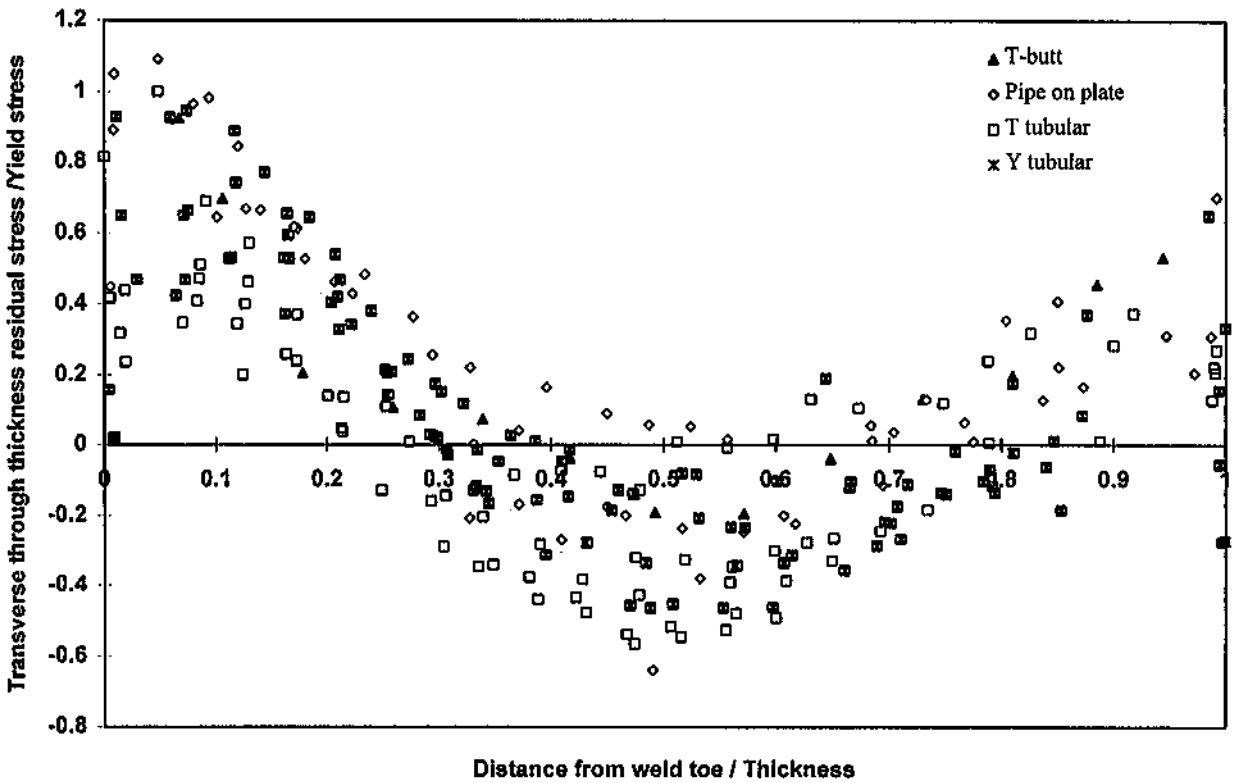

Figure 36: Transverse through-thickness residual stresses for T-butt, pipe on plate, and tubular joints

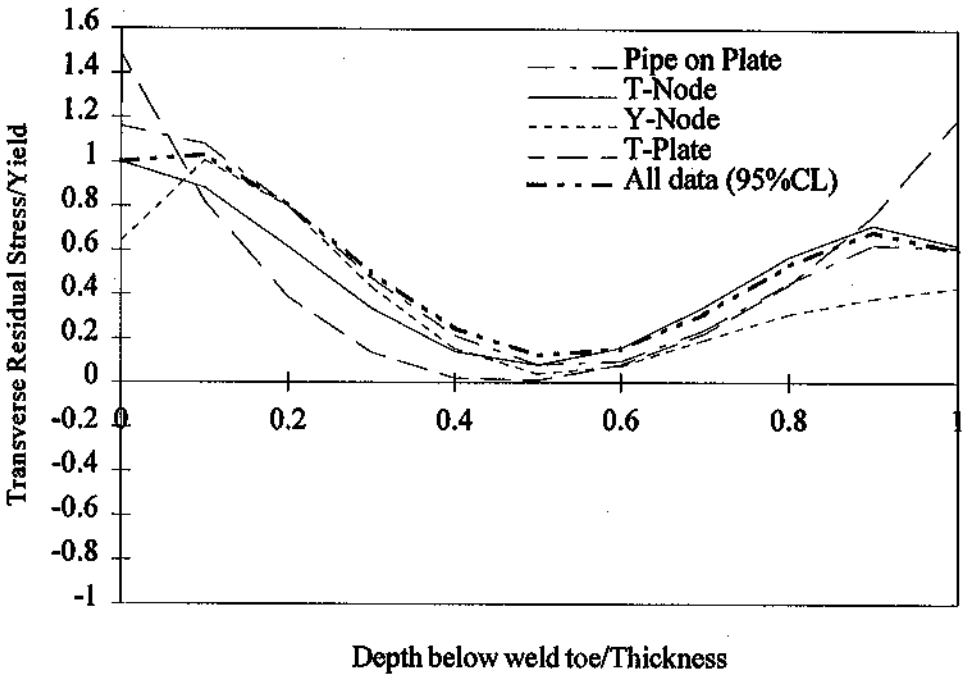

Figure 37 Comparison of upper bound stress profiles for transverse through thickness residual stress

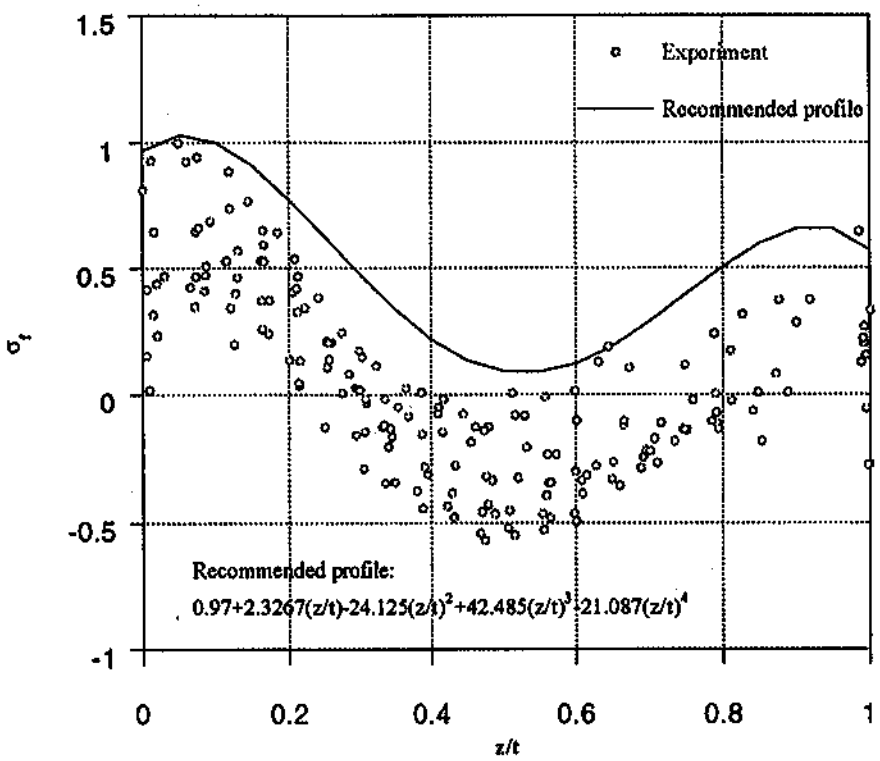

Comparison of recommended profile with measured transverse residual stress data for a T-node weld

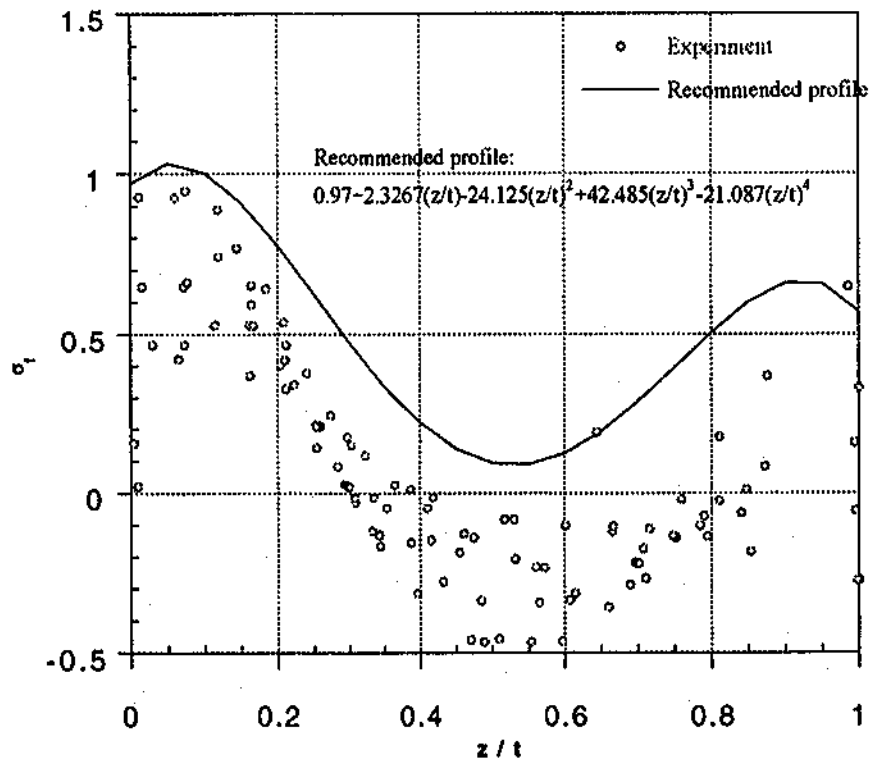

Figure 38 Comparison of recommended profile with measured transverseresidual stress data for a Y-node weld

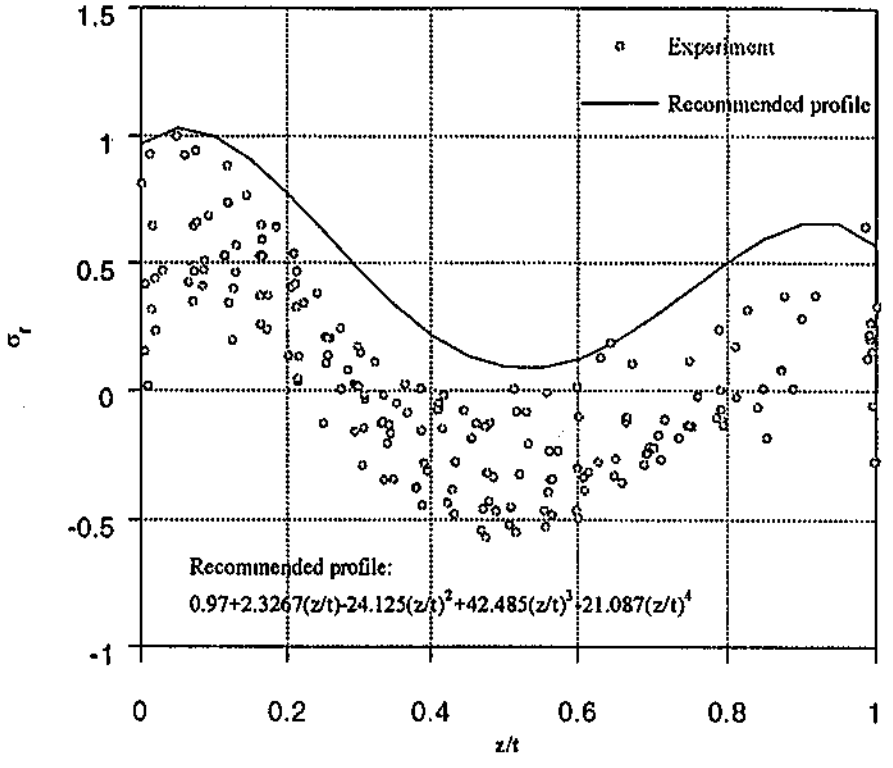

Comparison of recommended profile with measured transverse residual stress data for a T-node weld

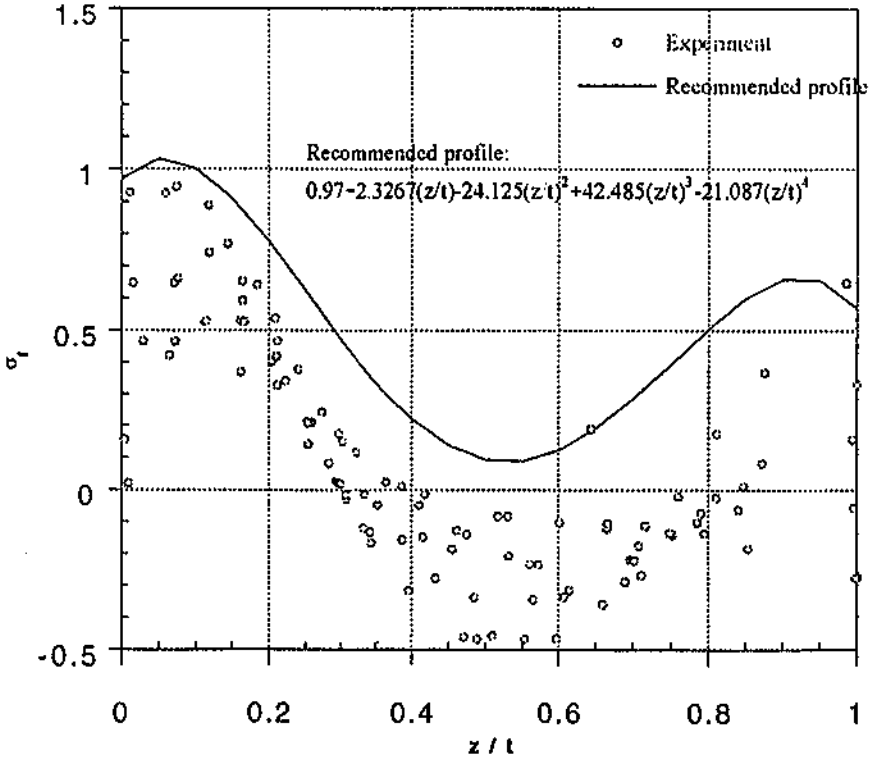

Figure 39: Comparison of recommended profile with measured transverseresidual stress data for a Y-node weld

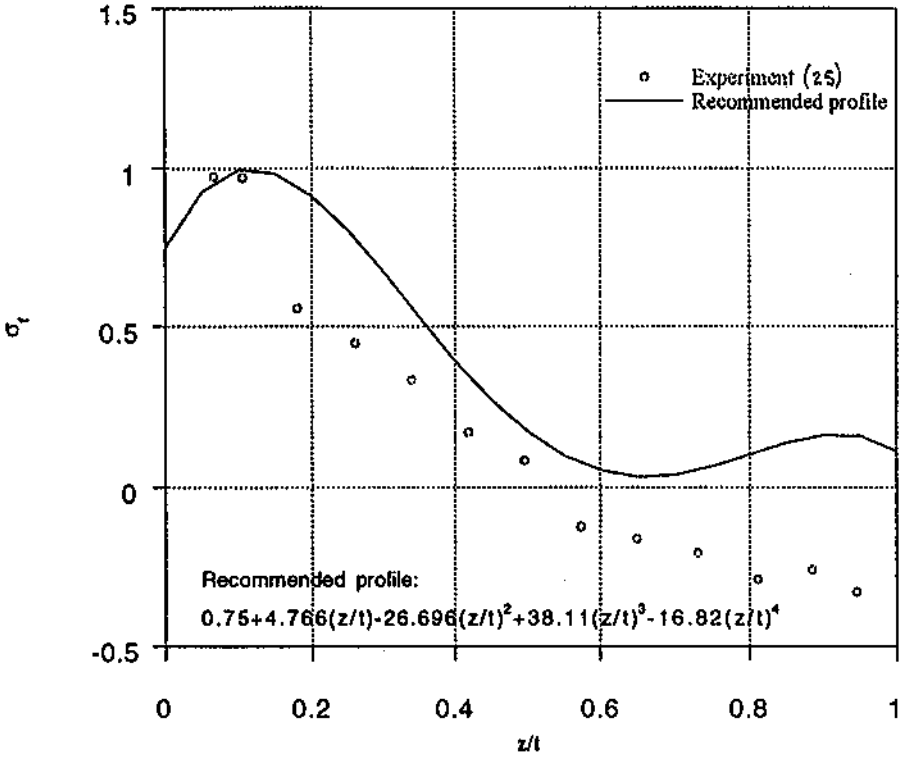

Figure 40: Comparison of recommended profile with measured longitudinal residual stress data for a plate T-butt weld

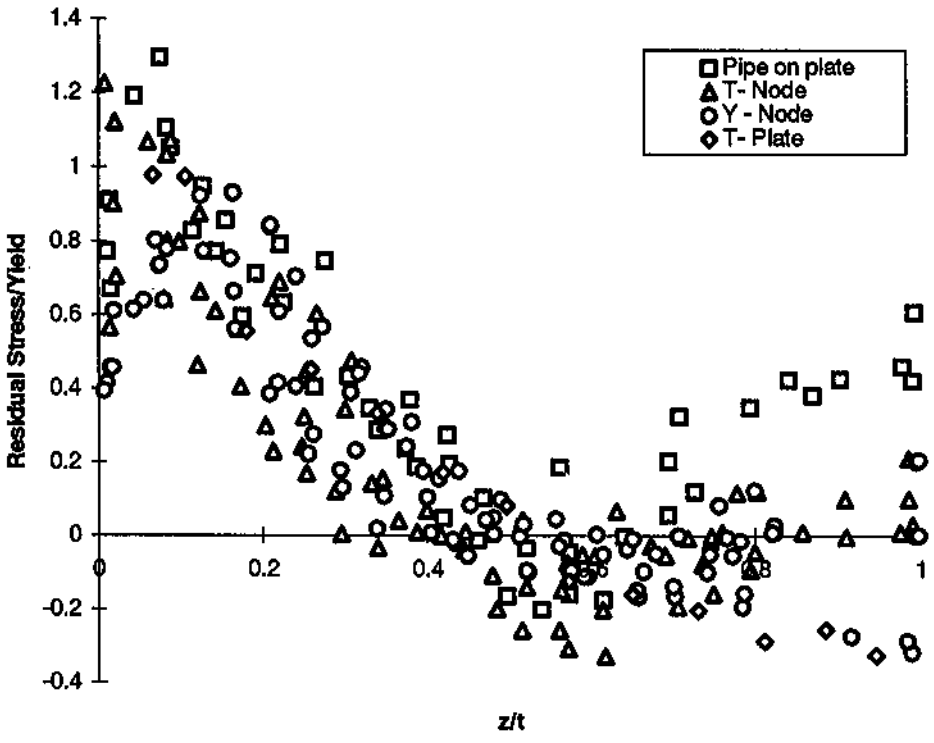

Figure 41: T-butt data obtained for longitudinal through thickness residual stress

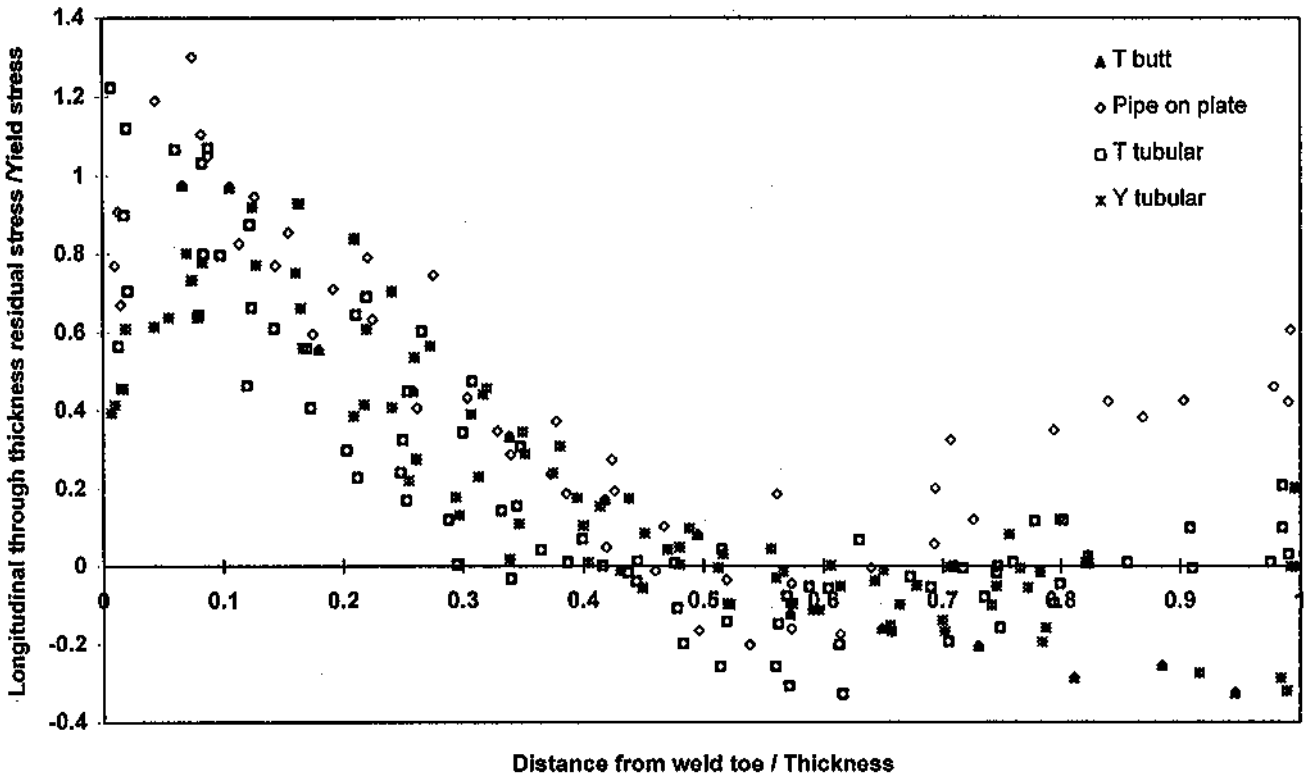

Figure 42: Longitudinal through-thickness residual stresses for T-butt, pipe on plate, and tubular joints

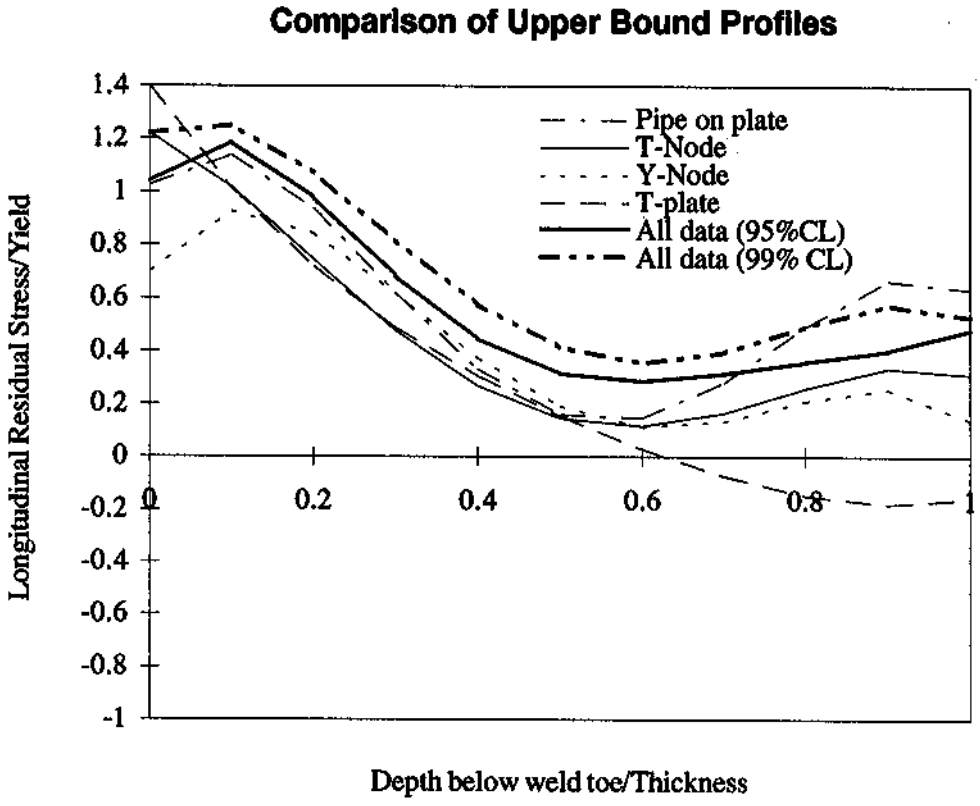

Figure 43 Comparison of upper bound stress profiles for longitudinal through thickness residual stress in T-butt joints

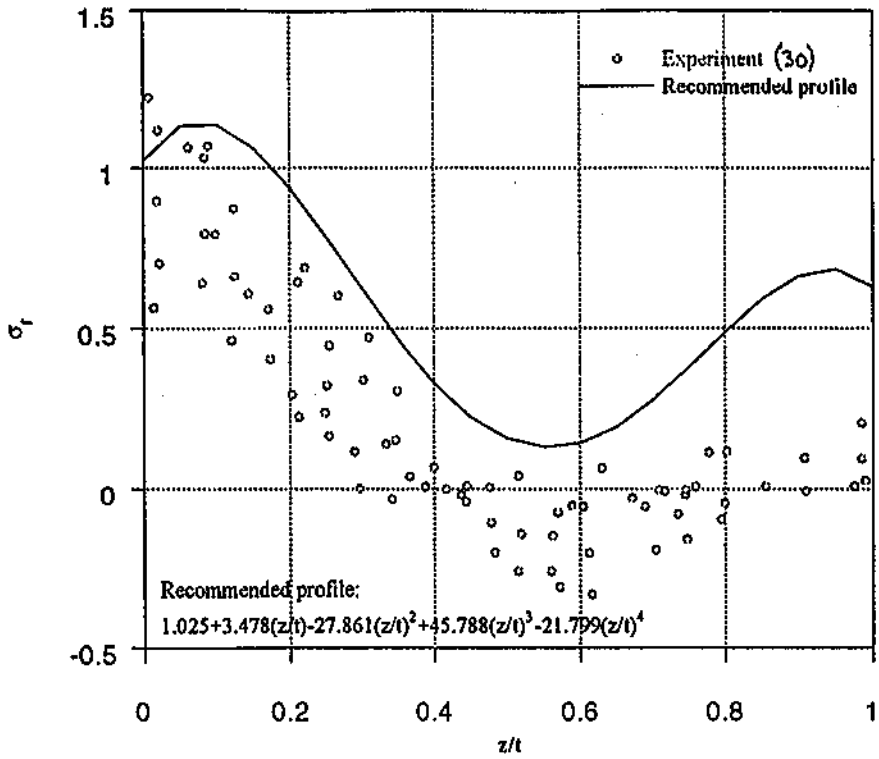

Figure 44: Comparison of recommended profile with measured longitudinal residual stress data for a tubular T-node weld.

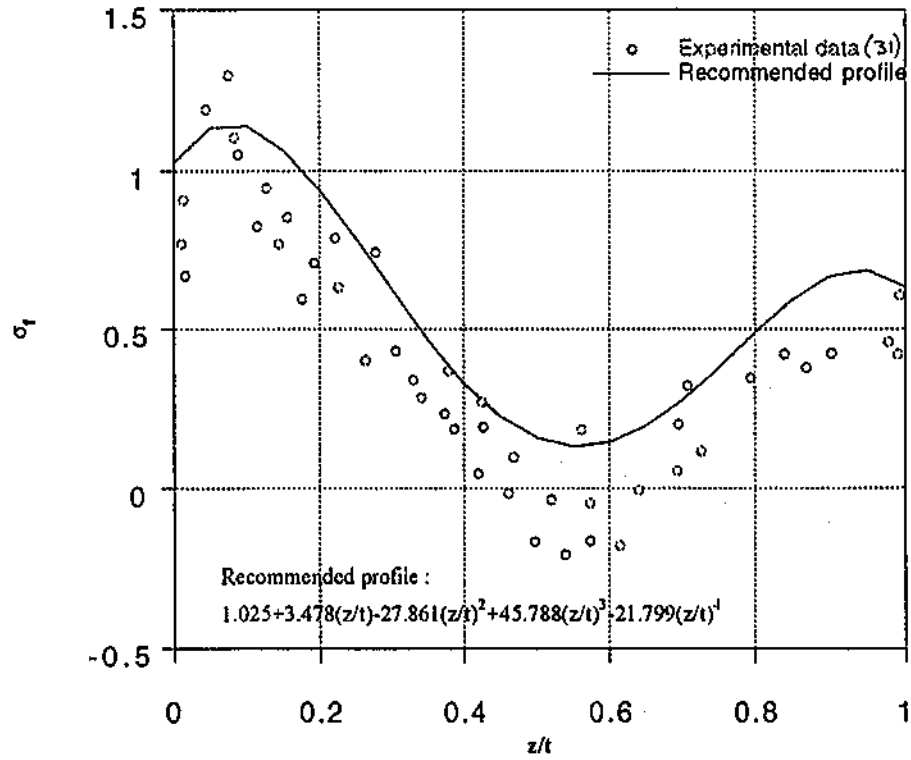

Figure 45: Comparison of recommended profile with measured longitudinal residual stress data for a pipe on plate weld

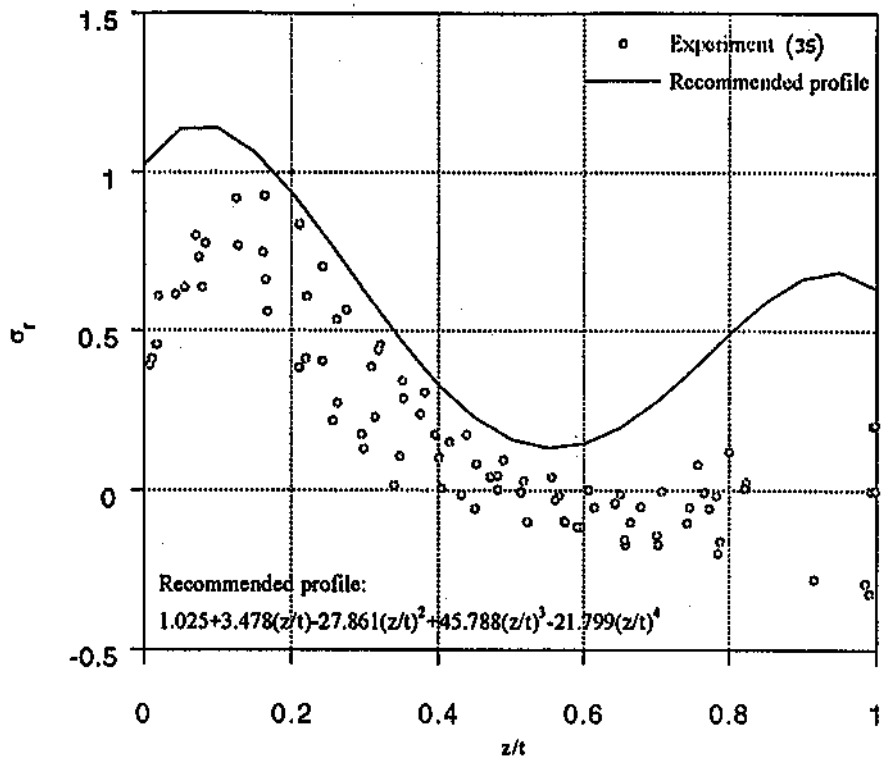

Figure 46: Comparison of recommended profile with measured longitudinal residual stress data for a Y-node weld

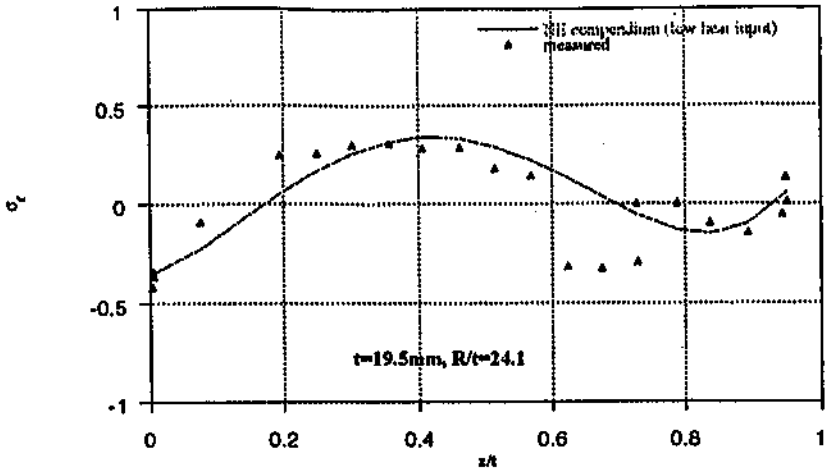

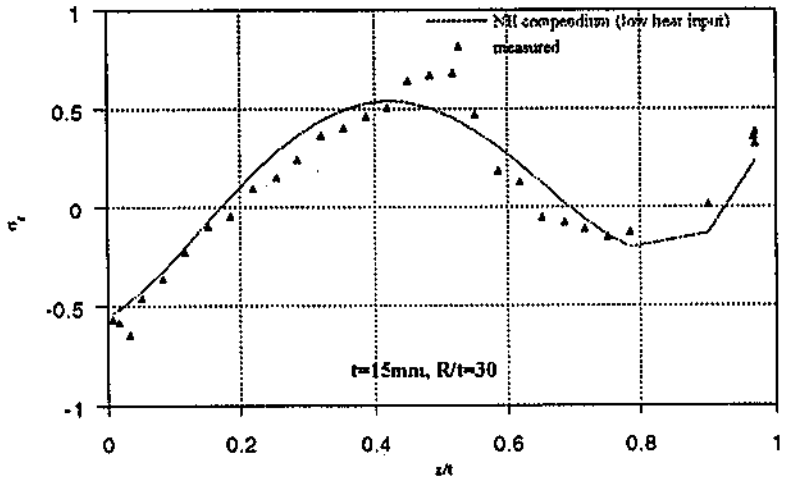

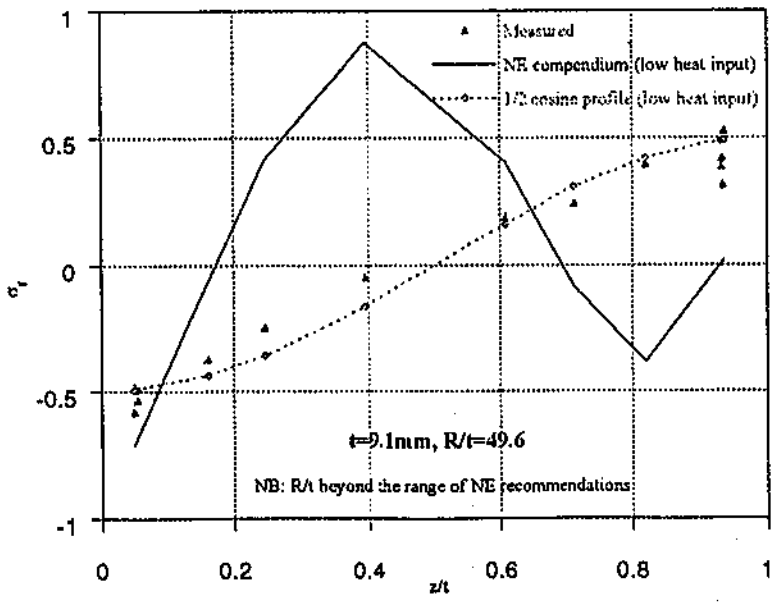

Figure 47: Comparison of Scaramangas' measured data with recommended profiles of NE and the 1/2 cosine profile for t=19.5, 15 and 9.1mm; and R/t=24.1, 30 and 49.6 respectively

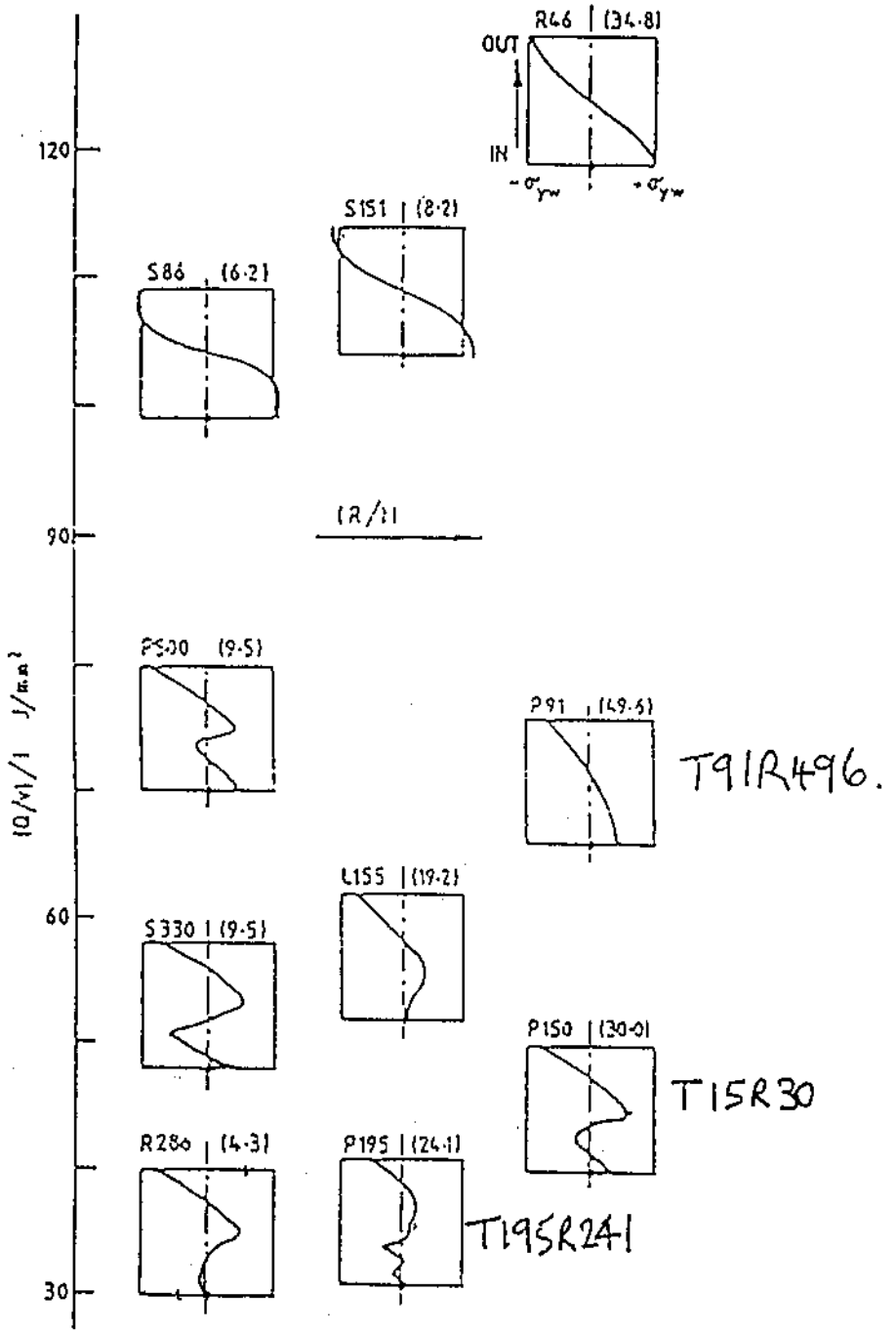

Figure 48: Illustration of effect of heat input and R/t on transverse residual stress profile of butt welded pipes [49]
(Bracket values indicate values of R/t)

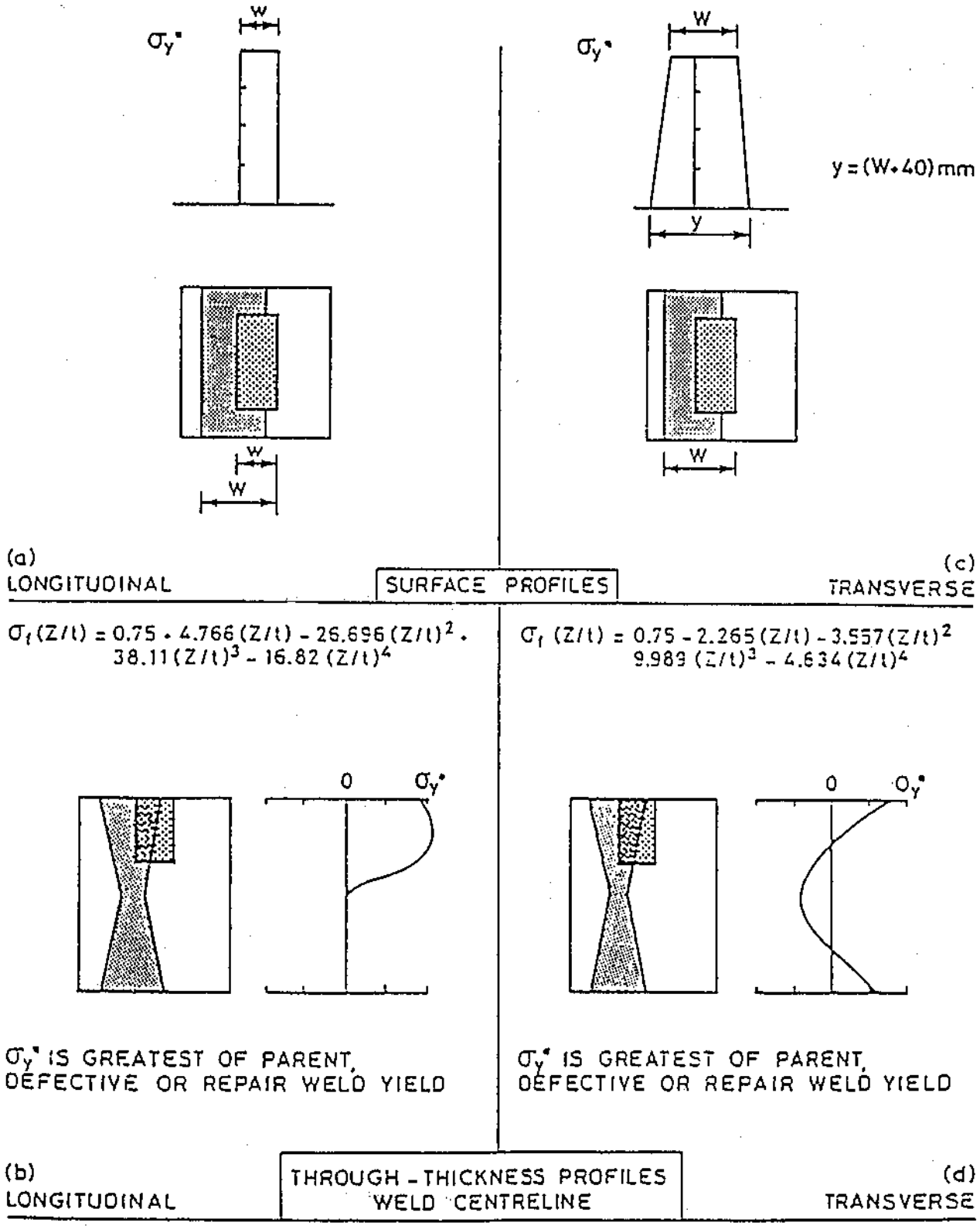

Figure 50: Repair welds: ferritic steels only [66]

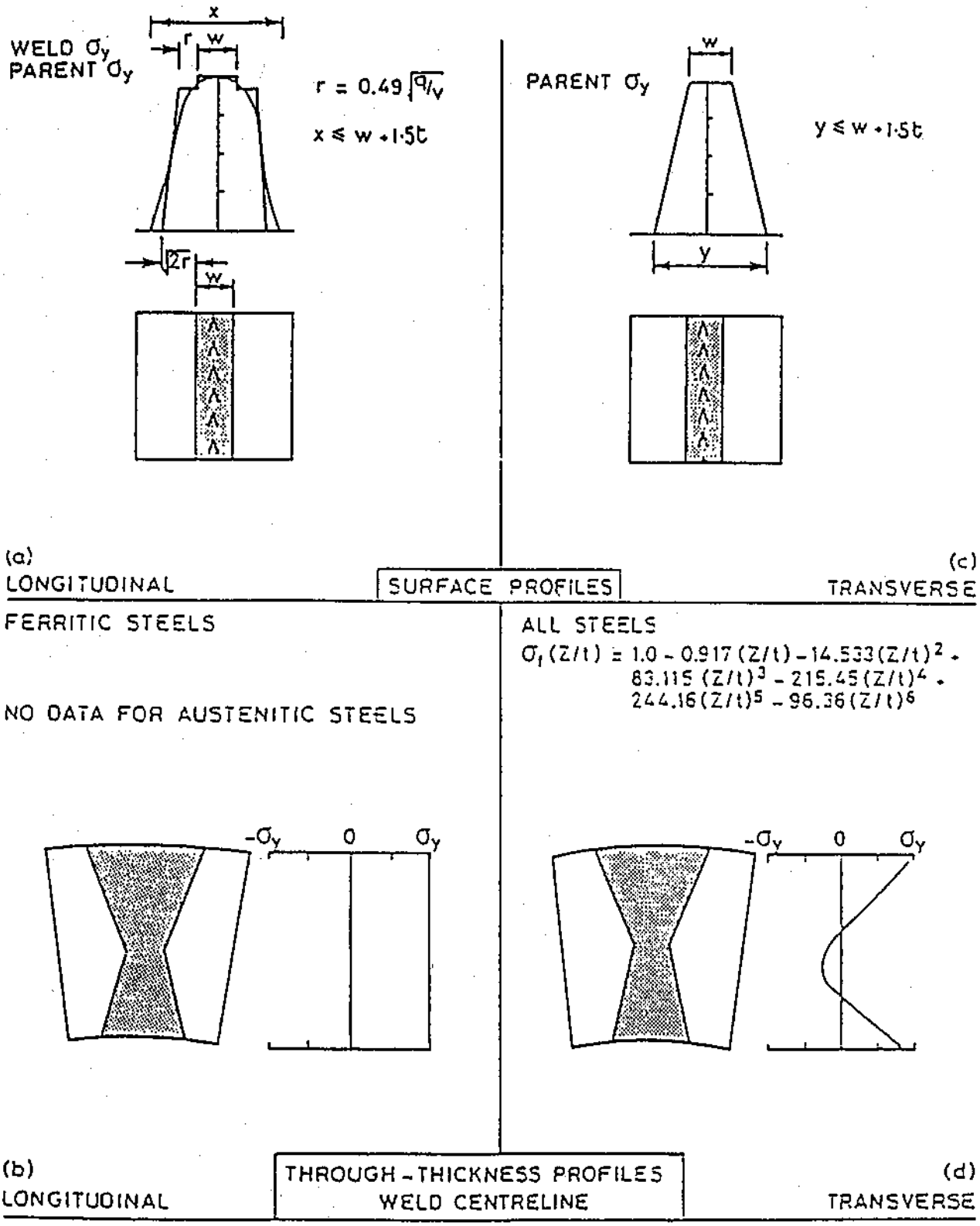

Figure 49: Geometry: pipe seam welds [66]

APPENDIX 1

REVIEW OF METHODS FOR EVALUATING RESIDUAL STRESS LEVELS AND DISTRIBUTIONS

D J Buttle
National NDT Centre
AEA Technology plc
Culham

REVIEW OF METHODS FOR EVALUATING RESIDUAL STRESS LEVELS AND DISTRIBUTIONS

D J Buttle
National NDT Centre, AEA Technology plc, Culham

REVIEW OF METHODS FOR EVALUATING RESIDUAL STRESS LEVELS AND DISTRIBUTIONS

1 INTRODUCTION

The purpose of this report is to review all available techniques for residual stress measurement, destructive, semi-destructive, nondestructive and numerical and assess the potential for offshore use. The techniques will first be described in detail, then their definition and performance summarised in Tables 1 to 3. The final section will discuss the suitability of the techniques for offshore application, summarised in Table 4. The material is based firstly on experience and expertise developed during the CEC BRITE programme P2082 'Development of Non-invasive Methods for Measurement of Stress in Welded Steel Structures' with industrial sponsorship from the Harwell Offshore Inspection Service, and which was therefore mainly directed at the offshore industry. One of the sponsors was HSE (taking over from the Department of Energy). Secondly, the technical literature has been briefly re-appraised, a sample of which appears in the Bibliography section.

2 DESTRUCTIVE AND SEMI-DESTRUCTIVE METHODS

Mechanical methods, (destructive and semi-destructive) all involve the removal of material, thereby relieving residual stresses, and monitoring the resulting displacements in the component. The methods of removal include saw cutting, slicing, hole drilling or trepanning and the methods of measurement precision callipers, optical methods or resistive strain gauges. The attachment of strain gauges requires preparation of a smooth surface.

2.1 Successive Layer Removal Methods

The sectioning method consists of cutting up the structure while measuring the relaxed strains on suitable free surfaces. First the part is removed from the component or structure and then successive thin layers of material are removed while monitoring strain relief with resistance gauges. The first stage results in relief of 'reaction' stresses and the second 'layer' stresses. Sometimes only the reaction stresses are required which can be determined rapidly. Conversely successive removal of surface layers is tedious and time consuming and evaluation of the initial internal stress state is complex, strain relief depending upon the size and shape of the removed part. Also influences from plasticity and strong residual stress gradients can cause uncertainties in the results. However destructive methods are universally applicable to materials and structures.

Theoretical relationships between the initial residual stress state and measured strain relief are established only for simple geometry's such as bars, rings, plates, tubes and rods. For tube geometry's the mechanical processes of 'turning off', 'boring out' and 'slitting-up' are applicable. These involve respectively, reducing the length, increasing the inner or reducing the outer diameter, cutting the tube open along its length.

For a thin walled tube circumferential and axial stresses can be evaluated separately if rotational symmetry is assumed. For circumferential stress evaluation sections of pipe are pickled to different depths before slitting each pipe. The subsequent change in diameter (deflection measurement) is measured in each case at least a distance from the ends of one diameter. The circumferential stress through the thickness can then be evaluated using appropriate stress deflection formulae. For axial stress evaluation a thin tongue of material of width less than one tenth of the diameter and length three diameters is removed. The surface is removed in successive layers and the deflection measured. The axial stress can then be evaluated in a manner similar to the curvature method. For both stress components a correction is required to account for partially remaining reaction stresses.

For rods and thick walled tubes the Sach's method has been developed for triaxial stress evaluation. This method requires measurements to be made at least one diameter away from the ends and assumes rotational symmetry of stress. For a rod an inner concentric hole is bored. For a thick tube outer or inner layers are removed. The changes in length and diameter are accurately measured due to stress relaxation. When the specimen has been reduced to a thin shell the remaining stresses can be determined using the procedure described above for thin pipes. Detailed formulae are established enabling the initial triaxial residual stress distribution to be evaluated.

All these methods require material removal without introducing additional strains from the machining. Also the techniques are very time consuming and require great expertise. Consequently the semi-destructive methods, such as the centre hole method are generally preferred.

2.2 Curvature Method

If a stress distribution exists in a thin strip, then removal of thin layers by progressive mechanical polishing will result the bending of the strip. By measuring the curvature as a function of surface removal it is possible to evaluate the internal stress levels before polishing. For a strip with an initial thickness, h, and curvature, F, the stress level is given from:

$$\sigma(z) = \frac{E}{6}\left(h^2 \frac{dF(z)}{dz} + hF(z) + \int_z^h F(z').dz' \right) \qquad [1]$$

where E is Young's modulus for the material. This evaluation makes the following assumptions: The initial strip is flat, the stress is uniaxial, the curvature is approximated as circular and no stresses are introduced by the mechanical polishing.

2.3 Through Hole and Centre Hole Methods

The drilling of a small hole into a stressed body results in local relief because at the sides of the hole the principal stress perpendicular to the surface and shear stress components must reduce to zero. This is the principle of the hole drilling method. In most applications, the drilled hole is blind with a depth equal to its diameter. However the through hole method is simple enough to enable an analytical solution for the stress relief to be evaluated.

For an initial uniaxial stress, σ_x, in a plate, the drilling of a hole of radius, R_0, through the plate results in relieved radial and tangential strains, ε_r and ε_θ, evaluated as:

$$\begin{aligned} \varepsilon_r &= \sigma_x(A + B\cos 2\alpha) \\ \varepsilon_\theta &= \sigma_x(-A + C\cos 2\alpha) \end{aligned} \qquad [2]$$

where the radius, R, is greater than R_0 and the coefficients A, B and C are given by:

$$A = -\frac{1+\upsilon}{2E}\left(\frac{1}{r^2}\right); \quad B = -\frac{1+\upsilon}{2E}\left[\left(\frac{4}{1+\upsilon}\right)\frac{1}{r^2} - \frac{3}{r^4}\right]; \quad C = -\frac{1+\upsilon}{2E}\left[-\left(\frac{4\upsilon}{1+\upsilon}\right)\frac{1}{r^2} + \frac{3}{r^4}\right] \qquad [3]$$

where $r=R/R_0$. Therefore the relieved strains vary in a complex way as a function of distance from the hole. As the strains generally decrease with distance it is desirable to measure them as close to the edge of the hole as possible. However, in the proximity of the hole parasitic effects can be significant. Therefore strain gauges are optimally positioned in the range $0.3<r<0.45$ where R is the radius to the longitudinal centre of the gauge. On the principal axis, the radial strain is much greater than the tangential strain. Therefore strain gauges are oriented with their longitudinal axis in the radial direction. Equations [2] and [3] indicate the relieved radial strain is always of opposite sign to the initial residual stress.

In cases of biaxial residual stress states the principle of superposition can be applied. This is valid for linear elastic material behaviour. The relieved radial strain is then evaluated as:

$$\varepsilon_r = A(\sigma_x + \sigma_y) + B(\sigma_x - \sigma_y)\cos 2\alpha \qquad [4]$$

There are three independent quantities σ_x, σ_y and α, requiring three angular measurements of ε_r and therefore three strain gauges positioned around the hole. For gauges positioned at angles α, α+45° and α +90° where α is the angle of the nearest principal stress to gauge 1, strain measurements ε_1, ε_2 and ε_3 can be inverted to yield:

$$\sigma_{max} = \frac{\varepsilon_1 + \varepsilon_3}{4A} - \frac{1}{4B}\sqrt{(\varepsilon_3 - \varepsilon_1)^2 + (\varepsilon_3 + \varepsilon_1 - 2\varepsilon_2)^2}$$

$$\sigma_{min} = \frac{\varepsilon_1 + \varepsilon_3}{4A} + \frac{1}{4B}\sqrt{(\varepsilon_3 - \varepsilon_1)^2 + (\varepsilon_3 + \varepsilon_1 - 2\varepsilon_2)^2} \qquad [5]$$

$$\tan 2\alpha = \frac{\varepsilon_1 - 2\varepsilon_2 + \varepsilon_3}{\varepsilon_1 - \varepsilon_3}$$

The strain gauges have a finite area which results in integrated averages or the radial strain over the length of the gauge. Also the finite width of the gauge introduces some sensitivity to the tangential strain. These problems are dealt with either by integration of equations [2] and [3] or, more accurately, by experimental calibration to evaluate modified coefficient values.

Centre or blind hole drilling is more usually used because components are rarely thin or flat. The drilling of a blind hole into a plane stress field produces a very complex stress state which cannot be evaluated analytically. However the general nature of the stress distribution is similar to an extent that the same equations [5] are used with modified coefficients, $\overline{A}$, $\overline{B}$ and $\overline{C}$. These coefficients must be obtained by finite element methods or experimental calibration. They include a functional dependence upon the dimensionless hole depth, defined as the ratio of the hole depth to the diameter of the circle joining the longitudinal centre-lines of the strain gauges. Normally the hole is drilled with this ration at 0.4 as an optimum for maximum strain relief and minimum damage.

The coefficients can be measured experimentally by using a prescribed uniaxial calibration. The results are then valid for materials with the same elastic properties using the same strain gauge rosette geometry and the same hole size. Also it is assumed that the stress is uniform with depth and biaxial.

Drilling of the hole must be carried out with great precision. Accuracy's of ±0.025 mm are normally achieved. Specially dressed end mills, high speed (400,000 rpm) air turbine and carbide cutters and abrasive jet machining methods have been used, the important consideration being not to introduce any local yielding (thus modifying the local stress state) or eccentricity. Also the diameter of the hole must be accurately known.

The accuracy of the technique is dictated by procedural considerations, the nature and magnitude of the residual stresses, the elastic-plastic characteristics of the test material and the precision to which the elastic constants are known. The most important procedural aspects are the avoidance of spurious strains and the accuracy to which the hole is drilled and measured. For stress levels below 50% of the yield stress, the overall accuracy is typically ≤ 8% of the maximum numerical stress in an equi-biaxial field, reducing to about 6% in pure shear and 4% in a uniaxial field. At higher stress levels the errors tend to increase because the hole acts as a stress raiser, accelerating the onset of plasticity at its periphery.

Finite element analysis based on an idealised elastic-plastic behaviour predicts that at full yield the stresses will be overestimated by 12% in an equi-biaxial field and by 9% in a uniaxial field. Direct measurements indicate they are smaller, i.e. +8% to +10%. At 70% of the yield stress the additional error is less than +3%.

2.4 Incremental Drilling Method

The blind hole drilling method has been developed by drilling the hole in incremental stages, in order to predict changes of stress with depth below the surface of a component. The modified centre hole coefficients $\overline{A}$ and $\overline{B}$ are generalised to dimensionless coefficients $\bar{a}$ and $\bar{b}$:

$$\bar{a} = -\frac{2E\overline{A}}{(1+\upsilon)}, \; and \; \bar{b} = -2E\overline{B} \qquad [6]$$

The coefficients $\bar{a}$ and $\bar{b}$ are independent and only weakly dependent upon the elastic constants respectively. For stresses which vary through the thickness the depth dependent coefficients can be evaluated by using a least squares fit between the normalised linear strain equations and the hole depth. A parabolic interpolation method can be used to interpolate the data. An alternative method, the integral method of analysis, uses incremental drilling strain gauge data to generate an equation for each depth sub layer. The equation unknowns represent an equivalent uniform stress acting over each sub layer. Data for dimensionless hole depths (defined above) greater than 0.4 to 0.5 show susceptibility to error and represent the limit of depth penetration for subsurface stress evaluation.

2.5 Deep Hole Method

The deep hole method attempts to measure stresses in the bulk of a component. It is one of the most comprehensive semi-destructive methods for bulk stress measurement. Some earlier work involved drilling relatively large diameter holes and mounting strain gauges on the side and bottom surfaces. Then the over-coring method is used to relax the stresses and finite element analysis applied to evaluate the initial stress state within the structure. However these techniques average over relatively large volumes and are not applicable to regions containing large stress gradients such as near a weld.

More recently a method has been developed using a 3.2 mm diameter deep hole to evaluate the three principal stress components averaged over a 10 mm diameter cylinder every 6 mm of cylinder length through the structure. The hole is over-cored and the subsequent diametral and axial shape changes to the hole measured along the length of the bore. The third principal stress is assumed to be parallel to the hole. Therefore three diametal and one axial measurement is required to evaluate the three principal stress levels and directions. Stress analysis is carried out with the aid of finite element analysis. The over coring must be carried out using a stress free machining process and diametral measurements of the central hole measured with a precision of 0.05 μm resulting in an accuracy of 2 to 5 MPa.

2.6 Holographic Interferometry with Blind Hole Drilling

Although blind hole drilling with rosette strain gauging is an effective method it requires very accurate positioning of the hole to avoid significant errors. Also the relieved strains decline rapidly with distance from the edge of the hole resulting in loss of sensitivity at the gauge position together with complex averaging effects. Finally the rosette occupies approximately 650 mm^2 of surface area at a given measurement location making it impractical in certain regions or on small parts.

Moiré interferometry has been used to measure the in-plane strain relief around a drilled hole, but application of the moiré grating is also time consuming and suffers from some of the same limitations as strain gauges. Holographic interferometry is an alternative method, which can be used to measure out-of-plane strain relief in addition to in-plane relief. The out-of-plane strain relief formula have a similar form to the in-plane components (equation[5]). Methods have been developed using either in-plane or out-of-plane strain relief measurement. The original in-plane method required three separate holograms to be produced with different illumination and viewing directions. This made the optical arrangement quite complex. Therefore more recently the out-of-plane measurement approach has been developed requiring only a single hologram measurement. Finally current research is concerned with electronic speckle pattern interferometry as another potential method of strain relief measurement.

2.7 Ring Core (Trepanning) Method

The ring core method is a variation of the centre hole method enabling greater measurement penetration. A rosette containing three strain gauges is attached to the surface and then a circular annulus is milled around the rosette in incremental steps of 0.2 to 0.5 mm. The cylindrical core is stress relieved and the resulting relaxation strains measured. As the milling depth increases the change in relaxation strain decreases. Therefore to obtain sub-surface stress values an experimentally determined 'declining' function is used. To obtain information below 5 mm the first core may be removed and another rosette fixed to the bottom of the hole before milling a second core. The theoretical basis of the method assumes a biaxial stress state which is co-planer with the surface. This may not always be the case below the surface for some geometry's and applications. Also results from subsequent coring are perturbed by the presence of the hole.

The declining function, K, expressed in terms of the sensitivity to the strain measured in direction i, ε_i, with annulus depth, z, is evaluated from:

$$\frac{d\varepsilon_1(z)}{dz} = K_1(z)\frac{\sigma_1(z)}{E} \qquad [7]$$

A uniaxial test is needed to calibrate the function $K_1(z)$. For strain gauges positioned at angles α, α+45° and α+90° where α is the angle of the nearest principal stress to gauge 1, the strain measurements ε_1, ε_2 and ε_3 can be expressed in terms of the initial biaxial state as follows:

$$\sigma_{x,y} = \frac{\sigma_1+\sigma_2}{2} \pm \frac{1}{\sqrt{2}}\sqrt{(\sigma_1-\sigma_3)^2+(\sigma_3-\sigma_2)^2}$$

$$tan\,2\alpha = \frac{2\sigma_3-(\sigma_1+\sigma_2)}{\sigma_1-\sigma_2} \qquad [8]$$

where the stresses σ_1, σ_2 and σ_3 are given by:

$$\sigma_1 = \frac{E}{K_1^2(z)-\mu^2K_2^2(z)}\left[K_1(z)\frac{d\varepsilon_1}{dz}+\mu K_2(z)\frac{d\varepsilon_2}{dz}\right]$$

$$\sigma_2 = \frac{E}{K_1^2(z)-\mu^2K_2^2(z)}\left[K_1(z)\frac{d\varepsilon_2}{dz}+\mu K_2(z)\frac{d\varepsilon_1}{dz}\right] \qquad [9]$$

$$\sigma_3 = \frac{E}{K_1^2(z)-\mu K_2^2(z)}\left[K_1(z)\frac{d\varepsilon_3}{dz}+\mu K_2(z)\left(\frac{d\varepsilon_1}{dz}+\frac{d\varepsilon_2}{dz}-\frac{d\varepsilon_3}{dz}\right)\right]$$

The circular groove must be cut without introducing additional stresses. Air abrasion has been used on hard and tough materials but a method suited for use in most structural materials is Electr-Discharge (EDM) or Spark Erosion machining.EDM has the advantage of being relatively simple to apply because there are no rotating parts. However the part must be submerged in a suitable fluid, such as paraffin, and as a consequence the strain gauges need protection from this environment. Also local temperature changes may arise from EDM, which can influence the strain gauge response.

The minimum practical diameter for the strain gauge rosette implies a core width of at least 10 mm. The depth of the circular groove must be accurately machined. An error of 0.2 mm results in an error of 10% on stress. In the UK the centre hole method is currently preferred over the ring core method.

3 NON-DESTRUCTIVE METHODS

3.1 Diffraction Methods

3.1.1 X-ray Diffraction

X-ray diffraction is the most widely used nondestructive method for residual strain measurement. A monochromatic X-ray beam is used to measure selected crystallographic lattice spacings in the material using Bragg's law. The diffraction takes place in a thin surface (x,y) layer (≈20 μm) where it is assumed that the stress components, σ_z, τ_{xz} and τ_{yz} are zero. If the X-ray beam is incident on the sample in the iz plane, where i is a direction on the xy plane, the surface stress component, σ_i, is given by:

$$\sigma_i = \frac{E}{1+\upsilon}(\varepsilon_i - \varepsilon_z) \quad \text{(In general } \sigma_i \text{ will not be principal)} \qquad [10]$$

where E and υ are Young's modulus and Poissons ratio for the material. The geometry of the equipment does not permit the lattice spacing to be measured in the surface plane to obtain ε_i. Therefore measurements are made in directions z and inclined to the surface at an angle ψ (usually the x=z direction, 45°). In this case we find:

$$\sigma_i = \frac{E}{1+\upsilon}\frac{(\varepsilon_\psi - \varepsilon_z)}{sin^2\psi} \qquad [11]$$

In terms of lattice spacings, d, the term $(\varepsilon_\psi - \varepsilon_z)$ can be replaced by $(d_\psi - d_z)/d_z$. This relation is independent of the unstrained lattice spacing, d_0, achieved by assuming that strains are much smaller than 1.

To determine the surface biaxial stress state, σ_x, σ_y, it is necessary to evaluate the surface stress levels for at least three beam orientations.

To make residual stress measurements, lattice planes are selected to give large diffraction angles (usually 2 θ should be greater than 125° and preferably ~140°). Equation [11] is used (expressed in terms of lattice spacings) either with the two-tilt method as described above or, more accurately, with a range of tilt angles, ψ. When a range of angles is used least squares curve fitting is applied. This is known as the $\sin^2\psi$ method and usually 4 to 6 tilt angles are used with equal increments of $\sin^2\psi$. Typically diffraction angles can be measured to within ±0.01°, yielding a lattice spacing measurement accuracy of ±0.01 pm. For aluminium and steel this corresponds to an accuracy for stress determination of ±14 and ±41 MPa respectively. In practical situations errors can be larger than these theoretical estimates.

Problems arise when the ratio $(d_\psi - d_z)/\sin^2\psi$ is not a constant as suggested by equation [11]. This can occur when strong material texture is present such as from rolling and, although quite small, cannot be ignored in iron based materials. Other reasons include large grain materials, the existence of shear strains parallel to the surface and when significant stress gradients with depth are present. This is because the lattice strain deduced from changes in position of an X-ray diffraction peak represents an average value in a given direction only for those grain in the polycrystal which are oriented to diffract. However theoretical developments have addressed many of the problems. In the case of crystallographic texture it is possible to find angles of ψ in which the textured material has the same mechanical behaviour as in the isotropic case. To deal with significant shear stresses parallel to the surface the Dölle method has been developed. Finally when stress gradients are present the theoretical development must be extended to include the effective X-ray penetration depth. In this case it is assumed that the stress varies linearly with depth.

Recently research has been done to investigate the possibility of using high energy X-rays to enable much greater penetration into a component.

3.1.2 Neutron Diffraction

Neutron diffraction has a similar theoretical basis as X-ray diffraction but has the ability to penetrate much deeper into a component. The technique is currently the only nondestructive method available for measuring the whole stress tensor at a point within the sample. However an intense neutron beam source is required which is available only at a nuclear reactor or accelerator. Therefore the technique is often used to

test finite element codes, calibrate other techniques or undertake specific studies on relatively small components. The 'gauge volume' or volume sampled is defined by the intersection of the incident and scattered beams which are themselves defined by collimators.

Like X-ray diffraction the technique is based upon Bragg's law of diffraction. For lattice spacing of planes, d_{hkl}, with Miller indices hkl, the diffraction angles, θ_{hkl}, are given by:

$$2d_{hkl}\sin\theta_{hkl} = \lambda \quad \text{(neutron beam wavelength)} \qquad [12]$$

Polycrystalline materials give rise to cones of diffracted neutrons at angles $\varphi_{hkl} = 2\theta_{hkl}$ about the incident beam on the sample. The detector is scanned through φ_{hkl} to determine the peak count angle. A least squares method is used to determine the diffraction angle and width of the peak. The lattice strain tensor is then given from:

$$\varepsilon_{hkl} = \frac{(d_{hkl} - d_{0hkl})}{d_{0hkl}} = -\frac{cot\,\theta_{0hkl}(\varphi_{hkl} - \varphi_{0hkl})}{2} \qquad [13]$$

where the index '0' refers to values for the unstressed material. Obtaining values for d_0 and φ_0 can be difficult in practice. An annealed sample or an extreme part of a component may be used. Alternatively, a sum rule or boundary conditions may be used. To measure the strain in different directions the sample must be rotated accurately about the centre of the gauge volume. This contrasts with the X-ray method where the beam is rotated and the sample remains fixed. As with the X-ray method, large diffracted angles are preferred for high accuracy. To uniquely determine the full strain tensor at least six beam incident angles must be used as there are six independent components in the tensor. More angles can be used for higher accuracy.

An alternative to a steady reactor source of monochromatic neutrons is a pulsed white beam of neutrons given by a spallation source. In this case the polycrystalline diffraction is observed at a fixed φ and time of flight, t, is used to scan the different lattice planes. The advantage of this method is that strains may be measured from many lattice planes {hkl} at once. However the positioning of the sample is more critical as it influences the path length and hence the time of flight.

The stress tensor may be evaluated from the strain values with knowledge of the elastic constants of the test material. The principal axes are found by diagonalising the stress or strain matrix.

The accuracy of the diffracted angle can be measured to within ±0.005° corresponding to ±10 MPa. Practical path lengths in steel and aluminium are 50 and 100 mm respectively. Thus measurements up to 25 and 50 mm below the surface are achievable in these materials. Longer paths in the material, for deeper penetration, can be realised by sampling larger volumes. However, these may become unevenly illuminated by the neutron beam because of scattering and absorption. In principal, all crystalline materials can be examined, but some materials, such as nickel, scatter neutrons incoherently and others, such as titanium alloy, have small Bragg intensities making measurements at depth correspondingly more difficult.

The elastic constants used to evaluate the stress tensor, E and υ, depend upon the lattice planes {hkl} measured. This is because the elastic response of each grain to an applied stress is anisotropic. Often these constants are found by experimental calibration for the material. For steel the 211 Bragg reflection is a good choice.

3.2 Ultrasonic Methods

The velocity of ultrasound in any material is directly affected by the magnitude and direction of stresses in the material (acoustoelastic effect). Unfortunately the velocity changes introduced are small ($\sim 10^{-4}$) because acoustoelasticity is only a second order effect and, although such changes are easily measured in the laboratory, the effect can be swamped by other material changes, particularly preferred grain alignment (texture). Therefore it is imperative that material anisotropy effects are separated to enable correct stress assessment. For this reason the use of ultrasonics in the measurement of residual stresses is often limited to

particular cases. However it appears that ultrasonics could and has been used to measure changes in stress. Changes in observed velocity will be as a result of an integral of the stress field over the ultrasonic path. This has important consequences for example, for bending stress where the average stress may be zero through the specimen thickness. Ultrasonic methods fall into two categories, those using surface propagating waves and those using bulk waves. The literature in the last ten to fifteen years has been extensive and for more information the reader should refer to the bibliography in section 7.3.2.

The relationship between ultrasonic wave velocity, c, and stress, σ, for longitudinal waves and polarised shear waves are functions of the second and third order elastic constants. The relationships for these and other wave displacements are rigorously established (Thurston and Brugger 1964). For an isotropic solid:

$$c_{ij} = c_{ij0} + g_{ijk}\sigma_k \qquad [14]$$

where the index 'i' and 'j' refer to the ultrasonic propagation and particle displacement directions, and 'k' the stress direction. The index '0' refers to the unstressed state and g are the acoustoelastic constants. The acoustoelastic tensor is unsymmetrical. There are five different isotropic parameters but only three of them are independent. Values of g are expressed in terms of the Lamé second order elastic constants, λ and μ, the Murnaghan third order elastic constant , l, m, and n and the density, ρ of the material (Murnaghan 1951).

However the third order elastic constants are not generally known and research of them has concentrated on pure metals and alloys (Green 1973). Therefore because of this and also because velocity measurements are highly sensitive to microstructural features and mobile dislocation density, experimental calibration is usually carried out for the materials under study. It is often more practical to measure transit times rather than velocities as the Ultrasonic path length is usually not known to a sufficiently high precision.

Ultrasonic measurements are made using transducers operating at several MHz which are coupled to the test component using suitable jelly or grease. Early work concentrated on single crystals and polycrystalline aluminium (acoustoelastic constants are high and texture effects low in aluminium). However, to determine absolute stress levels, the velocities for unstressed material and the third order elastic constants are required. A number of methods have been developed to avoid many of the difficulties. Most of these rely upon combinations of bulk or surface wave velocity measurements.

3.2.1 Bulk Wave Methods

The longitudinal, V_L, and polarised shear wave velocities, V_1 and V_2, may be combined and normalised to obtain parameters independent of path length:

$$\textit{Compressive Parameter} = \frac{\left(V_L^2\right)}{\left(V_L^2 + V_1^2 + V_2^2\right)} \qquad \textit{Normalised Birefringence} = \frac{\left(V_1^2 - V_2^2\right)}{\left(V_L^2 + V_1^2 + V_2^2\right)} \qquad [15]$$

A plot of the compressive parameter against the normalised birefringence enables microstructural texture and biaxial stress levels to be separated in cases there the principal microstructural and texture axes are co-linear. The velocity anisotropy of polarised shear waves appears to be a linear function of stress anisotropy, σ_1-σ_2, although for absolute measurement the initial birefringence at zero stress is required. However the ultrasonic paths for the three wave modes must be the same in order to assume the same texture components in each case.

Phase difference techniques have been developed where accurate changes in stress levels can be measured. The approach is to measure the change in phase between the front and back faces of a plate when the stress level is changed. This change in phase is directly proportional to the sum of the residual stress levels, $\sigma_1+\sigma_2$. Measurements are made with ultrasonic transducers positioned on opposite sides of a plate and only an averaged through thickness measurement of the stress can be made. However careful field trials have indicated accuracy's of approximately ±15 MPa although ±10% of yield is more likely in general.

3.2.2 Surface Wave Methods

Surface wave velocities are related to residual stress levels in a similar manner to bulk waves. The penetration of these waves is approximately one wavelength which is typically 1 mm. Experimentally the surface acoustic waves (SAW) are generated by a wedge or electromagnetic acoustic transducer (EMAT). For absolute stress measurement the distance between the source and receiver transducers needs to be known with high precision. Again only the average stress level along the ultrasonic path can be measured. By making velocity measurements in orthogonal directions, stress and texture components can be separated. However, this separation depends upon the texture being accurately the same along two different paths and hence good material homogeneity.

Tomography methods have been used for Ultrasonics, yielding residual stress contours over the surface of a component from a prior knowledge of the third order elastic constants.

An alternative surface technique involves the measurement of the frequency dependence of the Rayleigh wave velocity (dispersion). The varying penetration can be used to provide information about the variation of stress with depth below the surface. For examples the reader is referred to the references.

3.3 Magnetic Methods

The magnetic properties of steels and other ferromagnetic materials are sensitive to internal stress levels due to magnetostriction and the subsequent magnetoelastic effect. Magnetostriction is the process thereby each magnetic domain is strained along its direction of magnetisation. Consequently a change in the stress level will result in a modification of the domain configuration so as to reduce the magnetoelastic energy. The energy of magnetisation, E, for a single crystal is given by:

$$E = K_1(\alpha_1^2\alpha_2^2 + \alpha_2^2\alpha_3^2 + \alpha_3^2\alpha_1^2) - \frac{3}{2}\lambda_{100}\left[\sigma_{11}\left(\alpha_1^2 - \frac{1}{3}\right) + \sigma_{22}\left(\alpha_2^2 - \frac{1}{3}\right)\sigma_{33}\left(\alpha_3^2 - \frac{1}{3}\right)\right] \qquad [16]$$
$$-3\lambda_{111}\left(\sigma_{12}\alpha_1\alpha_2 + \sigma_{23}\alpha_2\alpha_3 + \sigma_{31}\alpha_3\alpha_1\right) - M_s H\left(\alpha_1\beta_1 + \alpha_2\beta_2 + \alpha_3\beta_3\right)$$

where α_i and β_i are the direction cosines of magnetisation, M_s, and applied field, H, respectively, K_1 is the first magnetic anisotropy constant and λ_{100} and λ_{111} are the saturation magnetostrictions along the indicated axes. At minimum energy the magnetisation will align with the crystalline directions (the magnetic easy axes) indicated by the first term of the equation. When stress is applied in a polycrystal the second and third terms indicate that the relative numbers of domains aligned along each of the easy axes will change. For example for positive values of λ_{100} (e.g. steel) more domains will be aligned to the easy axes closest to the directions of maximum positive stress. The last term gives the energy of magnetisation in an applied field.

The magnetic hysteresis loop will be distorted as a consequence of stress so that there will be changes in the coercive field, remanence and permeability. However all these properties are also sensitive to the microstructure and mechanical properties of the material. Therefore for most experimental work, calibration against known stress levels is required. Additional magnetic methods employed for stress measurement include magnetic incremental permeability (μ_Δ), Barkhausen emission (BE), stress-induced magnetic anisotropy (SMA), magnetoacoustic emission (MAE) and magnetically induced velocity change (MIVC). For further information the reader is referred to the bibliograpy of section 7.3.3.

Practical measurements are normally carried out using an electromagnet to apply a magnetic field and various coils, magneto-resistors or Hall sensors to measure the electromagnetic signals. Measurements are usually limited to the surface of a component because of limited magnetic field penetration into the bulk. This arises from Eddy current screening, controlled by the frequency of both the applied and detected fields, and also from the physical size of the magnet. The MAE and MIVC techniques use ultrasonic transducers to detect the signal, in the former and generate and detect the signal in the later case.

Magnetic methods are usually rapid taking just a few minutes but an understanding the results enabling quantitative stress evaluation has traditionally been their weakness.

3.3.1 The Hysteresis Loop

A theoretical understanding of uniaxial stress upon the magnetic hysteresis loop has been well established for polycrystalline materials in recent years. The Langevin function representation the anhysteretic together with models of the polycrystalline magnetostriction have been used to predict and evaluate uniaxial stress levels. Full triaxial modelling has not been achieved however. Also full hysteresis loop measurement on plant components is usually not quantitatively possible because of the resulting non-uniform magnetic fields. Nevertheless a practical approach has been developed using low field magnetic suseptibility measurement for uniaxial stress level and direction measurement.

3.3.2 Coercive Field

Coercive field values can be made on practical components because at zero magnetic flux, B, there is no flux leakage. Therefore coercive field measurements (H at B=0) are independent of probe lift-off effects. However detailed studies by several workers have shown that sensitivity to the level of stress is much lower than to changes in microstructure, such as grain size or the effect of tempering. No practical system has been proposed using this method.

3.3.3 Permeability (μ)

Stress in the material results in partial domain alignment as discussed above. As a consequence the material becomes easier to magnetise along the maximum stress axis as compared to the minimum stress direction. Therefore the permeability is highest along this axis.

Measurement of incremental permeability, (μ_Δ), is achieved by superimposing a small amplitude secondary magnetic field upon a primary low frequency drive field. The frequency of the secondary must be high compared to the primary field but low enough to maximise penetration by minimising Eddy current effects. The permeability is related to the normalised modulus, $|\Delta Z/Z_0|$, of the electrical impedance variation $\Delta Z = Z-Z_0$ of the probe coil with respect to its value in free space of Z_0.

The uniaxial stress sensitivity is similar to that predicted for permeability using theoretical models when the stress and applied field are parallel. A monotonic relationship between stress and permeability is observed with maximum sensitivity to compressive stress levels.

A simplified method known as, Directional Effective Permeability, (DEP), has been developed for use in the field. This uses a fixed amplitude AC field electromagnet with Eddy current equipment for impedance measurement. The impedance or voltage is sensitive to the average permeability along the measuring direction. By rotating the probe, a directional effective permeability can be measured as a function of probe angle. In the absence of material texture, DEP will be constant and no magnetic anisotropy is measured in a stress free state. In a biaxial stress field, DEP will change sinusoidally as a function of the measuring angle, with maximum and minimum DEP along maximum and minimum stress axes respectively. DEP magnitudes are related to both the principal stress levels enabling, in addition to measurement of principal directions, a measure of the two principal surface stress values to be attempted.

Normally a biaxial calibration is carried out on the material of interest to enable absolute stress evaluation. However similar materials exhibit the same characteristics between stress and DEP, enabling some qualitative assessment without calibration. Understanding of the biaxial sensitivity can be understood in part by considering equation [16] together with the Langevin anhysteretic and magnetostriction formulation developed for magnetic hysteresis loops. However literature is mainly concerned only with uniaxial stress.

The weaknesses of the technique remain with its material sensitivity as well as the need for an unstressed reference DEP value.

3.3.4 Magnetic Anisotropy Methods

Anisotropy in the magnetic permeability is induced by stress as discussed above. There are two methods which make use of this effect to accurately measure the induced anisotropy and hence the stress parameter σ_1-σ_2 in the plane of the component surface.

The first method is known as stress-induced magnetic anisotropy (SMA). The Anisotropy induced by stress results in the rotation of an induced magnetic field away from the direction in which it was applied. For example if a uniaxial tensile stress exists in a steel component and the magnetic flux is applied at some angle with respect to that stress, the induced field will rotate towards the tensile axis. The maximum rotation occurs when the applied field is oriented at 45° to the tensile direction, while no rotation occurs when the magnetic field and stress axes are parallel or orthogonal.

To utilise this effect, an AC magnetic field is applied to the component by a C-core laminated mumetal electromagnet, and the rotation of the field away from its applied direction measured. This is achieved by inserting coils between the poles of the magnet. One set is aligned so as to measure the magnetic flux being applied by the magnet while the other is aligned so as to link to any flux in the orthogonal direction in the plane of the component surface. If the magnetic field is rotated away from its applied direction in the steel due to the presence of stress, the rotation angle of the field in the air just above the steel is simply related to the ratio of the voltages measured across the two sets of coils. The instrument then gives a voltage reading proportional to the rotation angle (the SMA signal).

The method employed is to rotate the whole probe, and therefore the applied magnetic field, and to measure the output voltage as a function of the rotation angle. The phase of this signal enables the principal stress directions to be determined while the amplitude is almost monotonically related to the size of the stress anisotropy present. If the steel has permeabilities μ_1 and μ_2 along the principal axes and the line joining the magnet poles makes an angle, α with μ_1 then it can be shown that, in the absence of hysteresis, the two rotation angles θ and ϕ, for the two field components **H** and **B** in air are related by:

$$Tan\theta = \frac{Tan(\phi-\alpha) - \frac{\mu_2}{\mu_1} Tan\phi}{\frac{\mu_2}{\mu_1} + Tan\phi . Tan(\phi-\alpha)} \qquad [17]$$

where θ and ϕ are measured in the opposite sense. When the probe is aligned along either of the principal directions (α=0 or 90°) we find $\theta = \phi = 0°$. The greatest field rotation angles and hence the largest SMA signal occurs whenever the probe direction approximately bisects the principal axes.

Theoretical development has yielded a relationship between the SMA signal and the stress anisotropy enabling the technique to be used for quantitative stress evaluation. The technique has the advantage of being a 'null' method. I.e. on flat plate when the stress is zero the SMA signal is almost zero. Therefore very high accuracy is achievable and a zero stress reference is not required. However, material anisotropy, such as grain alignment, does result in some measured SMA at zero stress, although this is usually small compared to the stress sensitivity. Similarly the two principal stress axes on the component surface can be accurately determined as the probe is rotated.

The second method, known as MAS, is similar, but the sensing coils are replaced by a second C-core magnet positioned orthogonally with respect to the energising magnet. The MAS signal is given by the voltage induced across a coil wound on this second C-core.

3.3.5 Barkhausen Emission (BE)

The magnetic Barkhausen effect is observed as transient pulses induced across a search coil placed near or around the ferromagnetic material undergoing a change in magnetisation. These pulses can either be observed individually by counting and amplitude sorting or as an rms signal as a function of the applied

magnetic field. The BE signal arises from irreversible magnetic domain wall movements as domain walls become successively pinned and jump over obstacles in the material. These obstacles are typically dislocation defects, second phases or grain boundaries and consequently the technique is particularly sensitive to the microstructure and mechanical properties of the component. The technique is also sensitive to the internal stress state because of the partial domain alignment along the maximum principal stress axis. Thus tensile and compressive stresses usually increases and decrease the BE signal respectively.

Correlation of BE behaviour with B-H loops and other magnetic parameters is complex and the high signal frequencies (1 to 100 kHz) limit penetration resulting in a strong bias towards near surface layers and thus surface condition.

The technique has been investigated for stress measurement for over 30 years and commercial equipment is available unlike most other magnetic techniques. However full experimental calibrations using known stresses are required on identical material to the components under test if quantitative stress information is required. The technique has been used to measure uniaxial, and in some cases, biaxial stress together with principal stress directions. The approach is to measure BE as a function of probe rotation and find the directions of maximum and minimum BE signal. These angles correspond to the principal stress axes in cases where the magnetic anisotropy due to stress is large compared to that due to material anisotropy such as rolling texture.

3.3.6 Magnetoacoustic emission (MAE)

When a ferromagnetic material is taken through its hysteresis loop the magnetisation of the steel takes place by creation of domains, movement of their boundaries and subsequent annihilation of these domains. In steel the effect of magnetostriction is to make each domain longer along its direction of magnetisation and shorter in the orthogonal directions. There is thus a small strain field associated with domain magnetisation. Consequently if the direction of the magnetostrictive strain changes as a result of abrupt domain wall movement (90° domain walls in steel), elastic waves will be generated locally (MAE). MAE is therefore composed of millions of discrete acoustic emissions which together form a continuous largely incoherent noise signal.

If the steel is subjected to stress, this will interact with the magnetisation process as discussed above resulting in partial alignment of the magnetisation vectors towards the tensile axis, or away from the compressive axis. MAE is highly sensitive to stress due, in part, to this partial domain alignment. MAE signal amplitudes decrease for increasing tension and compression.

Some uniaxial and biaxial modelling of the technique has been done using a simple model for polycrystalline magnetostriction. However theoretical development is generally weak.

The MAE signal is normally detected by a piezo-electric transducer while the component under test is subjected to a varying magnetic field. The rms signal as a function of applied field is measured. Typical signal bandwidths are 10 to 1000 kHz while applied fields are usually between 0.1 and 1000 Hz. The penetration for measurement is normally much greater than other magnetic methods because the acoustic signal is not attenuated by Eddy currents in the test component.

Like BE, MAE measurements as a function of probe orientation may be used to determine principal stress axes and, with calibration, stress level information. However this is often not effective because the signal amplitude decreases for stress of either sign making inversion to stress ambiguous. The MAE technique does not provide enough information for unique biaxial stress evaluation but must be used together with further information. This has been achieved by using MAE together with SMA measurements.

A unique development of the technique has been to measure variations of stress with depth. This was achieved by varying the measurement penetration by changing the frequency and using a complex biaxial stress model to invert the data to stress.

All work with this technique has been limited to laboratory studies.

3.3.7 Magnetically Induced Velocity Changes (MIVC)

Ultrasonic velocity is sensitive to the magnetic field strength in the material as well as the internal stress state. Both bulk and surface stresses can be investigated by using either bulk longitudinal and shear waves or surface Ultrasonic waves. The velocities are much less sensitive to preferred grain alignment compared to Ultrasonic stress measurement methods because the technique is principally based upon the magnetoelastic effect not acoustoelasticity.

Measurement of wave velocities as a function of applied magnetic field enables the uniaxial stress level to be determined. At zero stress as the field is increased the velocity increases. Typical increases in velocity are ~0.1%. When uniaxial tensile stress is present the increase in velocity is less marked but still monotonically related to the applied field. However compressive stress levels show a decrease in velocity for relatively low magnetic filed strengths, followed by an increase as the field is increased further. Thus both the sign and magnitude of the stress can be inferred from the wave velocity vs applied field data.

Further information can be obtained by measuring changes in the ultrasonic attenuation as a function of the applied field.

3.3.8 Magnetic Technique Combinations

In order to improve accuracy of measurement and reduce the influence of extraneous factors such as microstructure recent researches have used a combination of two or more magnetic methods. These are usually incorporated into a single instrument to ease use and maintain a rapid method. One examples includes a combination of BE, coercivity and permeability and a second one a combination of DEP, SMA and coercivity. Both are incorporated into portable systems for in-field use, the first being available commercially. The second system has been developed specifically for absolute biaxial stress measurement while the first has general use in NDT for materials characterisation.

3.4 Thermal Methods

Methods such as SPATE and TERSA make use of the thermoelestic effect to measure stress levels in a component remotely. The thermoelastic effect arises from conservation of energy and momentum resulting in small temperature changes accompanying changes in stress level. Although much smaller than 1 K, these temperature variations can be detected by modern intrared equipment.

3.4.1 The SPATE Method

The temperature difference, θ, above a reference temperature, T_0, for a linear isotropic material satisfies the following relation (Boley and Weiner 1960):

$$k\nabla^2\theta = \rho C_\varepsilon \frac{\partial\theta}{\partial t} + \alpha T_0 \frac{\partial S}{\partial t} \qquad [18]$$

where k, ρ, C_ε and α are the thermal conductivity, density, specific heat under constant strain and coefficient of linear expansion respectively for the material. S is the sum of the principal stresses and t the time. If thermal conduction can be neglected (adiabatic) the simple expression below can be derived:

$$\frac{\Delta T}{T_0} = -K\Delta S \quad where\ K = \alpha/(\rho C_\varepsilon) \qquad [19]$$

where ΔT and ΔS are changes in the temperature and bulk stress and K is known as the thermoelastic constant. Equation [19] is applied in the SPATE system (Stress Pattern Analysis by measurement of Thermal Emission) for stress analysis, and therefore the method is only valid when the rate of loading is significantly higher than the rate of thermal diffusion. For most metals >10 Hz cyclic loading is required.

SPATE is a computer controlled system with a liquid nitrogen cooled infrared detector operating in the 8-12 μm spectral range. The amplification must be phased locked to the mechanical cycling in order to achieve sufficient sensitivity (0.001 °C). Stress variations of resolution 0.4 and 1 MPa in aluminium and steel respectively can be observed using a stand-off distance of 25 cm and a spatial resolution of 0.5 mm. Calibration is often carried out using a strain gauge reference. However components must be coated with a thin matt black paint.

The technique has been applied to a wide range of materials including metals, plastic composites and bones. Application to fracture studies yields stress intensity factors and the extent of the plastic zone. The method can also be used for validation of finite element codes.

3.4.2 The TERSA Method

TERSA (Thermal Evaluation for Residual Stress Analysis) is being developed to address measurement of *static* residual stresses. The application of heat to a body results in a temperature change which depends upon the specific heat and thermal conductivity of the material. In an analogous manner to pressure in gases, the specific heat and conductivity depend upon the internal stress state.

The approach involves using an infrared laser as a focused heat source on the surface of the component while measuring the temperature rise with a very sensitive radiometer. Temperature rise monitored over time yields information about the stress level. The work is in its early research phase.

3.5 Optical Methods

3.5.1 Photoelastic Method

The photoelastic or stress birefringence method measures the stress from its birefringent effect upon otherwise optically isotropic material. To use the technique models of the component are made from photoelastic material. The model is loaded at a temperature above the critical temperature and sectioned after cooling and removal of the load. A transmission polariscope measures the fringe pattern enabling the stress to be assessed at each point in the section.

The sensitivity of the method depends upon the stress-optical coefficient, S, and the fringe-stress coefficient, F, for the photoelastic material. The fractional velocity difference per unit stress, S is expressed as:

$$S = \frac{(c_1 - c_2)}{c_0(\sigma_x - \sigma_y)} \quad and \; F = \lambda / S \qquad [20]$$

where c_0 is the wave velocity in the unstressed material, c_1 and c_2 the wave velocities in the stressed material and σ_x and σ_y the principal stress levels in the plane perpendicular to the propagation direction. λ is the wavelength of light. F is defined as the stress required to produce one fringe.

3.5.2 Photoelastic Coating Method

The use of models can be avoided by using a photoelastic coating and refection polariscope. Special foils of thickness 1.2 to 3.2 mm are glued or a coat of lacquer is sprayed onto the surface. A linear -polarised light illuminates the object while loaded. Interference patterns occur in the surface layer as an indication of the difference in the principal stress levels. The direction of the principal stresses are also indicated by the interference lines.

Photoelastic methods have the advantage of giving a global overview of a component.

3.5.3 Moiré Method

The surface of the component is coated with a fine grid pattern and compared with a reference grid after loading. The resulting Moiré fringe pattern is measured optically. Limits on strain sensitivity are set by the grid (~$4x10^{-6}$ m) which is produced by microtoming. The reference grid may be a second grid or a double exposure of the grid before and after loading.

3.5.4 Holography Method

A hologram is produced of the object before and after loading and an interference pattern generated. Changes in strain are imaged as black lines. The method is used to analyse dynamic loading effects. The strains evaluated are those parallel to the direction of visual observation.

3.5.5 Speckle Method

A laser beam incident upon a rough surface appears as a spot with a speckles, due to random variation in path length for light scattered to the observer. When imaged on a screen through a lens, the speckle size is proportional to the ratio of the light wavelength and lens aperture. To measure the strain in the plane of the surface, speckle images are formed before and after loading the object. When recorded onto photographic film and subsequently illuminated by laser, a fringe pattern is observed enabling displacements in the range 1 μm to 1 mm to be estimated.

3.6 Other Methods

3.6.1 Indentation Measurements

An indentation results in high stress concentrations in the vicinity of the area of contact, enabling the yield stress to be measured. However, in the presence of significant levels of residual stress, the stress distribution is modified resulting in unisotropic yielding around the indent. This can be measured quantitatively using optical interference. The approach has been effective for uniaxial residual tensile stress but is less sensitive to uniaxial compression and biaxial stress states.

3.6.2 Nuclear Hyperfine Methods

The internal strain field affects the coupling of the nuclear magnetic and elastic moments to the surrounding atomic lattice. NMR and perturbed angular correlation methods have shown sensitivity to internal strain. However some of these techniques require the material to contain an element isotope which possesses the appropriate nuclear property. For example, the Mössbauer effect requires ^{57}Fe to be present, and perturbed angular correlation requires an appropriate radioactive nuclide.

In NMR the stress field influences the electric field gradient produced in the vicinity of an ion by the surrounding ions and electrons. The resulting influence on the electric quadrupole moment of the ion in the lattice perturbs the NMR signal. This effect is currently limited to laboratory research. The NMR technique requires a large magnet with size limitations on the component under test.

4 NUMERICAL METHODS

Several approaches have been developed for quantitative analytical methods to predict residual stress distributions in manufactured components and parts. With the advent of widely available computers, numerical tools such as the finite element method (FEM) and finite difference method (FDM) were extensively applied to solving residual stress problems. The reader is referred to section 4.4 for summaries of computational residual stress analysis methods. The main areas of interest are in the fields of welding, forming and heat treating.

Consider the welding process. Equations for the temperature distribution due to a moving heat source were published by Rosenthal. Early attempts to predict residual stresses due to welding by Tall and Vaidyanathan, applied simplified analytical approaches which indicated the distribution of stress but had limited accuracy. The development of finite element computer codes enabled numerical solution of the

heat transfer and structural response and was applied by Hibbitt, Friedman and Hsu, identified welding parameters such as power and torch speed as being more important than material properties or cooling conditions. Rybicki and co-workers in the USA calculated temperature distributions using the Rosenthal equations and applied these to the elastic-plastic finite element stress analysis for a range of weld geometry's of butt welded pipes and plates. Argyris and others in Germany, incorporated the effect of phase changes during solidification into a finite element analysis of the entire thermoelastic-viscoelastic process.

Phase changes were found to alter stress histories during cool-down but to have only a small effect on steady state stresses apart from some relatively minor local variations. In the UK work has been carried out by The Welding Institute where Leggatt used an empirical/analytical approach to predict residual stresses. Recently simplified approaches, suitable for application on PCs, have been reconsidered by Japanese researchers such as Umemoto. These approaches argue, on the basis of comparison with measurements, that the last welding pass dominates the residual stress distribution and the dependence of material behaviour on temperature is of no importance after the material cools from its re crystallisation temperature.

Two approaches can be undertaken to determine temperature distributions during welding. The first approach based on the classical equations of a moving heat source developed by Rosenthal, has the advantage of being analytically tractable and programmable for a PC. However it contains simplifications which tend to limit its accuracy. However it is considered useful because it enables a range of welding parameters to be easily and cheaply investigated. A second approach is to model transient heat transfer due to welding by finite element analysis. This enables factors, such as surface heat loss and weld area, not easily included in the analytical approach to be incorporated. Temperature distributions obtained in this way can be easily applied in a structural model.

The first approach can be used to predict the temperature distribution in a wide finite width plate with adiabatic surfaces produced by a heat source travelling in a line anywhere through its thickness. A method of superimposing solutions for a number of imaginary heat sources can be used. Input data for computer code comprises the welding parameters of interpass temperature, heat rate, torch speed and weld efficiency and the thermal properties and thickness of the plate. Examples of temperature distributions can be calculated at different times enabling investigation of parameters.

The second approach for thermal analysis of the welded plates is carried out using a two-dimensional unit thickness finite element model. A number of software codes exit for performing the analysis. The appropriate assumed boundary conditions should be applied and only the final weld pass normally needs to be considered. The approach is to consider two sets of temperature fields. The first just before the final pass weld torch heat was applied (interpass condition) and the other just after the deposit of the final pass filler material. The weld top surface is then allowed to cool down to the estimated recrystallisation temperature.

A two-dimensional finite element model program is then used to carry out linear and non-linear analysis of residual stresses. In the linear (elastic) case the resultant stress field is determined by considering the welding cycle as a two stage operation (heat up and cool down), where the weld material is considered to have no strength during the first stage. Stresses are determined by summation of the results from both phases. For the non-linear (elastic/plastic) analysis, typical room temperature work-hardening characteristics are used for the parent and as-deposited weld materials. Stresses due to the cool down phase are then determined.

Finite element analysis can also predict the distortion of the plate due to the final weld pass.

Computer codes for modelling of residual stresses is still under development. However, many codes developed for specific functions predict stress distributions in good general agreement with measurement methods. Work is usually limited to relatively simple geometry's.

5 OFFSHORE POTENTIAL

There is currently little residual stress measurement carried out in the offshore industry, so that conservative estimates have to be made of fatigue life. However there growing interest and some use of semi-destructive methods such as the centre-hole technique for specific critical problems. Also finite element calculation has been applied to offshore nodes. Virtually no NDT methods have been used except a few magnetic BE measurements which the industry has found to be of limited reliability. Bearing in mind the working environment and the size and nature of the structures, there will always be limitations on the application of all such techniques.

Destructive techniques require enormous preparation and effort and have largely given way to the use of semi-destructive methods as these have become established. Even so, semi-destructive methods are slow compared with NDT methods, and besides greater cost per measured strain, slightly damage the component. There could be some growth in centre-hole strain-gauging, especially in combination with finite-element modelling or NDT measurement.

In contrast, in the past NDT technology for stress measurement has not been sufficiently well developed to compete in terms of reliability and accuracy. However X-ray diffraction has now been established over a number of years and small portable equipment is available for rapid measurement of surface stresses. The technique has some limitations, not least its very low penetration making surface preparation critical. Corrections due to preferred grain alignment, stress gradients and triaxial stress would also be difficult to make in-situ. It is therefore difficult to see a large growth in it application offshore.

Other NDT techniques such as ultrasonic and more recently magnetic methods, have made up ground both in the theoretical establishment of principles and in practical implementation. These methods do not measure stress or strain directly but properties of the material which are influenced by the internal stress state, which must in turn be calibrated in terms of stress. Therefore data has always been difficult to interpret and sensitivity to other material aspects needed to be addressed before the technology could be practical enough for use outside the laboratory. Ultrasonic techniques can only give a line average measurement along the propagation path of the ultrasound and will suffer from access problems because of the need of using probe pairs on either side of the measurement location. Local variations in preferred grain alignment to which the technique is extremely sensitive, makes it difficult to use in practice, except for specific applications such as monitoring stress changes. It is likely that there will be some increase in the use of ultrasonic strain gauges in the context of for instance monitoring the tightening of bolts and connectors.

Magnetic methods also have access limitations because of the need of placing the probe directly over the measurement area which must be flat or gently curved. Therefore measurements below the weld cap, where the stress is likely to be highest, cannot be obtained. Also magnetic methods require careful calibration for each type of steel. This may not be a great restriction if only a few steel types are predominantly used in offshore structures. A substantial programme is under way (funded by the CEC Thermie initiative) to prepare AEA's MAPS system for offshore use, and the results of this are awaited with great interest.

Optical and thermal methods offer the ultimate in rapid coverage of large areas but the developed technology is limited to measurement of dynamic stress changes.

Numerical methods are now quite powerful for evaluation of residual stress distruibutions in and around welds. Of course the approach is generic and will not indicate which, of a number of similar welded joints, contains high or low stress levels due for instance to variations in procedure, but it will give an indication of where the stresses are likely to be serious and what influence reaction stresses will have from the rest of the structure. We recommend an alliance between finite element calculation and NDT measurements. Finite element is generic because input quantities such as heat input, torch speed etc. have to be estimated and typical values used. However one or two NDT results from a particular weld may enable characteristic trends from finite element analysis to be better 'anchored' for each specific weldment. Convesely

characteristic trends from finite element may enable NDT data to be extrapolated into key inaccessible regions such as within the weld.

Table 4 summarises the application and potential of stress measurement techniques in the context of the offshore industry.

6 TABLES

Technique	Measured Quantities	Required Information	Measurement Time per Location	Spatial Resolution	Penetration	Measured Quantities of Stress Tensor	Accuracy of Principal axes Determination	Accuracy of Stress Level Determination
Successive Layer Removal Methods	Strain relief by releasing stresses measured with resistance gauges	Elastic constants Sectioning formulae coefficients			Depends on method. Can be throughout specimen	Biaxial or Triaxial throughout specimen		±10 MPa
Curvature	Curvature measurement during surface removal	Elastic constants			Throughout specimen thickness	Uniaxial stress		
Centre Hole	Strain relief from drilled hole measured with resistance gauges	Elastic constants Centre hole coefficients A, B	1 to 2 hours	>0.5 mm^2 but hole separation > 3 diameters (3 mm)	Depth equal to hole diameter ≤5 mm	Surface biaxial		±8% for $<0.6\sigma_y$ Larger (<15%) for $>>0.6\sigma_y$
Incremental Drilling	Incremental strain relief from incrementally drilled hole measured with resistance gauges	Elastic constants Incremental centre hole coefficients a, b with depth		>0.5 mm^2 but hole separation > 3 diameters (3 mm)	Depth equal to hole diameter ≤5 mm	Biaxial as a function of depth (currently limited to eqi-biaxial)		Unestablished
Deep Hole	Shape changes of drilled hole after over coring measured with resistance gauges	Elastic constants		100 mm^2	No limitation, (averaging over 6 mm depth increments)	Triaxial at discrete depths		<±10%
Optical Method with Centre Hole	Strain relief from drilled hole measured with optical methods	Elastic constants Centre hole coefficients A, B		>0.5 mm^2 but hole separation > 3 diameters (3 mm)	Depth equal to hole diameter ≤5 mm	Surface biaxial.		

Ring Core (Trepanning)	Strain relief from milled annulus measured with resistance gauges	Elastic constants Ring core declining factors		150 mm^2 but separation of rings greater	5 mm (multiples achievable by removing earlier cores)	Surface and subsurface biaxial		±10 MPa achieved probably similar accuracy as centre hole in general.

Table 1. Destructive and Semi-destructive Techniques: Definition and Performance.

Technique Type	Techniques	Measured Quantities	Required Information	Material Limitations	Access Limitations	Relative Sensitivity to Stress & Microstructure	Current State of Development	Contact or Non contact	Portable Equipment
Diffraction	X-ray Diffraction	Lattice spacing using measured diffraction angles	Elastic constants	Crystalline materials, usually metallic	Smooth surface required	Some problems from large grains, severe plastic damage, rolling and second phase microstructures	Established theoretical and practical technology.	Noncontact	Yes. Commercial equipment widely available.
	Neutron Diffraction	Lattice spacing using measured diffraction angles	Lattice spacing for unstressed material. Elastic constants to evaluate stress	Crystalline materials	Component must be portable and fit in Diffractometer. Maximum thickness ~50 and 100 mm for steel and aluminium.	As X-ray diffraction but less severe for large grains due to greater sampled volumes	Relatively highly developed. Some further theoretical understanding needed.	Noncontact	No. Future development may include portable method
Ultrasonic	Bulk Methods	Longitudinal and shear wave velocities	Third order elastic constants and unstressed reference	Few limitations in theory but many in practice	Bulk ultrasonic wave propagation directions limited in practical applications	Technique much more sensitive to material anisotropy than stress but separation achieved in some cases	Laboratory based for absolute stress. In-field equipment for stress changes. Theory understood	Contact. Ultrasonic transducers must be acoustically coupled	Yes Some equipment commercially available
	Surface Methods	Rayleigh & skimming longitudinal wave velocities	Third order elastic constants and unstressed reference	Few limitations in theory but many in practice	Requires velocity measurement in two orthogonal directions	Technique much more sensitive to material anisotropy than stress	Laboratory equipment. Theory understood	Contact when using Ultrasonic transducers. Noncontact for EMAT's	Yes

Table 2. Nondestructive Testing Techniques - Technique Definition, Advantages and Limitations.

Technique Type	Techniques	Measured Quantities	Required Information	Material Limitations	Access Limitations	Relative Sensitivity to Stress & Microstructure	Current State of Development	Contact or Noncontact	Portable Equipment
Magnetic	Hysteresis Loop	B-H Loop	Various material constants and unstressed reference	Ferromagnetic materials only.	Requires flat or curved surface under probe. Measurement only directly under probe.	Sensitive to microstructure and stress	Mostly laboratory work. Some in-field work and equipment. Theory for uniaxial stress understood	Contact	Yes one system known
	Coercive Field	Coercive field	Unstressed reference and full experimental calibration	Ferromagnetic materials only.	Requires flat or curved surface under probe. Measurement only directly under probe.	Much more sensitive to microstructure than to stress	Laboratory work only. Theory weak.	Contact	No
	Permeability Methods	Probe impedance	Unstressed reference and experimental calibration	Ferromagnetic materials only.	Requires flat or curved surface under probe. Measurement only directly under probe.	Sensitivity to microstructure and stress is comparable	Laboratory and in-field work. Theory for uniaxial stress understood.	Contact	Yes Not commercially available
	Anisotropy Methods	Magnetic field rotation	Some experimental calibration	Ferromagnetic materials only.	Requires flat or curved surface under probe. Measurement only directly under probe.	Usually much more sensitive to stress than material anisotropy, but some sensitivity to rolling texture.	Increasing amount of in-field work. Theory understood for biaxial stress	Contact	Yes Commerciall y available.

Table 2 (contd). Nondestructive Testing Techniques - Technique Definition, Advantages and Limitations.

Technique Type	Techniques	Measured Quantities	Required Information	Material Limitations	Access Limitations	Relative Sensitivity to Stress & Microstructure	Current State of Development	Contact or Noncontact	Portable Equipment
Magnetic Continued	Barkhausen Emission	Electro-magnetic pulses induced across coil vs applied field	Full experimental calibration and unstressed reference	Ferromagnetic materials only.	Requires flat or curved surface under probe. Measurement only directly under probe.	Generally more sensitive to microstructure than stress	More field work than other magnetic methods. Some theoretical principals understood for uniaxial stress	Contact	Yes Commerciall y available.
	Magneto-acoustic Emission	Acoustic emission generated from domain wall motion vs applied field	Full experimental calibration and unstressed reference	Ferromagnetic materials only.	Requires flat or curved surface under probe. Measurement only directly under probe.	Sensitivity to microstructure and stress is comparable	Limited to laboratory work. Theoretical understanding is growing	Contact	Yes Not commercially available
	Magnetically Induced Velocity Change	Shear wave velocities as a function of applied magnetic field	Experimental calibration and unstressed reference	Ferromagnetic materials only.	Requires relatively uniform magnetic field along ultrasonic path length	Sensitivity to microstructure and stress is comparable	Limited to laboratory work	Contact	No
	Magnetic Technique Combinations	Various of the above	Experimental calibration and theoretical modelling	Ferromagnetic materials only	Requires flat or curved surface under probe. Measurement only directly under probe.	More sensitive to stress than microstructure	Laboratory work and early field work	Contact	Yes, some commercially available, others as prototype

Table 2(contd). Nondestructive Testing Techniques - Technique Definition, Advantages and Limitations.

Technique Type	Techniques	Measured Quantities	Required Information	Material Limitations	Access Limitations	Relative Sensitivity to Stress & Microstructure	Current State of Development	Contact or Noncontact	Portable Equipment
Thermal	SPATE	Temperature changes	Thermoelastic constant, strain gauge reference	Wide range of materials.	Component must be painted matt black		Used for in-field work	Noncontact - remote sensing	Yes
	TERSA	Temperature changes	Absorption, emissivity constants, and thermal properties	Wide range of materials		Unestablished	In early research phase	Noncontact - remote sensing	No
Optical	Photoelasticity	Polarised light interference pattern	Stress-optical coefficient for photoelastic material	Must be done on optically birefringent model of component	Component itself not accessed	Not applicable	Established usage. Not directly applicable for residual stress measurement	Noncontact - remote sensing	Yes
	Photoelastic Coating	Polarised light interference pattern	Stress-optical coefficient for photoelastic material	Wide range of materials	Surface of material must be coated	Not applicable	Established usage.	Noncontact remote sensing	Yes

Table 2(concluded). Nondestructive Testing Techniques - Technique Definition, Advantages and Limitations.

Technique Type	Techniques	Measurement Time per Location (excl set-up time)	Spatial Resolution	Penetration	Measured Quantities of Stress Tensor	Accuracy of Principal Axes Determination	Accuracy of Stress Level Determination
Diffraction	X-ray Diffraction	10 seconds. 15 minutes using 9 value ψ $\sin^2\psi$ method	<1 mm^2	5 to 30 μm	σ_x.and σ_y in the surface plane	± using $\sin^2\psi$ method	±40 MPa
	Neutron Diffraction	Typically 1 to 30 minutes per strain. 6 to 180 minutes for full tensor measurement	≥1 mm^3 volume	25 mm in steel. 70 mm in aluminium	All six independent quantities of strain tensor measured	±1° for full angular scan ±2 to 5° for 6 beam directions	±15 MPa in crystalline materials
Ultrasonic	Bulk Methods	~30 seconds	>5 mm^2	Through thickness line average	In principal σ_x, σ_y, σ_z by using 3 propagation directions but usually only σ_x & σ_y or σ_x -σ_y.	Assumes principal axes aligned with material anisotropy axes	±5 to 10% of yield for measurement of stress changes. Poor for absolute stress evaluation
	Surface Methods	~20 seconds	≥50 mm^2	One to two wavelengths, typically 0.5 to 2 mm	σ_x -σ_y and information on subsurface gradients using dispersion method	±10°	±5 to 10% of yield for measurement of stress changes. Better than bulk methods for absolute.
Magnetic	Hysteresis Loop	1 - 5 minutes	>10 mm^2	0.5 to 10 mm	Uniaxial, σ_x.	Unknown	±10% of yield for compression Worse for certain biaxial tensile states

Table 3. Nondestructive Testing Techniques - Technique Performance.

Technique Type	Techniques	Measurement Time per Location (excl set-up time)	Spatial Resolution	Penetration	Measured Quantities of Stress Tensor	Accuracy of Principal Axes Determination	Accuracy of Stress Level Determination
Magnetic Continued	Coercive Field	~ 1 second for each probe orientation	>10 mm^2	0.5 to 10 mm	Uniaxial or σ_x -σ_y by comparing orthogonal directions	Unknown	Unknown (±15 MPa using orthogonal measurement method in one material)
	Permeability Methods	1 - 2 minutes for complete probe rotation	~10 mm^2	0.1 to 10 mm	σ_x.and σ_y in the surface plane	±5°	±10% of yield for compression Worse for certain biaxial tensile states
	Anisotropy Methods	1 minute for complete probe rotation	~100 mm^2	0.1 to 10 mm	σ_x.-σ_y in the surface plane	±5°	±5% of yield
	Barkhausen Emission	0.5 or 10 minutes for singular rms and field scan respectively for complete probe rotation	~10 mm^2	20 to 300 μm	Uniaxial, σ_x. Possibly σ_x.and σ_y in the surface plane	±10°	
	Magneto-acoustic Emission	1 or 20 minutes for singular rms and field scan respectively for complete probe rotation	~100 mm^2	0.1 to 20 mm	Uniaxial, σ_x. Also ~σ^2_x+σ^2_y in the surface plane. Information on subsurface gradients using frequency scan method	±15° to ±25° when $\lvert\sigma_x\rvert \neq \lvert\sigma_y\rvert$ else ambiguous	

Table 3(contd). Nondestructive Testing Techniques - Technique Performance.

Technique Type	Techniques	Measurement Time per Location (excluding set-up time)	Spatial Resolution	Penetration	Measured Quantities of Stress Tensor	Accuracy of Principal Axes Determination	Accuracy of Stress Level Determination
Magnetic Continued	Magnetically Induced Velocity Change	10 seconds	Equal to ultrasonic path length ≥50 mm^2	Bulk waves - through thickness line average. Surface waves - 0.5 to 2 mm.	Uniaxial, σ_x. Possibly biaxial with more work	Unknown	Unestablished (±35 MPa in one study)
	Magnetic Technique Combinations	1 minute	50 mm^2	2 mm in structural steels	σ_x and σ_y in the surface plane	±5°	<40 MPa
Thermal	SPATE	Rapid 'rough' large area scan or high resolution fine scan	0.5 mm^2	Surface and subsurface stresses influence measurement	Dynamic changes in sum of principal stresses $\Delta\sigma_x$,+$\Delta\sigma_y$,+$\Delta\sigma_z$	Cannot normally be measured	Dynamic changes of ±1 MPa
	TERSA	Unestablished	9 mm^2 not established	Penetration controlled by heat input but is unestablished	Sum of principal stresses	Cannot normally be measured	Unestablished
Optical	Photoelasticity	Need to make model of component		Entire stress distribution throughout volume measured	Difference in principal stresses, σ_x-σ_y		
	Photoelastic Coating			Surface measurement	Difference in principal stresses, σ_x-σ_y		

Table 3(concluded). Nondestructive Testing Techniques - Technique Performance.

Technique	Application	Potential	Comments
Successive Layer Removal Methods	Full bulk stress characterisation of small parts	Limited use for special fracture studies	Very time consuming and hence expensive. Use semi-destructive methods in preference
Curvature Method	Uniaxial stress measurement of strips	Not appropriate for offshore	
Centre Hole and Incremental Drilling Methods	Surface and subsurface biaxial stress characterisation with penetration of 5 mm. Some stress variation with depth possible.	Probably already used for topside and construction yard use. Potential for underwater unclear.	Relatively slow (and thus expensive) compared with NDT methods. Method largely accepted by industry, where surface damage is acceptable.
Deep Hole Method	Through thickness triaxial stress assuming biaxial stress parallel to surface plane.	Could be used topside and at construction yard. Unlikely to be able to apply underwater.	Slow measurement. The need for stress-free overcoring requires care in offshore environment. Relatively low spatial resolution for high stress gradients near welds. Some damage must be acceptable; potential therefore limited.
Holographic Interferometry with Blind Hole Drilling	Same as centre hole method.	Limited to topside and construction yard.	Same as centre hole method but not subject to limitations of resistance strain gauges.
Ring Core (Trepanning) Method	Surface and subsurface biaxial stress with penetration of 5 or potentially as high as 25 mm	Likely to be limited to topside and construction yard	In UK the centre hole methods (almost equivalent) are usually preferred.
X-ray Diffraction	Close surface biaxial stress characterisation	Use at construction yards and topside.	Portable miniature PSD detectors allow easy in-situ use. Underwater use would require considerable development (est. £750k). Surface finish and removal of damage critical. Significant preparation required before measurement

Table 4 Application and potential of destructive, semi-destructive, nondestructive and numerical methods for use in the offshore industry.

Technique	Application	Potential	Comments
Neutron Diffraction	Triaxial stress measurement throughout bulk to depth 25 mm in steel	Not an in-situ technique therefore limited to model weldments or nodes which can be accommodated on a diffractometer	Could be used to validate numerical methods or nondestructive measurement techniques. Cost controlled by neutron beam charges..
Ultrasonic Surface and Bulk Methods	Uniaxial, stress anisotropy, biaxial stress averaged over propagation length	Absolute measurement likely to be limited to laboratory for some time. Commercial system (IzfP) available for measuring stress changes eg in bolts (*internal* strain gauge).	Could be used topside and, with development, underwater. Avoids the need for surface polishing required by strain gauges. Strong grain textural sensitivity may require fingerprinting critical regions first. Very quick.
Magnetic Hysteresis Loop, Coercivity and Permeability Methods	Uniaxial and biaxial stress with penetration of a few mm	Could be used topside and at construction yards with development. Underwater use possible with development	Requires calibration. Magnetic technique combinations are likely to be more accurate and reliable. Very quick.
Magnetic Anisotropy Methods	Difference between two principal stress levels in surface plane. Penetration of a few mm	Could be used topside and at construction yards with minimal system development. Also potential underwater use.	More reliable than most magnetic techniques, but gives less information on stress field (only stress differences). Very quick
Magnetic Barkhausen Emission	Uniaxial and possibly biaxial stress with penetration ~0.3 mm in steel	Can be used topside or construction yard with existing systems. Underwater use would require some development.	Requires calibration. Sensitivity to microstructure and surface condition likely to limit confidence in measurements. A stress relief heat treatment changes sensitivity significantly. Very quick. Poor record with some operators.
Magnetoacoustic Emission	Uniaxial and limited biaxial stress with penetration up to 10 mm. Also potential for stress as a function of depth information.	Could be used topside and at construction yards with system development. Also potential underwater use.	Requires low acoustic noise environment. Stress information limited unless combined with other technique. Complicated technique, but very quick.

Table 4(contd) Application and potential of destructive, semi-destructive, nondestructive and numerical methods for use in the offshore industry.

Technique	Application	Potential	Comments
Magnetically Induced Ultrasonic Velocity Changes	Uniaxial stress as line average along propagation direction.	Requires a lot more development than ultrasonic methods but otherwise potential is similar. Less sensitive to preferred grain alignment.	Could be used topside and underwater with development. A complicated technique, but avoids the need for surface polishing required by strain gauges.
Magnetic Technique Combinations	Biaxial stress with penetration of a few mm	Two types of system (MAPS, 3MA) available. Largely developed for topside and construction yard use. Underwater use potential.	The best choice for magnetic NDT methods. Give higher reliability although some calibration required for each steel type. One system (MAPS) already designed for offshore industry. Relatively quick to operate.
The SPATE Method	Dynamic changes in sum of principal stresses. Surface and subsurface stresses influence measurement.	Rapid coverage of large areas. Currently in use on construction plant. Should be applicable topside and on construction yard.	Does not measure residual stresses.
The TERSA Method	Similar to SPATE but sensitive to static stresses	Greater potential than SPATE but totally undeveloped. Possible problems for quantitative method.	When developed may be powerful for rapid (at least) qualitative stress assessment.
Optical Methods (except photoelastic)	Dynamic changes in difference in principal stresses in surface.	Limited to topside and construction yard. Rapid coverage.	Does not measure residual stresses. Photoelastic method does, but only for optically birefringent models.
Indentation Measurements	Uniaxial tensile stress at surface.	Could be used but appears to be somewhat qualitative.	Limited stress information.
Numerical Methods	Calculates all stress components throughout structure bulk. Also calculates other important material aspects.	Could be used to assess likely stress distributions for different welded geometries. Potential for extrapolation of stresses from experimental measurements to inaccessible regions such as under weld caps.	Once correct model exists for given application, method is cheap and rapid. By itself, subject to absolute errors. Should be pursued in combination with some measurements, eg centre hole-drilling or magnetics.

Table 4 (concluded) Application and potential of destructive, semi-destructive, nondestructive and numerical methods for use in the offshore industry.

7 BIBLIOGRAPHY

7.1 General Reviews

M.R. James and O. Buck (1980). 'Quantitative Nondestructive Measurements of Residual Stresses', Critical Rev. Solid State Mat. Sci. **9**(1), pp61-105.

C.O. Ruud (1982). 'A Review of Selected Non-destructive Methods for residual Stress Measurement', N.D.T. Int. Feb., pp15-23.

T.R. Finlayson (1982). 'Residual Stress Analysis: A Review', Met. Forum. **6**, No.1, Focal Point: residual Stress, Dec. 2, pp4-10.

S. Takahashi and K. Shimizu (1984). 'Development of Experimental Stress-Strain Analysis and Its Contribution to Practical Design', Nondestructive Testing J., Japan, vol.**2**, No.3, pp125-131.

V. Hauk (1987). 'Techniques for Determination of Residual Stresses - International State of the Art', N.D.T. Proceedings of 4th European Conf., **3**, 13-17 Sept. 1987, Eds. J.M. farley and R.W. Nickol, pp1580-1592.

Residual Stresses in Science and Technology (1988). Vols 1 & 2, Eds. E. Macherauch and V. Hauk, Int. Conf. on residual stresses, 1986, Garmisch-Partenkirchen (FRG), Verlag.

Southwest Research Institute (1989). 'Review of Pipeline Integrity - Stress State Measurement Techniques', SWRI Report 17-2221, San Antonio, Texas, USA.

J. Shackelford and B.D. Brown (1990). 'A Critical Review of Residual Stress Technology', Inv. Adv. N.D.T., **15**, pp195-215.

B. Pathiraj, G. Ekambaranathan, P. Brand, P.C.P.M. Teirlinck amd B.H. Kolster (1991). 'Non-destructive Evaluation of Internal or Residual stresses by Different Techniques', Adv. Materials: Cost Effectiveness, Quality Control, Health and Environment, Eds. A. Kwakernaak and L. van Arkel, Pub. Elservier Science, pp301-311.

L. Mordist (1993). 'Residual Stresses: Nondestructive Evaluation', Encyclopedia Materials Characterisation, Eds. R.W. Cahn and E. Lifshin, Pergamon Press, pp417-422.

7.2 Destructive and Semi-destructive Methods

E.M. Beaney (1976). 'Accurate Measurement of Residual Stress on Any Steel Using the Centre Hole Method',Strain **12**, no 3, pp99-106.

F. Witt, F. Lee and W. Rider (1983). 'A Comparison of Residual-stress Measurements Using Blind-hole, Abrasive-jet and Trepan-ring Methods', Exp. Tech. 7, no 2, pp41-44.

D.H. Mitchell (1985). 'Deep Hole Residual Stress Measurements in Metallic Specimens', IEE Colloquium (Digest), no 1985/31, Pub. IEE, London, Eng., P5, 1-5, 2.

D.V. Nelson and J.T. McCrickerd (1986). 'Residual Stress Developement Through Combined Use of Holographic Interferometry and Blind-hole Drilling', Exp. Mech. **26**, no4, pp371-378.

E. Procter (1986). 'Principles and Practice of Centre-Hole Residual Stress Measurements',Conf. Impact Surface Treatment, Bedford, England, Pub. Elserier Applied Science Pub.,London & New York, pp23-30.

A.N. Huntz and J.G. Zhao (1988). 'A curvature Method for Determining the Stress Distribution in a Duplex Oxide-metallic Substrate System', in Residual Stresses in Science and Technology (1988). Vols 1 & 2,

Eds. E. Macherauch and V. Hauk, Int. Conf. on residual stresses, 1986, Garmisch-Partenkirchen (FRG), Verlag, pp223-230.

G.S. Schajer (1988a). 'Measurement of Non-uniform Residual Stresses Using the Hole Drilling Method: Part I. Stress Calculation Procedures', J. Engineering Materials ant Technology, Vol.**110**, No.4, Oct., pp 338-343.

G.S. Schajer (1988b). 'Measurement of Non-uniform Residual Stresses Using the Hole Drilling Method: Part II. Practical Application of the Integral Method', J. Engineering Materials ant Technology, Vol.**110**, No.4, Oct., pp 344-349.

R.W. Hampton and D.V. Nelson (1989). 'On the Use of the Hole Drilling Technique for Residual Stress Measurements in Thin Welded Plates', Nondestructive Evaluation, NDE Planning and Application, The 1989 ASME Pressure Vessels and Piping Conf., Honolulu, Usa, Ed R.D. Streit, pp163-170.

M. Beghini and L. Bertini (1990). 'Residual Stress Modelling by Experimental Measurements and Finte Element Analysis', J. of Strain Anal. **25**,no2, pp103-109.

G. Nicoletto (1990). 'Moire Interferometry Determination of Residual Stresses in Presence of Gradients', Proc. 1990 SEM Spring Council on Exp. Mech., Alburquerque, USA, pp299-303.

S.T. lin and C.P. Hu (1992). 'Improved Holographic Blind-hole Methods for Measuring Residual Stresses', Proc. of the 13th World Conf. on NDT, San Paulo (Brazil) **1**,pp391-398, Eds C. Hallai and P. Kulcsar.

7.3 Non-destructive Methods

7.3.1 Diffraction Methods

M.E. Hilley, J.A. Larson, C.F. Jatczak and R.E. Ricklefs (eds) (1971). 'Residual Stress Measurements by X-Ray Diffraction', SAE Information Rep. J. 784a. SAE Pennsylvania.

W.P. Evans, R.E. Ricklefs, R.A. Hanson and J.A. Larson (1972). Society of Automotive Engineers, Pamphlet 720244, SAE SP-362.

R.H. Marion and J.B. Cohen (1974). Adv. X-Ray Anal., **18**, pp466-501.

A. Peiter (1976). Harterei-Techn. Mitt, **31**, pp158-165.

H. Dolle and V. Hauk (1976). Harterei-Techn. Mitt, **31**, pp165-168.

M.R. James and J.B. Cohen (1976). Adv. X-Ray Anal., **19**, pp695-708.

M.R. James and J.B. Cohen (1978). J. Testing Evaluation, **6**, pp91-97.

C.O. Ruud and G.D. Farmer (1979). 'Residual Stress Measurement By X-rays, Errors, Limitation, and Application', Nondestructive Evaluation of Materials. Segamore Army Materials Research Conference Proceedings **23**, Eds J.J. Burke and V. Wiess, pp101-115, Plenum Press.

M.R. James and J.B. Cohen (1980). 'The Measurement of Residual Stresses by X-Ray Diffraction Techniques', Treatise on Materials Science and Technology **19A**, chap 1, pp2-55.

G. Maeder, J.L. Lebrun and J.M. Sprauel (1981). 'Present Possibilities for the X-Ray Difraction Method of Stress Measurement', NDT Int., October, pp235-247.

A.J. Allen, M.T. Hutchings and C.G. Windsor (1985). 'Neutron Diffraction Methods for the Study Of Residual Stress Fields', Adv. Phys. **34**, pp445-473.

M.T. Hutchings (1991). 'Neutron Diffraction Measurement of Residual Stress Fields: Overview and Points For Discussion', Proc. NATO Advanced Research Workshop on Measurement of Residual and Applied Stress Using Neutron Diffraction, Eds M.T. Hutchings and A.D. Krawitz, NATO ASI Series E: Applied Sciences **216**.

M.T. Hutchings (1992). 'Neutron Diffraction Measurement of Residual Stress Fields - the Engineers Dream Come True?', Neutron News **3**, no 2, pp14-19.

M.T. Hutchings (1993). 'Residual Stresses: Measurement Using Neutron Diffraction', Encyclopedia Materials Characterisation, Eds. R.W. Cahn and E. Lifshin, Pergamon Press, pp412-417.

7.3.2 Ultrasonic Methods

F.D. Murnaghan (1951). 'Finite Deformation of an Elastic Solid', Wiley, New York.

R.N. Thurston and K. Brugger (1964). Phys. Rev., **133**, A1604.

R.E. Green (1973). Treatise on Materials Science and Technology, **3**, Eds H. Herman, Academic Press, New York.

B.G. Martin (1974). 'The Measurement of Surface and Near-Surface Stress in Aluminium Alloys Using Ultrasonic Rayleigh Waves', Materials Evaluation, November, pp229-234.

R. Bruce Thompson (1976). 'Strain Dependence of Electromagnetic Generation of Ultrasonic Surface Waves In Ferrous Metals', Applied Physics Letters **28**, no 9, pp483-485.

L. Alder, K.V. Cook, B.R. Dewey and R.T. King (1977). 'The Relationship Between Ultrasonic Rayleigh Waves and Surface Residual Stress', Materials Evaluation, July, pp93-96.

A.J. Boland, T.J. Davis, S.R. Doctor, T.P. Harrington, B.P. Hildebrand, D.K. Lemon, G.J. Posakony, and J.R. Skorpik (1980). 'Development of Ultrasonic Tomography for Residual Stress Mapping', EPRIRP 504-2 Final Report (Electric Power Research Institute, Palo Alto, USA).

A. Moro, C. Farina and F. Rossi (1980). 'Measurement of Ultrasonic Wave Velocity of Steel for Various Structures and Degrees of Cold Working', NDT Int. **13**, pp169-175.

E. Schneider and K. Goebbels (1982). 'Determination of Residual Stress by Linearly Polarised Ultrasonc Waves', Proc. Conf. on Periodic Inspection of Pressure Vessels, pp103.

R.B. King and C.M. Fortunko (1983). 'Determination of In-Plane Residual Stress States in Plates Using Horizontally Polarized Shear Waves', J. Appl. Phys. **54**, no 6, pp3027-3035

R.B. Thompson, J.F. Smith and S.S. Lee (1984). 'Microstructure-Independent Acoustoelastic Measurement of Stress', Appl. Phys. Lett. **44**, no 3, pp296-298.

D.R. Allen (1984). 'The Measurement of Residual Stresses Using Ultrasonics', Harwell Report AERE R-11445.

D.R. Allen and C.M. Sayers (1984). 'The Measurement of Residual Stress in Textured Steel Using and Ultrasonic Velocity Cobinations Technique', Ultrasonics **22**, pp179-187.

Y. Pao, W. Sachse and H. Fukuoka (1984). 'Acoustoelasticity and Ultrasonic Measurements of Residual Stresses', Physical Acoustics **XV11**, chapter 2, Eds. P. Mason and R.N. Thurston, pp61-143.

C.M. Sayers, D.R. Allen and G.E. Haines (1985). 'Texture Independent Determination of Residual Stresses in Metals Using Ultrasonic Surface Waves', Proc. Conf. Ultrasonics International **85**, pp306

R.B. Thompson, S.S. Lee and J.F. Smith (1986). 'Angular Dependence of Ultrasonic Wave Propagation in a Stressed Orthorhombic Continuum: Theory and Application to the Measurement of Stress and Texture', J. Acoustical Soc. Am. **80**, no.3, pp921-931.

G.D. Swanson (1986). 'Investigation of Ultrasonic Methods for Residual Stress Measurement', Topical Report BDX-613-3490, Allied Bendix Aerospce.

S.S. Lee, J.F. Smith and B.R. Thompson (1986). 'Evaluation of the Absolute Acousoelastic Stress Measurement Technique', Reveiw of Progress in Quantitative N.D.E.4', Eds D.O. Thompson and D.E. Chimenti, Plenum Press.

A.V. Clark, J.C. Moulder, R.B. Mignogna and P.P. DelSanto (1987). 'A Comparison of Several Ultrasonic Techniques for Absolute Stress Determination in the presence of Texture', Proc. ONR Symposium on Solid Mechanics Research for Quantitative Non-destructive Evaluation', Eds. J.D. Achenback, and Y. Rajapokse, Pub. Martinus Nijoff 1987, Nothern Univ. Evanston IL, USA, Sept. 1985.

H. Fukuoka (1987). 'Ultrasonic Measurement of Residual Stress', Proc. ONR Symposium on Solid Mechanics Research for Quantitative Non-destructive Evaluation', Eds. J.D. Achenback, and Y. Rajapokse, Pub. Martinus Nijoff 1987, Nothern Univ. Evanston IL, USA, Sept. 1985.

S.E. Pritchard (1987). 'Residual Stress Analysis Using Ultrasonic Techniques', N.D.T. Proceedings of 4th European Conf., **3**, 13-17 Sept. 1987, Eds. J.M. farley and R.W. Nickol, pp1775-1782.

T. Luthi (1990). 'Determination of Biaxial and Triaxial Stress Distributions Using Ultrasonics', N.DT International **23**, no 6, pp351-356.

7.3.3 Magnetic Methods

R.W. Leep (1967). 'The Barkhausen Effect and it's Application in Nondestructive Testing', Proc. Symp. on Physics and NDT, 439, Gordon and Breach.

W.L. Donaldson and R.L. Pasley (1967). 'A New Method of Nondestructive Stress Measurement', Proc. 6th Symp. nde of Aerospace and Weapons Systems Components and Materials, 563, Los Angeles: Western Periodicals.

S. I. Tiitto (1976). 'Influence of Elastic and Plastic Strain on the Magnetization Processes in Fe-3.5%Si, IEEE Trans. Magn. **12**, pp6.

G.A. Matzkanin, R.E. Beissner and C.M. Teller (1979). 'The Barkhausen Effect and it's Applications to Nondestructive Evaluation', SWRI, Report No NTIAC-79-2, 5.

K. Ono and M. Shibata (1979). 'Magnetomechanical Acoustic Emission for Residual Stress Measurements in Railroad Rails and Wheels', Proc. Conference on NDT for Measuring the Longditudinal Force in Rails. Federal Railway Adm. and American Assoc. of Railroads, Washington DC.

O. Sundström and K. Törrönen (1979). 'The Use of the Barkhausen Noise Analysis in Nondestructive Testing', Materials Eval. **37**, pp51.

H. Kusanagi, H. Kimura and H. Sasaki (1979b). 'Stress Effect on the Magnitude of Acoustic Emission During Magnetisation of Ferromagnetic Materials', J. Appl. Phys., **50**, pp2985.

W.A. Theiner, J. Grossman and W. Repplinger (1980). 'New Methods of Nondestructive Testing of Materials and their Application Especially in Nuclear Engineering', Proc. Int. Symp., Saarbrücken, Germany, 17-19 Sept. 1979, pp245-254, Berlin: Deutsche Gesellschaft für Zerstörungsfreie Prüfung e.v.

K. Ono and M. Shibata (1981a). 'Magnetomechanical Acoustic Emission for Residual Stress and Prior Strain Determination', Advances in Acoustic Emission, Eds H. L. Dunegan and W. F. Hartman, Dunhart, Knoxville, TN, pp154.

K. Ono and M. Shibata (1981b). 'Magnetomechanical Acoustic Emission - A New Method for Nondestructive Test Measurement', NDT Int. **14**, pp227.

K. Ono, M. Shibata and M. Kwan (1981). 'Determination of Residual Stress by Magnetomechanical Acoustic Emission', Residual Sress for Designers and Metalurgists, Eds L. J. Van de Walls, ASM, pp223.

G.L. Burkhardt, R.E. Beissner,G.A. Matzkanin and J.D. King (1982). 'Acoustic Methods for Obtaining Barkhausen Noise Stress Measurements', Mat. Eval., **40**, pp669.

R.A. Langman (1983). 'Nondesructive Evaluation of Stress in Steel by Magnetic Methods', Nondestructive Testing, Australia, pp14.

D.L. Atherton and D.C.Jiles (1983). 'The Effects of Stress on the Magnetisation of Steel', IEEE Trans. Magn., **19**, pp2021.

W.A. Theiner and I. Altpeter (1983). In New Procedures in Nondestructive Testing, ed. P. Holler, Berlin: Springer-Verlag.

G.V. Lomaev, V.S. Malyshev and A.P. Degterev (1984). 'Review of the Application of the Barkhausen Effect in Nondestructive Testing', Translated from Defektoskopiya, **3**, pp54.

E. Scheider, I. Altpeter and W.A. Theiner (1984). 'Nondestructive Methods for Material Property Determination', ed. C.O. Ruud and R.E. Green Jr, pp115-122, New York, Plenum Press.

D.C. Jiles and D.L. Atherton (1986). 'Theory of Ferro-magnetic Hysteresis', J. Magn. Mat. **61**, pp48-60.

D.J. Buttle, C.B. Scruby, G.A.D. Briggs and J.P. Jakubovics (1987). 'The Measurement of Stress in Steels of Varying Microstructure by Magnetoacoustic and Barkhausen Emission', Proc. R. Soc., London, A **414**, pp469.

D.C. Jiles (1988). 'Review of Magnetic Methods for Nondestructive Evaluation', NDT Int., **21**, pp311.

R.A. Langman (1988). 'Measurement of Stress by a Magnetic Method', in Nondestructive Testing, eds. J.M. Farley and R.W. Nichols, Pergamon, Oxford, pp1783-1799.

M.J. Sablik and D.C. Jiles (1988). 'A Model for Hysteresis in Magnetostriction', J. Appl. Phys., **64**, pp5402-5404.

M.J. Sablik (1989). 'Modelling Stress Dependence of Magnetic Properties for NDE of Steels', Nondest. test. Eval., **5**, pp49-65.

D.C. Jiles (1991). 'Introduction to Magnetism and Magnetic Materials', Chapman and Hall, London, pp165-172.

D.J. Buttle and M.T. Hutchings (1992). 'Residual Stress Measurement at NNDTC', Brit. J. NDT, **34**, pp175-181.

C.B. Scruby, G. Antonelli, D.J. Buttlle, W. Dalzell, M. Gori, J.A. Gulliver, C. de Michelis, F.A. Ravenscroft and M. Ruzzier (1993). 'Development of Non-Invasive Methods for Measurement of Stress in Welded Steel Structures', European Journal of NDT **3**, no 2, pp46-54.

7.3.4 Thermal Methods

B.A. Boley and J.H. Weiner (1960). 'Theory of Thermal Stresses', Wiley, New York.

P. Stanley and S. Saha (1985). 'Quantitative Stress Analysis by Means of the Thermoelastic Effect', J. Strain Anal. Eng. Des., **20**, 3, pp129-137.

D.E. Oliver, W. Reuter and G.M. Everett (1985). 'Non Contacting Measurement of Stresses in Engineering Structures', ISTA 85 - 14th Int. Symp. on Automotive Technology and Automation, proc. Vol.1, Graz, Australia, 23-27 Sept. 1985, Automotive Automation, 42 Lloyd Park Av., Croydon CR0 5SB, UK, Paper ISATA 85018, pp207-218.

D.S. Mountain and G.P. Cooper (1989). 'TERSA _ A New Technique for Assesing Residual Stress', Strain, February, pp15-19.

N. Harwood, W.M. Cummings and A.K. MacKenzie (1991). 'An Introduction to Thermoelastic Stress', in 'Thermoelastic Stress Analysis', eds. Harwood and Cummings, Hilger, Bristol, UK, 1991, pp1-34.

A.K. Wong (1993). 'Stress Distribution: Analysis Using Thermoelastic Effect', Encyclopedia Materials Characterisation, Eds. R.W. Cahn and E. Lifshin, Pergamon Press, pp483-487.

7.3.5 Optical Methods

D. Post (1971). In 'Techniques of Metals Research', vol. **V**, ed. R.F. Bunshah, New York, Interscience, p 339.

A.S. Kuo and H.W. Liu (1979). In 'Nondestructive Evaluation of Materials', eds. J.J. Burke and V. Weiss, New York, Plenum, p385.

J.M. Webster, J.K. Hepworth and C. Forno (1981). 'Strain in Transition Joints Measured by High Resolution Moire-photography', Exp. Mech. Vol **21**, 5, pp 195-200.

P. Blümel, E. Hosp, R. Ritter and B. Simon ((1982). 'Optische Verfahren in der Experimentellen Spannungsanalyse', VDI Ber Nr **439**, pp 97-121.

7.3.6 Other Methods

J.H. Underwood (1973). Exp. Mech., **9**, p373.

C.M. Yagnik and R.L. Collins (1976). Proc. Workshop on Nondestructive Evaluation of Residual Stress, Report NTIAC-76-2, Nondestructive Testing Information Analysis Center, Southwest Research Institute, San Antonio, Texas.

7.4 Numerical Methods

L. Tall (1964). 'Residual Stresses in Welded Plates: - A Theoretical Study', Welding Journal, Research Supplement, **43**, No 1, pp 10s - 23s.

S.V. Vaidyanathan, A.F. Todaro and I. Finnie (1973). 'Residual Stress due to Circumferential Welds', J. Engineering Materials and Technology, pp 233 - 237.

H.D. Hibbit and P.V. Marcal (1973). 'Numeric Thermomechanical Model for Welding and Subsequent Loading of a Fabricated Structure', J. Comp. and Structures, **3**.

E. Friedman (1975). 'Thermomechanical Analysis of the Welding Process using the Finite Element Method', ASME J Press Vess Tech, pp 206 - 213, Aug.

M.B. Hsu. 'Analysis of Welds by the Finite Element Method', MARC Analysis Research Corporation, Palo Alto, California.

E.F. Rybicki et al (1977). 'Residual Stresses at Girth Butt Welds in Pipes and Pressure Vessels', Final Report prepared for US Nuclear Regulatory Commission, Battelle Columbus Laboratories, NUREG-0376, June.

E.F. Rybicki, D.W. Schmueser, R.B. Stonesifer, J.J. Groom amd H.W. Mishler (1978). 'A Finite Element Model for Residual Stresses and Deflections in Girth Welded Pipes', ASME J Pressure Vessel Technology, Vol **100**, pp256-262, Aug..

E.F. Rybicki and R.B. Stonesifer (1979). 'Computation of Residual Stresses due to Multipass Welds in Piping Systems', ASME J. Pressure Vessel Technology, **101**, pp149-154.

K. Masubuchi (1980). Analysis of Welded Structures. 'Residual Stresses, Distortion and Their Consequences. Ed. D.W. Hopkins, Pergamon Press, Oxford.

D. Johnson (1981). TAU-A Computer Program for the Analysis of Temperature in Two- and Three-Dimensional Structures, Using the UNCLE Finite Element Scheme', Central Computer Services, Risley, ND-R-503(R), June.

Arggris et al (1982). 'Computational Aspects of Welding Stress Analysis', Computer Methods in Applied Mechanics, **35**, p 635.

R.H. Leggat (1982). 'Residual Stresses at Circumferential Welds in Pipes', The Welding Institute Research Bulletin, pp181-188, June.

K. Masubuchi (1982). 'Residual Stresses and Distortion in Weldments: A Review of the Present State-of-the-art', in Residual Stress and Stress Relaxation, Proc, 28th Sagamore Army Materials Research Conf., eds. E. Kula and V. Weiss, Plenum Press, New York, p49.

T. Richardson (1982). 'CAUSE: Two- and Three-Dimensional Stress Analysis of Continue, using the UNCLE Finite Element Scheme', Central Computer Services, Risley, ND-R-503, April.

E. Macherauch (1984). 'Residual Stresses', Application of Fracture Mechanics to Materials and Structures, Proc. Int. Conf., Freiburg, West Germany, 20-24 June, 1983, pp157-192, Eds. G.C. Sih, E. Sommer, W. Dahl, Pub. Martinus Nijhoff.

T. Umemoto and S. Tanaka (1984). ' A Simplified Approach to Calculate Weld Residual Stress in a Pipe', IHI Engng Rev **17**, No 3, pp177 - 183.

(1985). 'The UNCLE Finite Element Scheme', Risley Nucl Power Dev Est, ND-R-1131(R), Nov.

R.H. Leggat (1988). 'Computer Modelling of Transverse Residual Stresses in Repair Welds', IIW Document No. X-1176-88, May.

T. Umemoto and S. Furuya. (1989). 'A Simplified Approach to Assess Weld Residual Stress Distribution through Pipe Walls', Nuclear Engineering and Design, pp 159 - 171.

P. Palanichamy, A. Joseph, D.K. Bhattacharya and Baldev Raj (1992). 'Residual Stresses and Their Evaluation in Welds', in Welding Engineering Hand Book ISBN: 81-85373-02-7, Radiant Publications Private Limited, Secunderabad, India.

Printed and published by the Health and Safety Executive
C2 3/98

MAIL ORDER
HSE priced and free
publications are
available from:
HSE Books
PO Box 1999
Sudbury
Suffolk CO10 6FS
Tel: 01787 881165
Fax: 01787 313995

RETAIL
HSE priced publications
are available from
good booksellers

HEALTH AND SAFETY ENQUIRIES
HSE InfoLine
Tel: 0541 545500
or write to:
HSE Information Centre
Broad Lane
Sheffield S3 7HQ

HSE home page on the World Wide Web:
http://www.open.gov.uk/hse/hsehome.htm

ISBN 0-7176-2411-0

£65.00 net